ISSN 1916-9698 (Print)
ISSN 1916-9701 (Online)

INTERNATIONAL JOURNAL OF CHEMISTRY

Vol. 9, No. 3, August 2017

CANADIAN CENTER OF SCIENCE AND EDUCATION

International Journal of Chemistry

An International Peer-reviewed and Open Access Journal for Chemistry

International Journal of Chemistry (IJC) is an international, peer-reviewed, open-access journal, published by Canadian Center of Science and Education. The journal is published Quarterly (February, May, August and November) in both print and online versions. IJC aims to promote excellence through dissemination of high-quality research findings, specialist knowledge, and discussion of professional issues that reflect the diversity of this field.

The scopes of the journal include:

- Analytical
- Biochemistry
- Inorganic
- Materials
- Neurochemistry
- Nuclear Chemistry
- Organic
- Physical Chemistry

The journal is included in:

- Academic Journals Database
- Bibliography and Index of Geology
- CABI
- CAS (Chemical Abstracts Service, ACS)
- EBSCOhost
- Elektronische Zeitschriftenbibliothek EZB
- Google Scholar
- Ulrich's

Open-Access Policy

We follow the Gold Open Access way in journal publishing. This means that our journals provide immediate open access for readers to all articles on the publisher's website. The readers, therefore, are allowed to read, download, copy, distribute, print, search, link to the full texts or use them for any other lawful purpose. The operations of the journals are alternatively financed by publication fees paid by authors or by their institutions or funding agencies.

Copyright Policy

Copyrights for articles are retained by the authors, with first publication rights granted to the journal/publisher. Authors have rights to reuse, republish, archive, and distribute their own articles after publication. The journal/publisher is not responsible for subsequent uses of the work.

Submission Policy

Submission of an article implies that the work described has not been published previously (except in the form of an abstract or as part of a published lecture or academic thesis), that it is not under consideration for publication elsewhere, that its publication is approved by all authors and tacitly or explicitly by the authorities responsible where the work was carried out. However, we accept submissions that have previously appeared on preprint servers (for example: arXiv, bioRxiv, Nature Precedings, Philica, Social Science Research Network, and Vixra); have previously been presented at conferences; or have previously appeared in other "non-journal" venues (for example: blogs or posters). Authors are responsible for updating the archived preprint with the journal reference (including DOI) and a link to the published articles on the appropriate journal website upon publication.

iThenticate® Professional Plagiarism Prevention

The publisher and journals have a zero-tolerance plagiarism policy. We check the issue using the plagiarism prevention tool and a reviewer check. All submissions will be checked by iThenticate before being sent to reviewers.

IJC accepts both Online and Email submission. The online system makes readers to submit and track the status of their manuscripts conveniently. For any questions, please contact ijc@ccsenet.org.

International Journal of Chemistry; Vol. 9, No. 3; 2017
ISSN 1916-9698 E-ISSN 1916-9701
Published by Canadian Center of Science and Education

EDITORIAL TEAM

International Journal of Chemistry; Vol. 9, No. 3; 2017
ISSN 1916-9698 E-ISSN 1916-9701
Published by Canadian Center of Science and Education

Content

International Journal of Chemistry; Vol. 9, No. 3; 2017
ISSN 1916-9698 E-ISSN 1916-9701
Published by Canadian Center of Science and Education

Synthesis of Network Polymers Containing Si-Vinylene Units by Mizoroki-Heck Reaction

Naofumi Naga[1], Yasuto Sugano[1], Arie Senda[1]

[1]Department of Applied Chemistry, Materials Science Course, College of Engineering, Shibaura Institute of Technology, 3-7-5 Toyosu, Koto-ku, Tokyo 135-8548, Japan

Correspondence: Naofumi Naga, Department of Applied Chemistry, Materials Science Course, College of Engineering, Shibaura Institute of Technology, 3-7-5 Toyosu, Koto-ku, Tokyo 135-8548, Japan. E-mail: nnaga@sic.shibaura-it.ac.jp

Received: April 5, 2017 Accepted: May 2, 2017 Online Published: May 9, 2017

doi:10.5539/ijc.v9n3p1 URL: https://doi.org/10.5539/ijc.v9n3p1

Abstract

Network polymers containing Si-vinylene units have been synthesized by Mizoroki-Heck reaction of cyclic siloxane or cubic silsesquioxane compounds with vinyl groups, as joint molecules, and dibromo aryl compounds, as linker molecules, using a Pd catalyst. The reaction of 1,3,5,7-tetravinyltetramethylcyclotetrasiloxane (TVMCTS) or octavinyloctasilsesquioxane (PVOSS) with *o*, *m*, *p*-dibromobenzene (DBB) or 4,4'-dibromobiphenyl (DBBP) yielded the corresponding network polymers, except TVMCTS-oDBB system. Optical properties of the network polymers were studied by UV-vis and photoluminescence spectroscopy, and absorption and emission derived from σ-π conjugation of the Si-vinylene units were detected. Copolymerization of TVMCTS-DBB/bromobenzene yielded $CHCl_3$ soluble fraction due to formation of the network fragments. The network polymers of TVMCTS or PVOSS with 2,7-dibromofluorene (BFl) or 9,9-dihexyl-2,7-dibromofluorene were synthesized by the same procedures. Scanning electron microscope image of TVMCTS-BFl network polymer indicated formation of porous structure. The network polymers have been also synthesized by the reactions of multifunctional aryl bromide, as the joint molecules, with divinyl or dially silane compounds, as the linker molecules. The molecular structure of the multifunctional aryl bromide affected the emission wavelengths of the network polymers. In the case of the 2,2',7,7'-tetrabromo-9,9'-spirobifluorene-based network polymers, the emission spectra widely ranged from 450 to 500 nm, which were sensitive to molecular structure of the divinyl or dially silane compounds.

Keywords: network polymer, Si-vinylene unit, Mizoroki-Heck reaction, optical properties

1. Introduction

Many kinds of π-conjugated polymers have been developed due to their characteristic photophysical features and application to organic light-emitting diodes (for example Burroughes, Bradley, Brown, Marks, Mackay, Friend, Burns, & Holmes, 1990). Among the π-conjugated polymers, poly(*p*-phenylene-vinylene), poly(thiophene), poly(*p*-phenylene), poly(fluorene), and poly(carbazole) are typical polymers that show high photoluminescence quantum yield. The copolymers based on these π-conjugated polymers have been synthesized to control the photophysical properties and/or increase solubility in organic solvents.

We have synthesized fluorene or carbazole-based alternating copolymers containing Si-vinylene units (Naga, Tagaya, Noda, Imai, & Tomoda, 2008; Naga, Ohkura, Tagaya, & Tomoda, 2011; Naga & Saito, 2016). The copolymers were obtained with Mizoroki-Heck reaction of dibromofluorene or dibromocarbazole with Si-containing divinyl or diallyl compounds. For example, the copolymerization of 9,9-dihexyl-2,7-dibromofluorene (BHFl) with divinyldimethylsilane (VMS) using palladium(II) acetate catalyst yielded the corresponding alternating copolymer in good yield. The copolymers showed absorption peaks derived from intramolecular charge transfer through the σ-π moiety.

Geometric variations of the conjugated polymers, such as hyper-branched, dendritic, and network structures, have been also investigated (for examples Jiang, Su, Trewin, Wood, Campbell, Niu, Dickinson, Ganin, Rosseinsky, Khimyak, & Cooper, 2007; Dawson, Laybourn, Clowes, Khimyak, Adams, & Cooper, 2009; Liu, Lam, & Tang, 2009; Hu, Lam, & Tang, 2013). Neckers et al. reported synthesis of Si containing unsaturated star polymers by hydrosilylation reaction of 1,3,5-triethynylbenzene (TEB) and (*p*-(dimethylsilyl)phenyl)acetylene (Wang, Kaafarani, & Neckers, 2003). Some organic-inorganic hybrid gels containing σ-π conjugated Si-vinylene units in the network were developed in our laboratory by the hydrosilylation reaction of TEB and 1,1,3,3-tetramethyldisiloxane or 1,4-bisdimetylsilylbenzene in toluene (Naga, Iwashita, Nagino, Miyanaga, & Furukawa, 2015). Although, the hydrosilylation reaction is one of the

effective methods to synthesize the network structures containing Si-vinylene units, the multifunctional ethynylene compounds, such as TEB, should be necessary. We thought about to synthesize the network polymers having Si-vinylene units using Mizoroki-Heck reaction. This method should widen the applicable monomers and make it possible to synthesize variety of network polymers having Si-vinylene units.

In this paper, we report synthesis of the network polymers containing Si-vinylene units by Mizoroki-Heck reaction of multi-functional siloxane compounds with vinyl groups and dibromo aryl compounds using a Pd catalyst, as shown in Scheme 1. The reaction of multifunctional aryl bromide with divinyl or dially silane compounds also conducted to yield the network polymers, as shown in Scheme 2. Absorptive and emissive properties of the network polymers were investigated with UV-vis and photoluminescence (PL) spectroscopy.

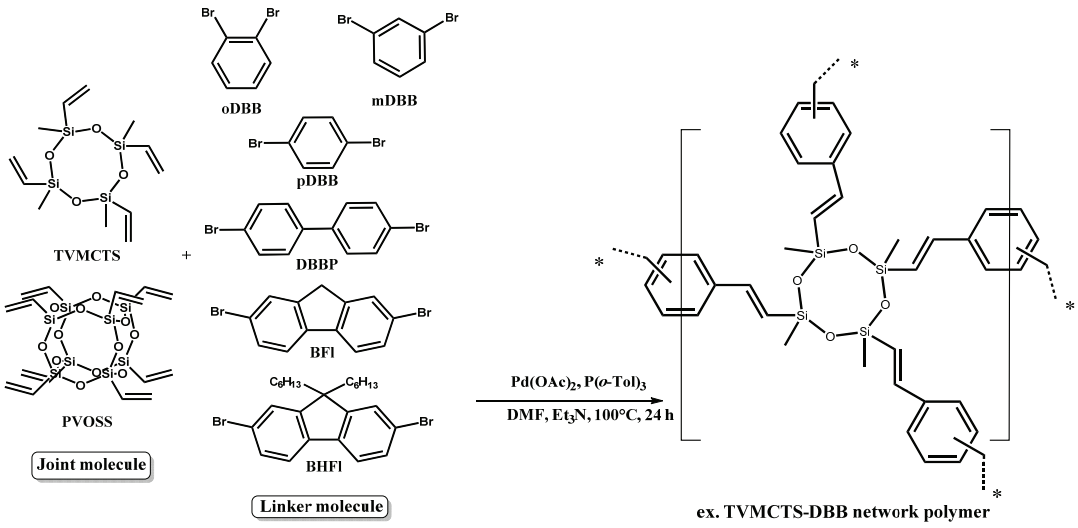

Scheme 1. Synthesis of network polymers by Mizoroki-Heck reaction of cyclic siloxane or cubic silsesquioxane compounds with vinyl groups-dibromo aryl compound systems

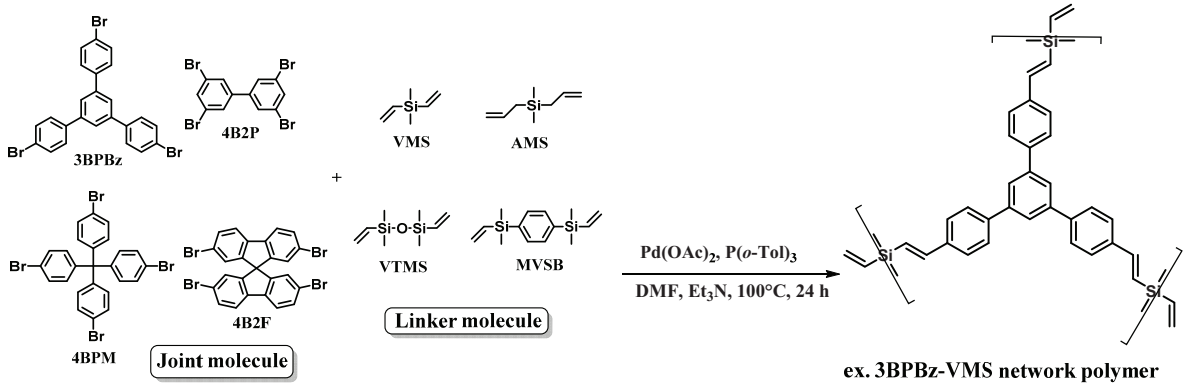

Scheme 2. Synthesis of network polymers by Mizoroki-Heck reaction of multifunctional aryl bromide-divinyl, diallyl silane systems

2. Method

2.1 Materials

1,3,5,7-Tetravinyltetramethylsiloxane (TVMCTS) (Chisso Co., Ltd.) and octavinyloctasilsesquioxane (PVOSS) (Aldrich Chemical Co., Ltd.) were used without further purification. 1,2-Dibromobenzene (oDBB), 1,3-dibromobenzene (mDBB), 1,4-dibromobenzene (pDBB), 4,4'-dibromobiphenyl (DBBP), bromobenzene (BB), 2,7-dibromofuluorene (BFl), and BHFl were commercially obtained from Tokyo Chemical Industry Co., Ltd., and used as received. 1,3,5-Tris(4-bromophenyl)benzene (3BPBz), 3,3',5,5'-tetrabromo-1,1'-biphenyl (4B2P), tetrakis(4-bromophenyl)methane (4BPM), 2,2',7,7'-tetrabromo-9,9'-spirobifluorene (4B2F) (Tokyo Chemical Industry Co., Ltd.), VMS (Aldrich Chemical Co., Ltd.), diallydimethylsilane (AMS) (Tokyo Chemical Industry Co., Ltd.), 1,1',3,3'-tetramethyl-1,3-divinyldisiloxane (VTMS) (Chisso Co., Ltd.), and 1,4,-bis(dimethylvinylsilyl)benzene (MVSB) (Shin-etsu Chemical Co., Ltd.) were commercially obtained and used without further purification. Palladium(II) acetate

($Pd(OAc)_2$) (Aldrich Chemical Co., Ltd.), tri-*o*-tolylphosphine ($P(o\text{-}Tol)_3$) (Kanto Chemical Co., Ltd.), triethylamine (NEt_3) (Kanto Chemical Co., Ltd.), and N,N-dimethylformamide (DMF) (dehydrated grade, Kanto Chemical Co., Ltd.) were commercially obtained and used as received.

2.2 Synthesis of Network Polymers

Synthesis of the network polymers was carried out in a 10 mL ample tube equipped with a magnetic stirrer. A reaction of TVMCTS with DBB is described as a reference. DBB (1 mmol), $P(o\text{-}Tol)_3$ (0.12 mmol), and $Pd(OAc)_2$ (0.02 mmol) were added to the ample tube under a nitrogen atmosphere. After the addition of TVMCTS (0.5 mmol), DMF (2.0 mL), and NEt_3 (1.5 mmol), the ample tube was sealed by burning off. The reaction was conducted at 100°C for 24 h. The polymerization was terminated by adding a small amount of methanol. The polymer was precipitated in a large excess of methanol and recovered by filtration. The polymer obtained was washed by chloroform and dried in vacuo at 50°C for 6 h. Other network polymers were synthesized by the same procedures with the molar ratio of vinyl or allyl to Br was 1.0.

2.3 Analytical Procedures

FT-IR spectra of the network polymers were recorded on a Jasco FT/IR-410 spectrometer in pulse Fourier transform mode as KBr discs. ^1H NMR spectra of $CHCl_3$ soluble fractions of TVMCTS-DBB/BB polymers were recorded on a JEOL-JNM-LA300 spectrometer in pulse Fourier transform mode in $CDCl_3$. The pulse angle was 45º and 32 scans were accumulated in 7 s of the pulse repetition. UV-vis absorption spectroscopy was conducted with SHIMADZU UV-2450. Photoluminescence (PL) spectroscopy was investigated with a SHIMADZU RF-5300PC. Scanning electron microscope (SEM) images were acquired by JEOL JSM-7400F.

3. Results and Discussion

3.1 Network Polymers from TVMCTS, PVOSS-DBB, DBBP

Mizoroki-Heck reaction of TVMCTS or PVOSS with DBB or DBBP has been investigated with $Pd(OAc)_2$ catalyst in DMF at 100ºC, as shown in Scheme 1. Polymerization results are summarized in Table 1. The reaction of TVMCTS with pDBB and DBBP yielded the polymers in good yields. The yield of the TVMCTS-mDBB polymer was much lower than that of the TVMCTS-pDBB polymer. Furthermore, the polymer was not obtained in the reaction of TVMCTS with oDBB. The sterically hindered o- and m- positions of Br in DBB should decrease the reaction conversion, which would cause the low polymer yields. The reactions with PVOSS yielded the polymers in good yields independent of the molecular structure of the dibromo aryl compounds used. Large number of vinyl groups, 8 groups per one molecule, should effectively form the network structure.

FT-IR spectra of TVMCTS-mDBB, pDBB, and DBBP are shown in Figure 1 (a), (b), and (c), respectively. The broad peaks derived from Si-O-Si structure of TVMCTS were detected at around 1050 cm^{-1}. The peaks derived from phenyl groups were detected at around 1500 cm^{-1} (C=C stretching of phenyl) and 750-800 cm^{-1} (C-H vending of disubstituted phenyl). The peaks derived from the unsaturated C=C units connected to Si, and Si-C units were detected at 1600 cm^{-1}, and 1275 cm^{-1}, respectively. These results clear the formation of the network polymers by Mizoroki-Heck reaction of TVMCTS with mDBB, pDBB, and DBBP. The network polymers with PVOSS showed similar spectral profiles derived from the corresponding network structure.

Absorptive and emissive features of the network polymers (solid state) were studied with UV-vis and PL spectroscopy. The UV-vis and PL spectra of TVMCTS-pDBB, TVMCTS-DBBP, and PVOSS-pDBB are shown in Figure 2. The λ_{max} wavelength of the spectra are summarized in Table 1. The network polymers showed broad absorption ranged from about 300 to 400 nm. Excitation of the network polymers with the λ_{max} wavelength of the absorption showed relatively sharp emission peaks. The network polymers with pDBB and DBBP showed the emission at longer wavelength than those with oDBB or mDBB. The red-shift of the network polymers with pDBB and DBBP would be due to the long and linear conjugated structure in the network derived from these *p*-substituted linker molecules.

Table 1. Synthesis and optical properties of TVMCTS, PVOSS-DBB, DBBP network polymers [a]

Run	Joint	Linker	Yield %	λ_{max} nm	
				absorption [b]	emission [b,c]
1	TVMCTS	mDBB	41	342	383
2	TVMCTS	pDBB	95	320	461
3	TVMCTS	DBBP	95	353	450
4	PVOSS	oDBB	87	312	365
5	PVOSS	mDBB	100	319	370
6	PVOSS	pDBB	100	354	457
7	PVOSS	DBBP	100	335	450

[a]Conditions: linker molecule (1 mmol), P(*o*-Tol)$_3$ (0.12 mmol), Pd(OAc)$_2$ (0.02 mmol), TVMCTS (0.5 mmol) or PVOSS (0.25 mmol), DMF (2.0 mL), NEt$_3$ (1.5 mmol), 100°C for 24 h. [b]Evaluated in solid state. [c] Excitation with λ_{max} of absorption.

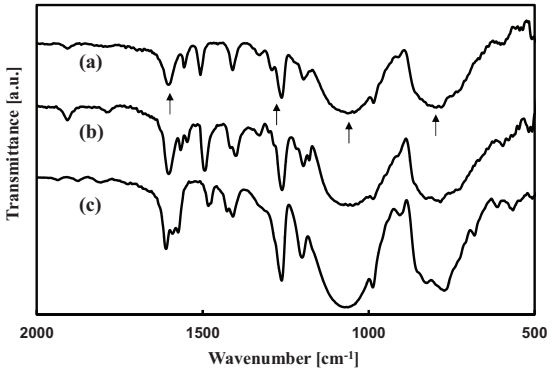

Figure 1. FT-IR spectra of (a) TVMCTS-mDBB, (b) TVMCTS-pDBB, and (c) TVMCTS-DBBP network polymers

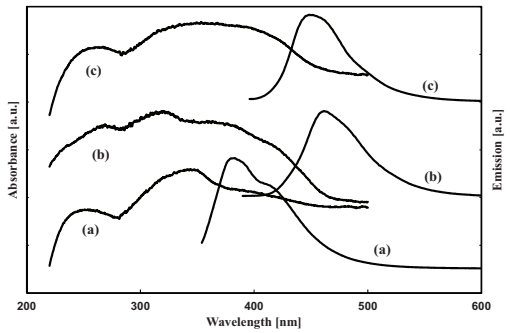

Figure 2. UV-vis (left) and PL (right) spectra of (a) TVMCTS-mDBB, (b) TVMCTS-pDBB, and (c) TVMCTS-DBBP network polymers (solid state)

3.2 Network Polymers from TVMCTS-pDBB/BB and TVMCTS/VTMS-pDBB Systems

Network polymers have been synthesized from TVMCTS-pDBB/BB systems. The results are summarized in Table 2. The network polymers contained chloroform soluble fraction, and its amount slightly increased with increasing of the BB feed ratio. Molecular structure of the chloroform soluble fraction was studied by ^{1}H NMR spectroscopy. Figure 3 shows the ^{1}H NMR spectrum and chemical shift assignment of the chloroform soluble fraction of a TVMCTS-pDBB/BB network polymer (Run 10). The peaks derived from vinylene units and methyl group connected to Si were detected at 6.0, 4.7 and 1.5 ppm, respectively. These results indicate that the molecular structure of the chloroform soluble fraction is parts of the network structure. Incorporation of mono-functional BB prevents from formation of infinite network, and yields the small fragments. The network polymers were also synthesized from TVMCTS/VTMS-DBB systems. Although the chloroform soluble fraction of the network polymers was detected, the fractions were small. Absorptive and emissive features of the TVMCTS-pDBB/BB network polymers of the chloroform soluble fractions were studied with UV-vis and PL spectroscopy in chloroform, as shown in Figure 4. Intensity of the absorption peak at around 300-320 nm in UV-vis spectra increased with increasing of the BB feed ratio in the reaction system. The fragments derived from the defect structure, which shows the absorption at long wavelength, would increase with increasing of the BB feed ratio.

Table 2. Synthesis and optical properties of TVMCTS–pDBB/BB, TVMCTS/VTMS-pDBB network polymers [a]

Run	Joint mmol		Linker mmol		Yield %	$CHCl_3$ sol.[b] wt%	λ_{max} nm	
	TVMCTS	VTMS	pDBB	BB			absorption[c]	emission[c,d]
8	0.30		0.56	0.06	97	10	271	424
9	0.27		0.47	0.15	81	15	271	430
10	0.23		0.31	0.31	60	16	264	443
11	0.28	0.03	0.59		78	-	-	-
12	0.23	0.08	0.55		72	5	287	447
13	0.16	0.16	0.47		63	7	280	451

[a]Conditions: P(*o*-Tol)$_3$ (0.125 mmol), Pd(OAc)$_2$ (0.025 mmol), DMF (2.0 mL), NEt$_3$ (1.56 mmol), 100°C for 24 h. [b]$CHCl_3$ soluble fraction. [c]Evaluated in $CHCl_3$. [d]Excitation with λ_{max} of absorption.

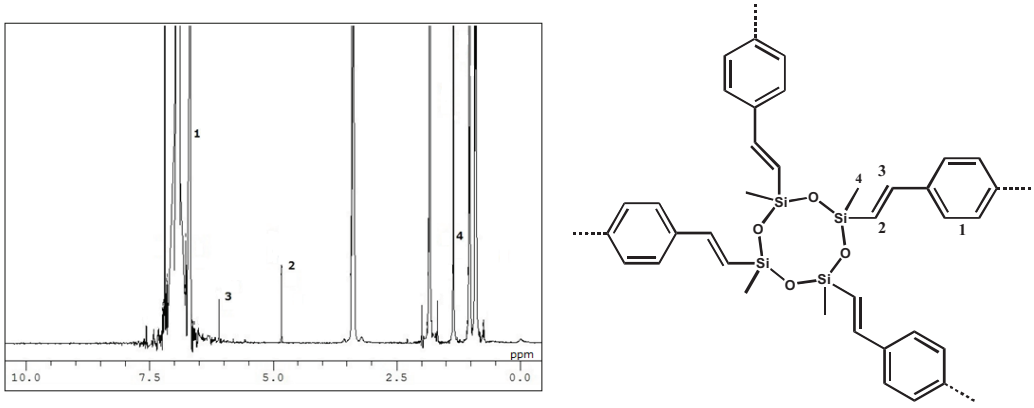

Figure 3. ^{1}H NMR spectrum of TVMCTS-DBB/BB polymer (Run 10), and assignment

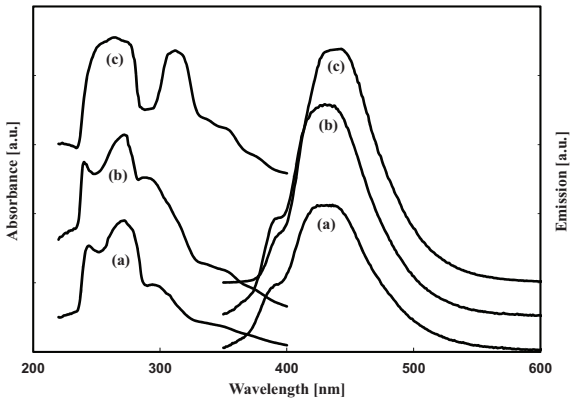

Figure 4. UV-vis (left) and PL (right) spectra of network polymers of chloroform soluble fraction of TVMCTS-pDBB/BB network polymers (chloroform solution), (a) Run 8, (b) Run 9, and (c) Run 10

3.3 Network Polymers from TVMCTS, PVOSS-BFl, BHFl

Network polymers have been synthesized from TVMCTS, PVOSS-BFl, BHFl systems, as shown in Scheme 1, to introduce the fluorescent fluorene units into the network. The results are summarized in Table 3. The corresponding network polymers were obtained in good yields.

FT-IR spectra of TVMCTS-BFl, TVMCTS-BHFl network polymers are shown in Figure 5 (a) and (b), respectively. The broad peaks derived from Si-O-Si structure of TVMCTS were detected at around 1050-1100 cm^{-1}. The peaks derived

from phenyl groups of fluorene units and unsaturated C=C units connected to Si were detected at around 1450 cm^{-1} (C=C stretching of phenyl) and 1650 cm^{-1}, respectively. These results clear the formation of the network polymers by Mizoroki-Heck reaction of TVMCTS with BFl and BHFl. The network polymers with PVOSS showed the similar spectral profiles derived from the corresponding network structure.

Absorptive and emissive features of the network polymers (solid state) were investigated with UV-vis and PL spectroscopy. The λ_{max} wavelengths of the absorption and emission spectra are summarized in Table 3. The spectra of the network polymers showed broad absorption peaks at around 315 nm or 350 nm, and emission peaks at around 450 nm or 480 nm. Definite correlation between the molecular structure and the absorption or emission wavelengths was not detected in these network polymers. The results indicated that the hexyl substituent of fluorene unit has little effect on the optical properties of the network polymer.

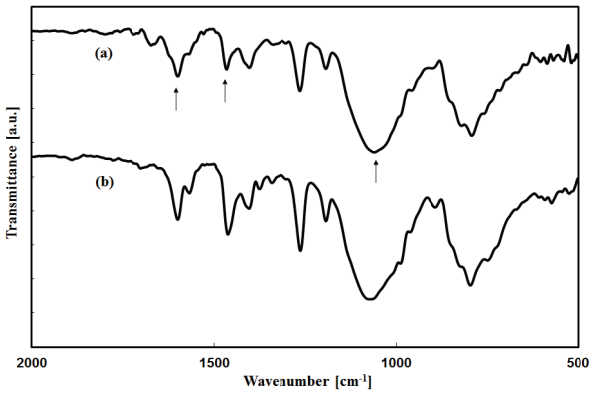

Figure 5. FT-IR spectra of (a) TVMCTS-BFl, and (b) TVMCTS-BHFl

Table 3. Synthesis and optical properties of TVMCTS, PVOSS-BFl, BHFl network polymers [a]

Run	Joint	Linker	Yield %	λ_{max} nm	
				absorption [b]	emission [b,c]
14	TVMCTS	BFl	54	316	449
15	PVOSS	BFl	51	352	451
16	TVMCTS	BHFl	64	318	477
17	PVOSS	BHFl	47	315	454

[a]Conditions: BFl or BHFl (1 mmol), P(*o*-Tol)$_3$ (0.12 mmol), Pd(OAc)$_2$ (0.02 mmol), TVMCTS (0.5 mmol) or PVOSS (0.25 mmol), DMF (2.0 mL), NEt_3 (1.5 mmol), 100°C for 24 h. [b]Evaluated in solid state. [c] Excitation with λ_{max} of absorption.

SEM images of TVMCTS-BFl and TVMCTS-BHFl network polymers are shown in Figure 6. TVMCTS-BFl network polymer showed the texture derived from porous structure. By contrast, the texture of TVMCTS-BHFl network polymer indicated smooth surface. One explanation for this result is effect of the substituent of BHFl on the network formation. The bulky hexyl group of BHFl would prevent from forming rigid network structure.

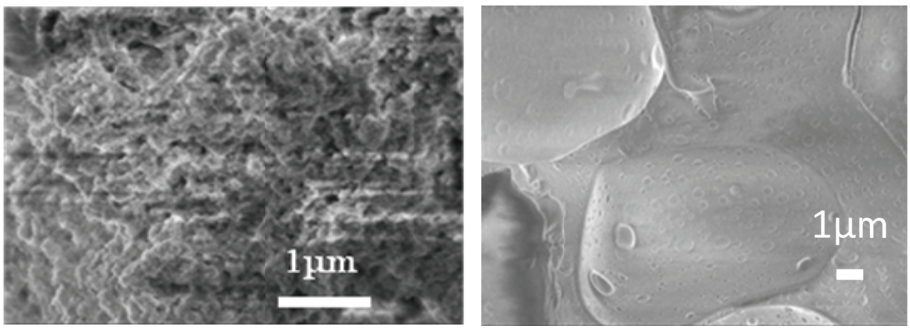

(a) (b)

Figure 6. SEM images of (a) TVMCTS-BFl, and (b) TVMCTS-BHFl network polymers

3.4 Network Polymers from Multifunctional Aryl Bromide and Divinyl, Dially Silane Compounds

Network polymers containing Si-vinylene units were also synthesized by the Mizoroki-Heck reaction of multifunctional aryl bromide (3BPBz, 4B2P, 4BPM, or 4B2F) with divinyl or dially silane compounds, VMS, AMS, VTMS, MVSB, as

shown in Scheme 2. The corresponding polymers were obtained in middle to good yields, 27-94% as summarized in Table 4. Figure 7 shows FT-IR spectra of 3BPBz-VMS, AMS, VTMS, MVSB network polymers. All the network polymers showed the peaks derived from stretching of C=C in vinylene, stretching of C=C in phenyl group, stretching of CH_3-Si-CH_3, and C-H vending of phenyl group, at around 1600 cm^{-1}, 1500 cm^{-1}, 1250 cm^{-1}, and 840-820 cm^{-1}, respectively. The spectrum of 3BPBz-AMS network polymer (Figure 7 (b)) or 3BPBz-MVSB network polymer (Figure 7 (d)) showed the peak derived from vending of Si-CH_2-CH= or stretching of Si-aryl at around 1150 cm^{-1} or 1130 cm^{-1}, respectively. Molecular structure of the other network polymers was also confirmed by the FT-IR spectra.

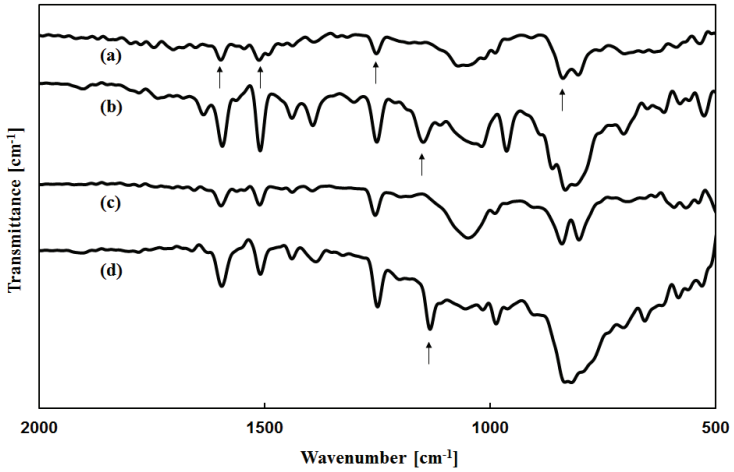

Figure 7. FT-IR spectra of (a) 3BPBz-VMS, (b) 3BPBz-AMS, (c) 3BPBz-VTMS, and (d) 3BPBz-MVSB network polymers

Table 4. Synthesis and optical properties of multifunctional aryl bromide-divinyl, diallyl silane network polymers [a]

Run	Joint	Linker	Yield %	λ_{max} nm	
				excitation [b]	emission [b,c]
18	3BPBz	VMS	84	378	428
19	3BPBz	AMS	94	362	430
20	3BPBz	VTMS	71	396	439
21	3BPBz	MVSB	69	390	435
22	4B2P	VMS	51	374	421
23	4B2P	AMS	32	---	---
24	4B2P	VTMS	68	371	416
25	4B2P	MVSB	52	363	411
26	4BPM	VMS	93	263	341
27	4BPM	AMS	87	263	344
28	4BPM	VTMS	69	258	342
29	4BPM	MVSB	57	264	341
30	4B2F	VMS	49	450	489
31	4B2F	AMS	64	419	463
32	4B2F	VTMS	80	458	496
33	4B2F	MVSB	27	385	448

[a]Conditions: linker molecule (0.188 mmol or 0.25 mmol), P(*o*-Tol)$_3$ (0.0375 mmol), Pd(OAc)$_2$ (0.0075 mmol), joint molecule (0.125 mmol), DMF (0.5 mL), NEt_3 (0.47 mmol), 100°C for 24 h. [b]Evaluated in solid state. [c]Excitation with λ_{max} of absorption.

Emission spectra of the network polymers (solid state) are shown in Figure 8. The excitation wavelength was determined by fluorescence excitation spectrum. The averaged maximal emission wavelength of the emission spectra, which were exited with 280-380 nm at intervals of every 10 nm, was used as the excitation wavelength, as summarized in Table 4. 1,3,5-Triphenylbenzene, biphenyl, tetraphenylmethane, and 9,9-spirobifluorene, which are moieties of the network structure in the network polymers with 3BPBz, 4B2P, 4BPM, and 4B2F, showed the emission peak with λ_{max} at 352 nm, 322 nm, 323 nm, and 310 nm, respectively. These wavelengths were different from those of the corresponding network polymers. These results indicate that the emission of the network polymers should be affected by the σ-π conjugation formed by Si-vinylene unit. Figure 8 (i) shows the emission spectra of 3BPBz-based network polymers. The emission spectra showed maximal peaks at around 430 nm. In the case of the 4B2P-based network polymers, Figure 8 (ii), the polymer with VMS, VTMS, and MVSB showed the emission peaks with the λ_{max} at around 410-420 nm. By contrast, 4B2P-AMS network polymer did hardly show emission, Figure 8 (ii)-(b). Methylene units between Si and vinylene in AMS should disturb formation of conjugation in the network, as previously reported in the similar liner polymers (Naga, Tagaya, Noda, Imai, & Tomoda, 2008). The 4BPM-based network polymers showed the emission peaks with the λ_{max} at around 340 nm independent of the structure of divinyl or dially-silane compounds (Figure 8 (iii)). These wavelengths were shorter than those of the 3BPBz and 4B2P-based network polymers due to the short excitation wavelength. In the case of the 4B2F-based network polymers, the λ_{max} of the emission spectra widely ranged from 450 to 500 nm, and depended on molecular structure of the divinyl or dially silane compounds (Figure 8 (iv)). One possibility to explain the results would be difference of the emission wavelengths, as summarized in Table 4. We studied the effect of the excitation wavelength on the emission wavelength of the 4B2F-based network polymers with fixed exaction wavelengths of 380 and 410 nm. The results cleared that the excitation wavelength did not affect the emission wavelength of those network polymers. The difference of the emission wavelengths of the 4B2F network polymers should be derived from the molecular structure of the divinyl or dially silane compounds. Substituent in 9,9-spirobifluorene molecule is sensitive to the emission wavelengths, as reported in some 9,9-spirobifluorene molecules (for example Abdel-Awwad, Luan, Messow, Kusserow, Wiske, Siebert, Fuhrmann-Lieker, Salbeck, & Hillmer, 2015). The molecular structure of the divinyl or dially silane compounds in the network structure with 4B2F should strongly affect the emission wavelengths.

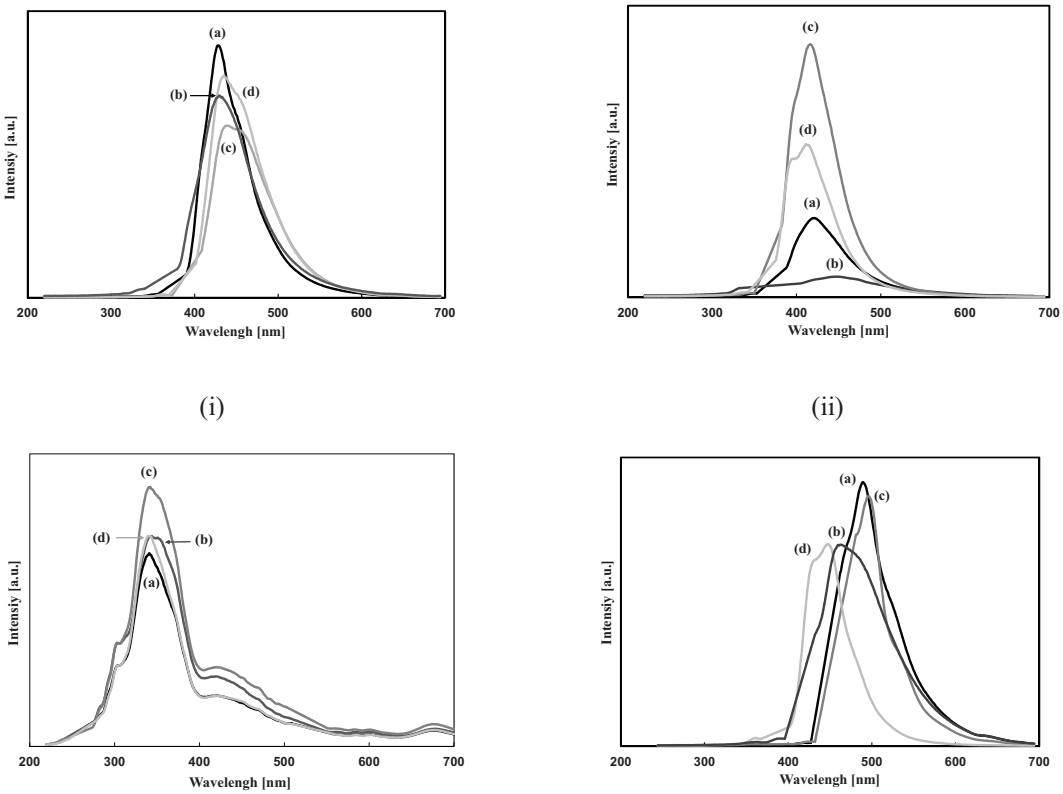

Figure 8. PL spectra of (i) 3BPBz-, (ii) 4B2P-, (iii) 4BPM-, and (iv) 4B2F- based network polymers with (a) VMS, (b) AMS, (c) VTMS, and (d) MVSB (solid state)

4. Conclusions

Mizoroki-Heck reaction of cyclic siloxane or cubic silsesquioxane compounds with vinyl groups, TVMCTS, PVOSS, as the joint molecules, and dibromo aryl compounds, as the linker molecules, gave the corresponding network polymers. The network polymers showed the emission derived from the σ-π conjugation. Molecular structure of the dibromo aryl compounds affected the emission wavelengths of the network polymers. Long conjugation structure with DBBP or BFl, and straight substituted structure with pDBB of the dibromo aryl compounds induced the long emission wavelengths. Copolymerization with mono-functional BB produced the $CHCl_3$ soluble fraction in the resulting network polymers. The SEM image of TVMCTS-BFl network polymer indicated formation of porous structure. The network polymers were also synthesized by the reaction of multifunctional aryl bromide, as the joint molecules, with divinyl or dially silane compounds, as the linker molecules. The emission wavelengths were depended on the molecular structure of the multifunctional aryl bromide. The emission wavelengths of 4B2F-based network polymers were sensitive to the structure of the divinyl or dially silane compounds, and widely ranged from 450 to 500 nm.

Mizoroki-Heck reaction of multi-functional siloxane compounds having vinyl groups with dibromo aryl compounds, or multifunctional aryl bromide with divinyl or dially silane compounds is one of the useful methods to synthesize the network polymers containing Si-vinylene units. The network polymers synthesized by the present methods would be widely usable due to their features: porosity, photophysical properties, thermal stability, and chemical resistance. Such experiments are under way, and the results will be reported elsewhere.

References

Abdel-Awwad, M., Luan, H., Messow, F., Kusserow, T., Wiske, A., Siebert, A., & Hillmer. H. (2015). Optical amplification and photodegradation in films of spiro-quaterphenyl and its derivatives. *Journal of Luminescence*, *159*, 47-54. https://doi.org/10.1016/j.jlumin.2014.10.065

Burroughes, J. H., Bradley, D. D. C., Brown, A. R., Marks, R. N., Mackay, M., Friend, R. H., & Holmes, A. B. (1990). Light-emitting diodes based on conjugated polymers. *Nature, 347*, 539-541. https://doi.org/10.1038/347539a0

Dawson, J. X., Laybourn, A., Clowes, R., Khimyak, Y. Z., Adams, D. J., & Cooper, A. I. (2009). Functionalized Conjugated Microporous Polymers. *Macromolecules, 42*, 8809-8816. https://doi.org/10.1021/ma901801s

Hu, R., Lam, J. W. Y., & Tang, B. Z. (2013). Recent Progress in the Development of New Acetylenic Polymers. *Macromol. Chem. Phys., 214*, 175-187. https://doi.org/10.1002/macp.201200389

Jiang, J. X., Su, F., Trewin, A., Wood, C. D., Campbell, N. L., Niu, H., & Cooper, A. I. (2007). Conjugated Microporous Poly(aryleneethynylene) Networks. *Angew. Chem.Int. Ed., 46*, 8574-8578. https://doi.org/10.1002/anie.200701595

Liu, J., Lam, J. W. Y., & Tang, B. Z. (2009). Acetylenic Polymers: Syntheses, Structures and Functions. *Chem. Rev., 109*, 5799-5867. https://doi.org/10.1021/cr900149d

Naga, N., & Saito, Y. (2016). Synthesis and Properties of Poly(ferrocenylsilane)s Containing Si-Vinylene Units in the Main Chain. *International Journal of Chemistry*, *8*, 86-93. https://doi.org/10.5539/ijc.v8n2p86

Naga, N., Iwashita, M., Nagino, H., Miyanaga, T., & Furukawa, H. (2015). Synthesis and optical properties of σ–π conjugated organic–inorganic hybrid gels. *Journal of Polymer Science: Part A: Polymer Chemistry*, *53*, 1360-1368. https://doi.org/10.1002/pola.27571

Naga, N., Ohkura, Y., Tagaya, N., & Tomoda, H. (2011). Synthesis and Chemosensing Behavior of Fluorene-Based Alternating Copolymers Containing Ether Side Chains and Si-Vinylene Units in the Main Chain. *Journal of Polymer Science: Part A: Polymer Chemistry*, *49*, 4935-4940. https://doi.org/10.1002/pola.24943

Naga, N., Tagaya, N., Noda, H., Imai, T., & Tomoda, H. (2008). Synthesis and Properties of Fluorene or Carbazole-Based Alternating Copolymers Containing Si and Vinylene Units in the Main Chain. *Journal of Polymer Science: Part A: Polymer Chemistry*, *46*, 4513-4521. https://doi.org/10.1002/pola.22788

Wang, F., Kaafarani, B. R., & Neckers, D. C. (2003). Synthesis of Silicon-Containing Unsaturated Polymers by Hydrosilylation Reactions. Phtophysical. *Macromolecules, 36*, 8225-8230. https://doi.org/10.1021/ma034618f

International Journal of Chemistry; Vol. 9, No. 3; 2017
ISSN 1916-9698 E-ISSN 1916-9701
Published by Canadian Center of Science and Education

New Spectrofluorimetric Method for Determining Cadaverine Following Derivation with Orthophthalaldehyde: Application in Fish Tissue

Moumouny Traoré[1], Khemesse Kital[1], Moussa Mbaye[1], Olivier Maurice Aly Mbaye[1], Cheikh Diop[1], Marina Koussemon Camara[2], Lamine Cissé[1], Mame Diabou Gaye Seye[1], Atanase Coly[1], Alphonse Tine[1]

[1]Laboratoire de Photochimie et d'Analyse (LPA) - Faculté des Sciences et Techniques, Université Cheikh Anta DIOP, Dakar, Sénégal. B.P. 5005 Dakar-Fann, Senegal

[2]Laboratoire de Biotechnologie et Microbiologie des Aliments-UFR des Sciences et Technologies des Aliments, Université Nangui Abrogoua, Cote d'Ivoire

Correspondence: Alphonse Tine, Laboratoire de Photochimie et d'Analyse (LPA) - Faculté des Sciences et Techniques, Université Cheikh Anta DIOP, Dakar, Sénégal. B.P. 5005 Dakar-Fann, Senegal. E-mail: alphtine@yahoo.fr

Received: March 23, 2017 Accepted: May 11, 2017 Online Published: May 14, 2017

doi:10.5539/ijc.v9n3p10 URL: https://doi.org/10.5539/ijc.v9n3p10

Abstract

A new spectrofluorimetric method was developed in this study for simple determination of cadaverine (CD) (1,5-diaminopentane) in flesh of mackerel fish. This method required homogenization of the flesh, solid phase extraction (SPE) with 0.4M HCl/methanol or water/methanol (25/75v/v), centrifugation and derivation with orthophthalaldehyde (OPA). Physico-chemical parameters that affected the sensitivity of the fluorescence signal of the cadaverine-dihydrochloride/orthophthalaldehyde complex (CD/OPA), were optimised; these included reaction time, temperature, solvent system, pH and reactants concentrations (OPA/CD). The study was conducted in acetate buffer (pH 3.5 and 7) and showed low limits of detection (LOD), 0.6 and 25.5 ng. mL^{-1} respectively. The limits of quantification (LOQ) obtained were 3.5 $ngmL^{-1}$ (pH 3.5) and 122 $ngmL^{-1}$ (pH 7). The sensitivity of the results allowed its satisfactory application for quantification of cadaverine in fish.

Keywords: spectrofluorimetric method, cadaverine, mackerel fish, extraction, derivation, orthophthalaldehyde

1. Introduction

Biogenic amine refers to a group of biomolecules with different chemical structures and a common amine group which have a biological origin. Those molecules are synthetized by micro-organism on human, animal and plants tissus (Ladero, Calles-Enríquez, Fernández, & Alvarez, 2010). This synthesis is done through the amino acid decarboxylation metabolic way. The mechanism of the reaction includes the elimination of the α –carboxyl group from the amino acid. The amino acid decarboxylase needs pyridoxal-5-phosphate or pyruvoyl coenzymes to catalyze the reaction (Kamath, Vaaler, & Snell, 1991). The product of this decarboxylation is an amine also called biogenic amine. However, only few classes of microorganisms are able to produce this biogenic amine according to their ability to synthetize specific carboxylase. This reaction has been said to optimally occur at pH ranging between 4.0 and 5.5 (Dapkevicius, Nout, Rombouts, Houben, & Wymenga, 2000). In addition, specificity of the biogenic amines produced is correlated to the strains (ten Brink, Damink, Joosten, & Huis in 't Veld, 1990). For example, *enterobacteria* are mainly producers of putrescine and cadaverine while *enterococcis* produce mostly Tyramine (ten Brink, Damink, Joosten, & Huis in 't Veld, 1990., Suzzi, & Gardini, 2003). These microorganisms are a part of the food flora or can be introduced by contamination before or during foodstuffs handling. Several factors like pH, conservation, and temperature can influence the decarboxylation of amino acids (Santos, 1996) . This is why most food that contains a high level of protein may have a large quantity of biogenic amines. So food substances that are prepared by the process of fermentation or exposed to microbial contamination during aging or conservation are likely to contain a large quantity of biogenic amines. As a result of this fact, the first stages of fermentation are crucial in the formation of biogenic amines (ten Brink, Damink, Joosten, & Huis in 't Veld, 1990., Latorre-Moratalla, Bover-Cid, & Vidal-Carou, 2010).

Biogenic amines are known as sources of nitrogen and precursors for the synthesis of hormones, alkaloids, nucleic acids and proteins (Bouchereau, Guénot, & Larher, 2000., Jansen, van Dusseldorf, Botterma, & Dubois, 2003). They can equally influence metabolic processes in an organism such as the regulation of body temperature, synapse transmission, allergic reaction, cellular division and proliferation of malignant cells, control of blood pressure, arterial pressure and cell growth (Bouchereau, Guénot, & Larher, 2000, Halász, & Baráth, 2002, Jansen, van Dusseldorf, Botterma, &

Dubois, 2003, Bashan, Holguin, & Bashan, 2004., Önal, 2007). This is why the amount of biogenic amines in fish products has been reported in many studies (Heidi, & Collin, 2005, Tine, & Douabale, 2008, Simat, & Dalgaard, 2011, Randy, & Wen-Hsin, 2012). In fact, the level of free amino acids present in fish increases progressively as a function of the degree of fish freshness, temperature and time of conservation because of the proteolysis of endogens and exogenous enzymes (Makarios-Laham, & Lee, 1993., Carelli, Centonze, Palermo, Quinto, & Rotunno, 2007). By the way, in non-fermented foods, the presence of biogenic amines is indicative of undesirable microbial activity (Shakila, Vasundhara, & Kumudavally, 2001., Anli, & Bayram, 2009). As a result of their special odors cadaverine and putrescine can be used as indicators of food quality, particularly fish (Chytiri, Paleologos, Savvaidis, & Kontominas, 2004., Ehsani, & Jasour, 2012). In fact, we can observe an increasing levels of putrescine and cadaverine after the fish is dead, in the flesh of badly conserved fish, while the rate of spermine and spermidine goes down (Ruiz-Capillas, & Fménez-Colmenero, 2004). Some biogenic amines are used as indicators of cancer in an organism due to the high amounts of cadaverine in blood and urine (prostate, diabetes, arthritis and fibrose), (Khuhawar, Memon, & Bhanger, 2000, Awan, Fleet, & Thomas, 2008).

Cadaverine ($NH_2(CH_2)_5NH_2$) known by the names 1,5-diaminopentane or pentamethylenediamine is a diamine (figure 1). It was isolated with putrescine in 1887 by Brieger (Brieger, 1887) as part of the *Vibrio cholerae* culture.

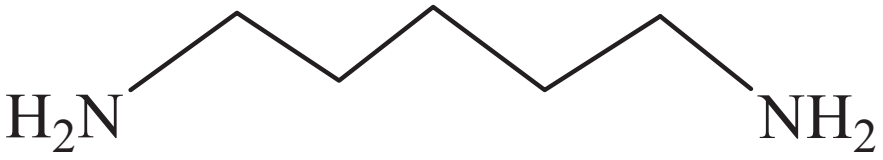

Figure 1. Structure of cadaverine

The stench of cadaverine comes from the hydrolysis of certain proteins during the putrefaction of dead bodies; hence his name (Antoine et al, 2004). It is mostly produced in foods by decarboxylation of lysine. This amine indicates the evaluation of the degree of microbial alteration of a very large number of fish as free lysine. It is present in many species of fish. The absence of cadaverine in a sample is therefore a reflection of the good quality of the fish (Li, Bao, Luo, Shen, & Shi, 2012). In food, the major concern of consumers is the ability of cadaverine to potentiate the toxicity of other amines, specifically histamine (Lehane, & Olley, 1999, Al Bulushi, Poole, Deeth, & Dykes, 2009, EFSA, 2011). In addition, cadaverine can react with nitrite when heated to form the n-nitrosopiperidine, which is a carcinogenic nitrosamine (Al Bulushi, Poole, Deeth, & Dykes, 2009); which constitutes an additional toxicological risk.

So it is important to monitor the amount of biogenic amines in foods particularly in fish products. The improvement of the sanitary quality of seafood has become a major preoccupation of governments and all stakeholders in this field.

Due to the increasing need for quality and hygiene of fish products, most countries had strengthened their regulation. This can explained why many analysis methods have been developed for the detection and quantification of biogenic animes in fish and fish products. These methods include, thin layer chromatography (Shalaby, 1995); high pressure liquid chromatography (Li et al., 2013., Önal, Tekkeli, & Önal, 2013., de Figueiredo et al., 2015., Ibarra et al.,2015., Lee, Yoo, & Shin, 2015), gas chromatography (Khuhawar, Memon, & Bhanger, 2000), (Almeida, Fernandes, & Cunha, 2012) and capillary zone electrophoresis (Arce et al., 1997). The revision of these chromatographic methods by Önal (Önal, Tekkeli, & Önal, 2013) shows that they often require sophisticated equipment with trained staff. Thus, the greater parts of these apparatus are not readily available in developing country, for routine work. Therefore a new simple, easier, sensitive and available method is needed. In this regard this work aimed at developing a new spectrofluorimetric method to determine cadaverine levels in fish products.

2. Experimental

2.1 Chemicals and Solvents

All reagents used were of analytical grade. Cadaverine dihydrochloride (CD, 99%, m/m), orthophthalaldehyde (OPA, 97%, m/m), methanol (MeOH), sodium hydroxide (NaOH, 98%, m/m) and hydrochloric acid (HCl, 37%, m/m) were bought at Sigma-Aldrich (Taufkirchen, Germany). Trichloroacetic acid (TCA, 99%, m/m), sodium acetate (CH_3COONa) and glacial acetic acid (CH_3COOH) were purchased from Carlo Erba (France). Distilled water was used for regent preparation.

2.2 Equipment

For measurements, a spectrofluorimeter Perkin Elmer LS-55 model connected to a microcomputer and driven by the FL WinLab software was used. A parallelepiped quartz cuvette (1 cm optical path, inside volume 3.5 ml) with five smooth

surfaces was used for the analytical measurements. For the centrifugation, it was used a Bioblock Scientific, Dusseldorf, Germany apparatus. Weighing was carried out using a precision balance of accuracy 0.1 mg from Sartorius AG Gottingen (Type BA 110S-OF1). The dilutions were performed using brand micropipettes Gilson, France. A pH meter from HANNA Instruments was also used.

2.3 Preparation of Solutions

Stock solutions of cadaverine ($1x10^{-2}$ M) and OPA ($1x10^{-2}$ M) were prepared; OPA required a little methanol to facilitate dissolution (1/10, v/v). Working solutions were obtained by diluting the stock solutions in the appropriate solvent.

All solutions were protected from light with aluminium foil and stored in a refrigerator at 278 K. The stock solutions of HCl (1M) and NaOH (1M) were prepared with distilled water and used with or without dilutions according to the case.

2.3.1 Samples Preparation

Extractions were performed as previously described by Richard (Richard, Pivarnik, Ellis, & Lee, 2011) and AOAC (AOAC, 1995). 25g of fish meat were removed (avoiding as much as possible the bones and the scales). The flesh removed was ground and 10g of the ground tissue are introduced into 65 mL of a mixture of HCl/methanol (25/75, v/v) or water/methanol (25/75,v/v). The resulting mixture was centrifuged at 1073 g for 5 minutes. The supernatant (containing extract) was collected and heated in a water bath at 333 K for 15 minutes to eliminate methanol. After cooling at room temperature, it was filtered using a whatman filter paper. The resulting extract was kept in the refrigerator at 278 K until analysis.

2.3.2 Method for Standard Addition

For a quantitative analysis of an analyte in a matrix, one often uses the method of standard addition to evaluate the degree of interference caused by the presence of other substances. It consists in adding a constant volume of unknown sample to standard solutions of increasing concentrations, the first addition being done in the blank. The linear increase allows the deduction of the concentration of the unknown sample by way of interpolation.

2.4 Data Analysis

All data were treated using MicroCal software, Origin Lab, Northampton and MA software version 8.5.

3. Results and Discussions

3.1 Preliminary Study

First, we proposed to study the stoichiometry of the reaction of complexation between cadaverine and orthophthalaldehyde (OPA) because cadaverine and OPA are non-fluorescent substances in water. To do this, concentrations of cadaverine ranging from 2×10^{-5} M to 2×10^{-4} M were added to a fixed concentration of OPA ($4x10^{-4}$ M) and fluorescence signal was measured for each concentration of cadaverine. The concentrations of OPA and cadaverine corresponding to the maximum fluorescence intensity allowed to determine the stoichiometry of the complex. Indeed, the fluorescence intensity of the complex OPA/CD is maximal when the reaction mixture contains an OPA concentration double that of cadaverine. We can pretend that each OPA molecule reacts with a group of amine where the stoichiometry is 2:1 in water.

The excitation and emission spectra (Figure 2) were recorded after complexation of both substances. The shape of spectra structure is the same in all solvents studied (two peaks of excitation and one peak of emission). In water, the excitation spectrum has two peaks localized at 234nm and 281nm respectively, while the emission spectrum was located at 313 nm (Figure 2).

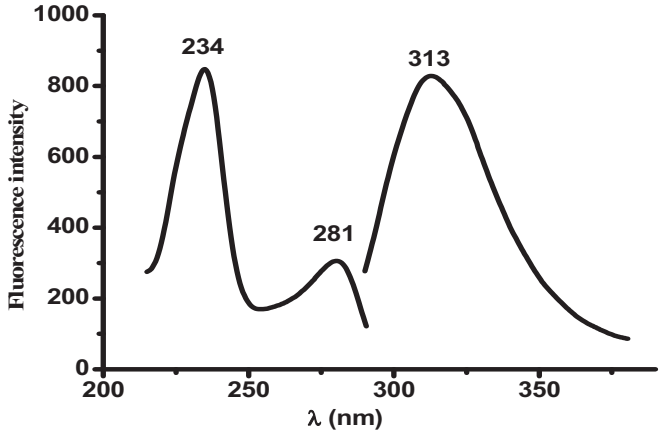

Figure 2. Fluorescence excitation and emission spectra of OPA/CD complex $2x10^{-4}$ M in water at 298K

3.2 Optimization of Analytical Parameters

3.2.1 Effect of pH in an Aqueous Medium

Studies reveal that the fluorescence signal of organic compounds is very sensitive in pH changes of the medium (Coly, & Aaron, 2009). The protonation or deprotonation of functional groups modifies profoundly many fluorophores in their excitation and emission spectra (Coly, & Aaron, 2009). This is why we planned to study the effect of pH on the fluorescence of OPA/CD complex. Figure 3 shows that the fluorescence intensity increases gradually between the values 1 and 3.5, while it slowly decreases between the values 3.5 and 9. The spectra of the complex OPA/CD formed in an acid medium have the same form as those obtained in basic medium. The curve shows a maximum at pH 3.5. From pH values higher than 9, the fluorescence intensity drops sharply as the pH increases. This indicates that in the basic medium, the complex OPA/CD is hardly detectable by fluorescence method. This significant decrease in fluorescence intensity is probably due to the dissociation of the complex. This observation leads us to the selection of the acid medium for the next stage of the study.

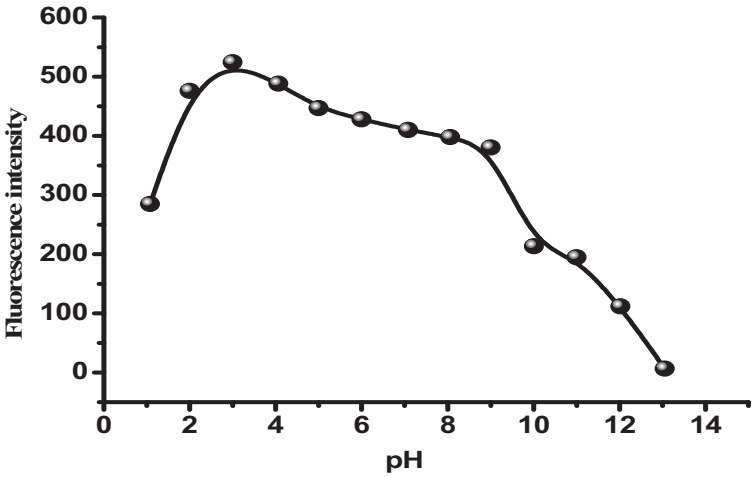

Figure 3. pH effect on the fluorescence intensity of OPA/CD complex $2x10^{-4}$ M in water at 298 K (λ_{ex} = 234 nm ; λ_{em} = 313 nm)

3.2.2 Kinetics of the OPA/CD Complex Formation

In order to improve the chosen fluorescence method, the stability of the complex formed was studied. We studied the complex for 5 minutes in water at optimal pH (3.5). After mixing the two reagents, the kinetic study started by monitoring the fluorescence signal over time. We noticed that the resulting complex was relatively stable in water (Figure 4).

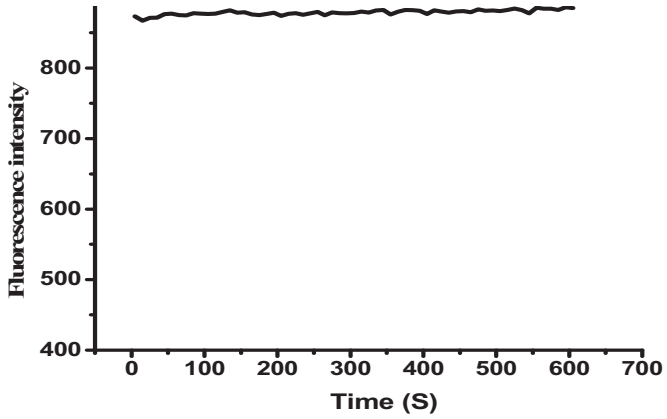

Figure 4. Evolution of the fluorescence intensity of OPA/CD complex $2x10^{-4}$ M in water at 298 K

3.2.3 Effect of Temperature on the OPA/CD Complex

Previous studies indicated that temperature has a remarkable effect on the kinetics of the complex OPA /histamine. So, it was deemed necessary to study the effect of heat on the fluorescence intensity of the complex OPA/CD. It was observed that, there was a decrease in the fluorescence intensity of the complex in correlation with the increase in temperature, (Figure 5). This increase in temperature causes the dissociation of the complex, which causes a reduction of the fluorescence intensity. This observation is in agreement with that reported in the literature (Khonté et al., 2015) . This process is reversible, because by cooling the solution, we observed an increase in fluorescence intensity due to the reconstitution of the complex. However, above a certain temperature (303K), it was observed that the decrease in the fluorescence signal was relatively slow.

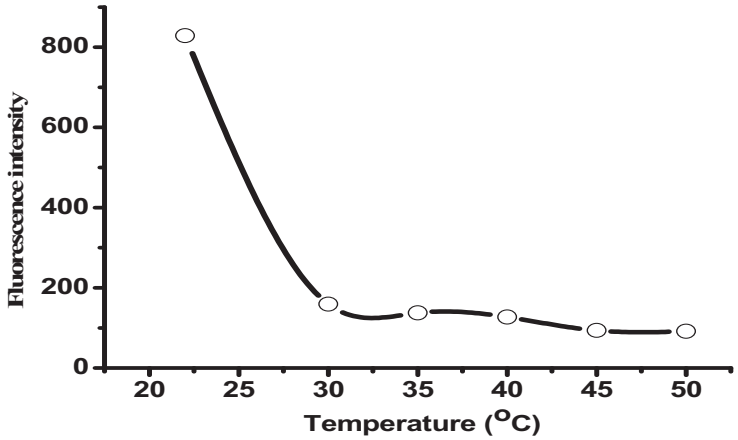

Figure 5. Effect of temperature on fluorescence intensity of OPA/CD complex ($2x10^{-4}$ M) in aqueous media

3.2.4 Effect of Binary Buffered Media (Water/MeOH) at pH 3.5 and 7

To predict the influence of methanol levels in water/MeOH mixture given the optimum analytical conditions of cadaverine, we varied the proportions of MeOH in different water/MeOH mixtures (Figure 6). We recorded the fluorescence spectrum of each buffer water/MeOH mixture at pH 3.5 and 7. In buffer solution pH 3.5, the fluorescence signal is highest for the water/MeOH mixture (95:5, v/v), while at neutral pH, methanol progressively inhibits the fluorescence signal. The progressive decrease in the fluorescence intensity with the addition of large amounts of MeOH could be due to the phenomenon of salvation (Khonté et al., 2015) . In addition, the continuous addition of methanol in the reaction medium increases the dissociation of OPA/CD complex where there is a decrease in the observed fluorescence intensity. After extraction of the cadaverine from the sample with the binary mixture water/MeOH, to avoid (the) inhibition of the signal, it would be wise to heat in order to drive off the traces of methanol.

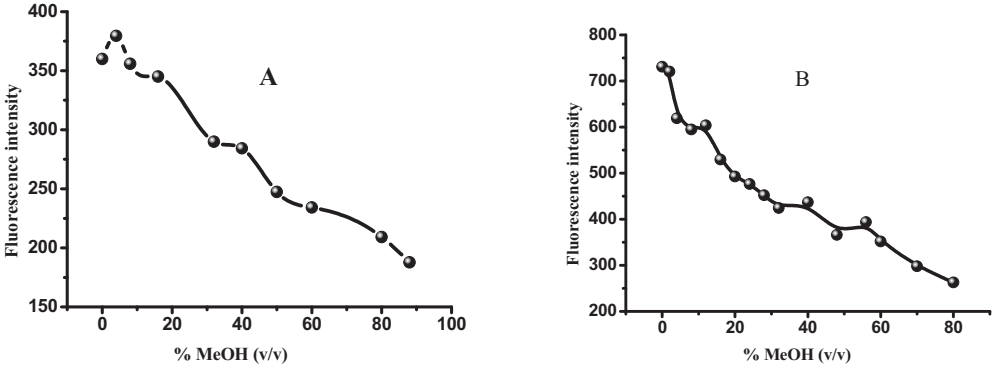

Figure 6. Variation effect of MeOH on the fluorescence signal of OPA/CD complex ($2x10^{-4}$ M) at 298 K, pH= 7 (A) and pH 3.5 (B). (λ_{ex} = 234 nm ; λ_{em} = 313 nm)

3.3 Analytical Performance

To evaluate the analytical effectiveness of our proposed method, we established a calibration curve of cadaverine in water at pH 3.5; and pH 7; comparing the two experimental results. We chosed this medium (pH 7 and 3.5) because it showed a very large intensity of emission of the complex (OPA/CD). We obtained a linear correlation between the fluorescence intensity and the concentration of the CD (Table 1) with a correlation coefficient ranging from 0.996 to 0.997, this indicated the precision of our measurements. Using the calibration curves, we determined some analytical parameters (Table 1).Ten measurements were used to achieve the results of the Table 1. The study of analytical performance of the method led to the detection limits (LOD) of 0.6; 25.5 $ngmL^{-1}$ and quantification limits (LOQ) of 3.5; 122 $ngmL^{-1}$, respectively at pH 3.5 and pH 7. The values of the relative standard deviation (RSD) are relatively low, these are evidence of good precision and reproducibility of our measurements. Statistical data indicated that better results were obtained in acetate buffer pH 3.5. Indeed, the acetate buffer presented many advantages, both in terms of stability and sensitivity of the complex OPA/CD.

Table 1. Spectrofluorimetric analytical figures of merit for the determination of CD in buffer (pH = 3.5 and pH = 7)

Medium	LDR[a] ($ngmL^{-1}$)	LOD[b] ($ngmL^{-1}$)	LOQ[c] ($ngmL^{-1}$)	RSD[d] ($ngmL^{-1}$)	r^{2e}
Water (pH = 3,5)	4 – 697	0.6	3.5	2	0,997
Water (pH = 7)	82 – 15601	25.5	122	5.6	0,996

[a]Linear dynamic range, [b]Limit of detection, defined as the amount of analyte giving a signal-to-noise ratio of 3, [c]Limit of quantification, defined as the amount of analyte giving a signal-to-noise ratio of 10, [d]Mid-range relative standard deviation (n = 6 – 8), [e] Correlation coefficients.

3.4 Analytical Application

To verify the presence of cadaverine in our fish sample, extraction was performed according to Richard and the AOAC methods (AOAC, 1995, Richard, Pivarnik, Ellis, & Lee, 2011), as previously described. Figure 7 shows that the excitation and emission spectra of the complex and the extract are perfectly superimposable, confirming the presence of cadaverine in the mackerel sample. The solvent 0.4M HCl/methanol (25/75, v/v) gave a greater fluorescence intensity of the complex OPA/CD. This results showed that this solvent was better and more selective for cadaverine extraction in fish samples. Indeed, some researchers reported that the solvent of extraction 0.4M HCl/methanol (25/75, v/v) allows for more recovery of cadaverine and putrescine in the flesh of fish. This, regardless of the fat content, the handling conditions and the size of the fish sample (Richard, Pivarnik, Ellis, & Lee, 2011).

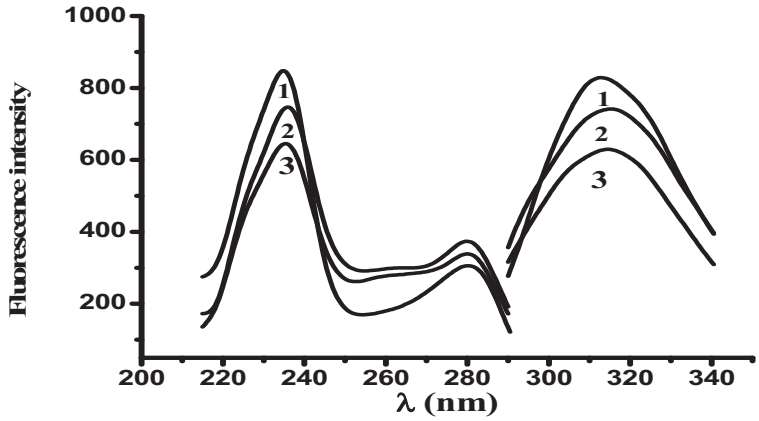

Figure 7. Fluorescence excitation and emission of OPA/CAD complex: Standard solution (1); after extraction in MeOH/HCl mixture (2) and MeOH/water mixture (5:95, v/v) (3)

Furthermore, for a better quantitative analysis of cadaverine in the sample, we prepared an additional curve to evaluate the degree of interference of other substances present in the matrix (Diaw et al., 2014, Khonté et al., 2015),. The slopes of the calibration curves and standard addition are very close (Figure 8). This parallelism of the two curves indicated lower sensitivity to interfering substances and negligible matrix effect (Khonté et al., 2015).

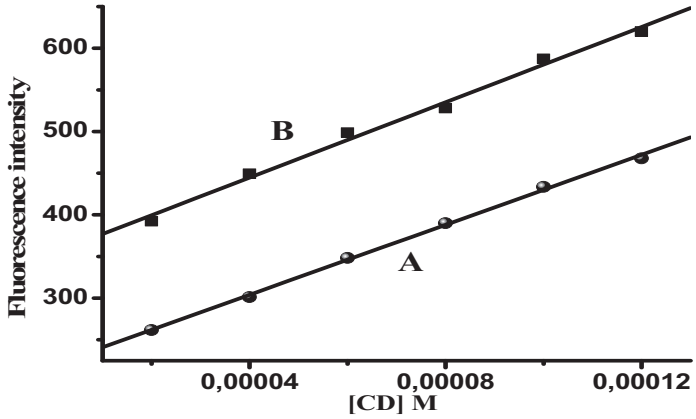

Figure 8. Straight calibration curve: Calibration curve of CD in water (A); Standard addition curve of the sample in fish (B) (λ_{ex} = 234 nm, λ_{em} = 313 nm).

This was confirmed by the satisfactory percentage recovery between 82.4 and 97.7 (Table 2).

The recovery rate (% R) was determined according to the following relationship below.

$$\%R = \frac{Ct}{Ca+C0} \times 100$$

This rate allowed to evaluate the interference effects for each concentration in the linearity domain of the calibration curve. Thus, to the extent of its applicability, in agreement with the validation of analytical methods, this rate must be between 80 and 120%.

Ct: concentration of CAD found, Ca: concentration added; C0: Blank concentration (13.5ng.mL^{-1}).

The average percentage recovery was very good (93%) which was not far from 100%. The relative standard deviation was low (5.19%) attesting to the good precision of our measurements (Table 2). These values were consistent with international standards for the validation of the analytical method (Khonté et al., 2015). Researchers have obtained a recovery percentage of 97% for mackerel (Richard, Pivarnik, Ellis, & Lee, 2011).

Table 2. Evaluation of recovery values in mackerel by solid-phase extraction procedure (SPE)

Added (Ca) ($ng.mL^{-1}$)	Found (Ct) ($ng.mL^{-1}$)	Recovery (%R)	Mean Recovery (%)
0	13.5	-	
3.5	14.0	82.4	
7.0	19.1	93.2	
10.5	23.5	980	93,0 ± 5.19
14.0	25.4	92.4	
17.5	30.3	97.7	
21.0	32.6	94.5	

4. Conclusion

In this work, a simple, sensitive, accurate and inexpensive method for the determination of cadaverine in fish sample (mackerel) was developed. We demonstrated the usefulness of the spectrofluorometric method of analysis with the optimization of different parameters which could affect the fluorescence intensity of the complex OPA/CAD in water. The analytical performances confirmed the good sensitivity and precision of our method. We also showed the applicability of the method for the determination of cadaverine in fish samples in the range of ng/mL with good recovery percentage values and low interference effects. Therefore, our method can be proposed for routine analysis. We intend to apply this method to other biological matrices other than fish.

Acknowledgments

This work was financed partly by a scholarship UE-ACP (PIMASO).

References

Al Bulushi, I., Poole, S., Deeth, H. C., & Dykes, G. A. (2009). *A Review Critical Reviews in Food Science and Nutrition, 49*(4), 369–377.

Almeida, C., Fernandes, J. O., & Cunha, S. C. (2012). *Food Control, 25*, 380-388. https://doi.org/10.1016/j.foodcont.2011.10.052

Anli, R. E., & Bayram, M. (2009). *Food Rev. Int., 25*, 86–102. https://doi.org/10.1080/87559120802458552

Antoine, F. R., Wei, C. I., Otwell, W. S., Sims, C. A., Littell, R. C., Hogle, A. D., & Marshall, M. R. (2004). *J. Food Prot., 67*, 2255–2262. https://doi.org/10.4315/0362-028X-67.10.2255

AOAC (1995). Official Methods of Analysis of the AOAC international, 16th ed. Method 970.12. Association of Official Analytical Chemists International. Washington, DC, USA

Arce, L., Rios, A., & Valcarcel, M. (1997). *Chromatographia, 46*(3), 4170–4176.

Awan, M. A., Fleet, I., & Thomas, C. L. P. (2008). *Food Chemistry, 111*(2), 462-468. https://doi.org/10.1016/j.foodchem.2008.03.068

Bashan, Y., Holguin, G., & Bashan, L. E. (2004). *Can. J. Microbiol, 50*, 521–577. https://doi.org/10.1139/w04-035

Bouchereau, A., Guénot, P., & Larher, F. (2000). *J. Chromatogr. B. Biomed Sci. Appl., 747*(1-2), 49-67. https://doi.org/10.1016/S0378-4347(00)00286-3

Brieger, L. (1887). Translated by, Roussy, J. Winter. Publisher, Doin, *1887*. Original from, the University of California. Digitized, Jan 24, 2007. Length, 235 pages.

Carelli, D., Centonze, D., Palermo, C., Quinto, M., & Rotunno, T. (2007). *Biosensors and Bioelectronics, 23*(5), 640–647. https://doi.org/10.1016/j.bios.2007.07.008

Chytiri, S., Paleologos, E., Savvaidis, I., & Kontominas, M. G. (2004). *J. Food Prot., 67*, 960-965. https://doi.org/10.4315/0362-028X-67.5.960

Coly, A., & Aaron, J. J. (2009). *Maced. J. Chem. Chem. Eng., 27*, 33-40.

Dapkevicius, M. L. N. E., Nout, M. J. R., Rombouts, F. M., Houben, J. H., & Wymenga, W. (2000). *International Journal of Food Microbiology, 57*, 107-114. https://doi.org/10.1016/S0168-1605(00)00238-5

De Figueiredo, T. C., de Assis, D. C., Menezes, L. D., da Silva, G. R., Lanza, I. P., Heneine, L. G., & Cançado Sde, V. (2015). *Talanta, 142*(1), 240-245. https://doi.org/10.1016/j.talanta.2015.04.056

Diaw, P. A., Mbaye, O. M. A., Gaye-Seye, M. D., Aaron, J. J., Coly, A., Tine, A., ... Oturan, N. (2014). *J. Fluoresc, 24*, 1319-1330. https://doi.org/10.1007/s10895-014-1418-8

EFSA Panel on Biological Hazards (BIOHAZ). (2011). Scientific Opinion on risk based control of biogenic amine formation in fermented foods. *EFSA Journal*, *9*(10), 2393. https://doi.org/10.2903/j.efsa.2011.2393

Ehsani, A., & Jasour, M. S. (2012). *Journal of Food Science and Technology, 77*(12), 664–668.

Halász, A., & Baráth, Á. (2002). *Food Science and technology, COST 917 Biogenically active amines in food volume VII.*6, 131-41EC Publication, Luxembourg

Heidi, S. M., & Collin, R. A. (2005). *Journal of Chromatography A.*, *1094*(1-2), 60-69. https://doi.org/10.1016/j.chroma.2005.07.088

Ibarra, A. A., Wrobel, K., Escobosa, A. R., Elguera, J. C., Garay-Sevilla, M. E., & Wrobel, K. (2015). *J. Chromatogr B Analyt. Technol. Biomed Life Sci., 1002*, 176-184. https://doi.org/10.1016/j.jchromb.2015.08.036

Jansen, S. C., van Dusseldorf, M., Botterma, K. C., & Dubois, A. E. (2003). *A review. Ann. Allergy Asthma Immunol, 91*(3), 233-240. https://doi.org/10.1016/S1081-1206(10)63523-5

Kamath, A. V., Vaaler, B. L., & Snell, E. E. (1991). *The Journal of Biological Chemistry, 266*, 9432-9437.

Khonté, A., Thiaré, D. D., Diop, C., Cissé, L., Delattre, F., Coly, A., ... Gaye-Seye, M. D. (2015). *International Journal of Chemistry, 7*, 85-98. https://doi.org/10.5539/ijc.v7n2p85

Khuhawar, M. Y., Memon, A. A., & Bhanger, M. I. (2000). *Jour. Chem. Soc. Pak., 22*(2), 267-270.

Ladero, V., Calles-Enríquez, M., Fernández, M., & Alvarez, M. A. (2010). *Current Nutrition Food Sci,.6*, 145-156. https://doi.org/10.2174/157340110791233256

Latorre-Moratalla, M. L., Bover-Cid, S., & Vidal-Carou, M.C. (2010). *Meat Science, 85*(3), 537-541. https://doi.org/10.1016/j.meatsci.2010.03.002

Lee, S., Yoo, M., & Shin, D. (2015). *LWT-Food Science and Technology, 62*(1), 350-356. https://doi.org/10.1016/j.lwt.2015.01.016

Lehane, L., & Olley, J. (1999). *National Office of Animal and Plant Health,AustraliaCanberra*.

Li, K., Bao, Y., Luo, Y., Shen, H., & Shi, C. (2012). *Journal of Food Protection, 75*, 2228–2233. https://doi.org/10.4315/0362-028X.JFP-12-143

Li, Y., Yang, H., Liao, H., Fan, H., Liang, C., Deng, L., & Jin, S. (2013). *Journal of Chromatography B, Analytical Technologies in the Biomedical and Life Sciences, 929*, 33-39. https://doi.org/10.1016/j.jchromb.2013.03.025

Makarios-Laham, I. K., & Lee, T. C. (1993). *Journal of Food Science and Technology, 58*(2), 310–313.

Önal, A. (2007) *Food Chem., 103*, 1475–1486. https://doi.org/10.1016/j.foodchem.2006.08.028

Önal, A., Tekkeli, S. E., & Önal, C. (2013). *Food Chemistry, 138*(1), 509-515. https://doi.org/10.1016/j.foodchem.2012.10.056

Randy, L. S, & Wen-Hsin, W. (2012). *Journal of Food Composition and Analysis, 27*(2), 169-173. https://doi.org/10.1016/j.jfca.2012.06.002

Richard, N. L., Pivarnik, L. F., Ellis, P. C., & Lee, M. C. (2011). *Journal of AOAC International, 94*(4).

Ruiz-Capillas, C., & Fménez-Colmenero, J. (2004). *Critical Rev. Food Sci. Nutrition, 44*(7-8), 489-499. https://doi.org/10.1080/10408690490489341

Santos, M. H. (1996). *International Journal of Food Microbiology, 29*(2-3), 213-231. https://doi.org/10.1016/0168-1605(95)00032-1

Shakila, R. J., Vasundhara, T. S., & Kumudavally, K. V. (2001). *Food Chemistry, 75*(2), 255–259. https://doi.org/10.1016/S0308-8146(01)00173-X

Shalaby, A. R. (1995). *Food Chemistry, 52*(4), 367-372. https://doi.org/10.1016/0308-8146(95)93283-W

Simat, V., & Dalgaard, P. (2011). *Food Science and Technology, 44*, 399–406.

Suzzi, G., & Gardini, F. (2003). *Int. J. Food Microbiol, 88*(1), 41-54. https://doi.org/10.1016/S0168-1605(03)00080-1

ten Brink, B. T., Damink, C., Joosten, H. M. L. J., & Huis in 't Veld, J. H. J. (1990). *International Journal of Food Microbiology, 11*, 73-84. https://doi.org/10.1016/0168-1605(90)90040-C

Tine, A., & Douabale, E. S. (2008). *Reviews in Fluorescence,* 195–218.

International Journal of Chemistry; Vol. 9, No. 3; 2017
ISSN 1916-9698 E-ISSN 1916-9701
Published by Canadian Center of Science and Education

Optimized HPLC -UV Method for Separation, Detection and Quantification of Endocrine Disrupting Estrogens in Low Quality Water

Sijaona Cassian Msigala[1], Faith P Mabiki[1], Bjarne Styrishave[2], Robinson H Mdegela[3]

[1]Department of Physical Sciences, Faculty of Science, Sokoine University of Agriculture, P.O. Box 3038, Morogoro, Tanzania

[2]Department of Pharmacy, Faculty of Health and Medical Sciences, University of Copenhagen, 2100 Copenhagen OE, Denmark

[3]Department of Veterinary Medicine and Public Health, College of Veterinary and Medical Science, Sokoine University of Agriculture, P.O. Box 3021, Morogoro, Tanzania

Correspondence: Sijaona Cassian Msigala, Department of Physical Sciences, Faculty of Science, Sokoine University of Agriculture, P.O. Box 3038, Morogoro, Tanzania. E-mail: sijaona99@suanet.ac.tz

Received: April 5, 2017 Accepted: May 3, 2017 Online Published: May 14, 2017

doi:10.5539/ijc.v9n3p19 URL: https://doi.org/10.5539/ijc.v9n3p19

Abstract

Endocrine disrupting estrogens are emerging contaminants in aquatic ecosystems and environment in general. There are no guidelines for routine monitoring of these chemicals, despite the existing evidences of their adverse health effect to living organisms at low concentrations. This study aimed at developing and validating an optimized HPLC-UV method for detection and quantification of estradiol and ethinylestradiol. Isocratic elution was used for separation and detection of ethinylestradiol and estradiol. The mobile phase was applied with A; water B; acetonitrile (50:50) at flow rate of 0.7mL/min and injection volume 10mL. The precision and accuracy of the method were within the acceptable range. Relative standard deviation of peak area for E2 ranged from 1.373 to 3.668%, and for EE2 ranged from 0.829 to 6.495 %. The percentage recovery for E2 ranged from 82.3 to 99.84 %, and for EE2 ranged from 84.6 to 103.52 %. Linearity of the method was realized at range of 2.5 to 50 ng/mL and 100 to 1000 ng/mL for both E2 and EE2. The linear regression coefficients were 0.9979 and 0.9973 for E2 whereas for EE2 were 0.9983 and 0.9976. Limit of detection were found to be 0.05 ng/mL and 0.08 ng/mL for E2 and EE2 respectively. The obtained limits of quantification were 0.18 and 0.28 ng/mL for E2 and EE2 respectively. In untreated sewage the concentrations of E2 and EE2 were 0.28 ng/ml and 0.18 ng/ml respectively. But in subsequent wastewater stabilization ponds the concentrations were below detection limit. Therefore, the optimized HPLC-UV method is suitable for detection and quantification of endocrine disrupting estrogens when a level of pollution is at least 0.15 ng/ml. At low extent of pollution would require use of the method in conjunction with ELISA technique.

Keywords: chromatographic method, development, validated, estrogens, analytical chemistry

1. Introduction

Estrogen hormones are emerging pollutants in water. There are natural and synthetic estrogens; the natural estrogens are not only produced by humans but also by other vertebrates as well as invertebrates particularly insects (Das, 2016). The synthetic estrogens are used for birth control, hormone replacement therapies, cancer drugs and other pharmaceuticals (Shook, 2011; Sood *et al*., 2014). Usually the estrogens are excreted from humans and animals mainly as conjugates of glucuronide or sulphate and a lesser amount as parent compounds in urine and faeces. The conjugates undergo deconjugation to form free estrogens by enzymatic action of bacteria or fungi (Kumar *et al*., 2012). The occurrence of these hormones in the environment is receiving considerable attention due to the fact that most of these compounds are endocrine disrupting chemicals (Christiansen et al., 2002; Cui et al., 2006; Zheng et al., 2013; Huang et al., 2016). Several studies have demonstrated that wastewater treatment systems are the main source of estrogens to aquatic environment (Ingrand et al., 2003; Swart & Pool, 2007; Yoon et al., 2012; Belhaj et al., 2014). A reliable analytical technique is necessary for separation, detection and quantification of the estrogens in the environmental matrix such as water.

In literature there are several analytical methods for detection and quantification of estrogens from environmental samples but the methods differ in sensitivity (Ingerslev & Halling-Sørensen, 2003). Among those methods are HPLC, LC-MS, GC-MS, and immunochemical methods. The LCMS/MS and GCMS/MS are advanced methods and most

sensitive for detection of estrogens (Faqehi et al., 2016), however their use is limited by high costs. Immunochemical methods are also sensitive but have poor selectivity compared to LCMS/MS and a single assay can only detect a single steroid (Ingerslev & Halling-Sørensen 2003; Faqehi et al., 2016).

High performance liquid chromatography is a dominant analytical technique due to its applicability to diverse analytes (Dong, 2013). The technique can quantify compounds in complex samples and can be coupled with different detectors such as UV, diode array detection (DAD), evaporation light scattering detection (ELSD), refractive index detector, fluorescence detection and mass spectrometry (MS) (Dong, 2013). The successful use of HPLC requires the right combination of variety of operating conditions such as the column length and diameter, column temperature, type of the column packing, type of the mobile phase, mobile phase flow rate, and injection volume (Settle, 2004). This implies that HPLC method development and validation are inevitable for successful application of HPLC.

Method validation ensures consistent capabilities of an analytical method by defining and confirming the analytical requirement for a specific application (Magnusson & Ornemark, 2014). The ISO/IEC 17025:2005 (2005), a guideline for competence testing and laboratory calibration, stresses that method validation is necessary requirement in analytical chemistry since it demonstrate that the method is fit for the purpose. Method validation include assessment of the parameters such as precision, linearity, accuracy, limit of detection, limit of quantification, specificity, range and robustness of the method (ICH, 2005; Magnusson & Ornemark, 2014).

Schellinger & Carr (2006) found that gradient elution gave a shorter overall analysis with similar resolution compared to isocratic elution. On the other hand isocratic elution remain preferable when the sample contains less than ten weakly retained components (Schellinger & Carr, 2006).

This study aimed at establishing an optimized HPLC-UV method for separation, detection and quantification of estrogens hormones from low quality water particularly from wastewater stabilization ponds. The study focused on the two most potent estrogens namely ethinylestradiol and estradiol.

2. Materials and Methods

2.1 Chemicals and Materials

Ethinylestradiol (EE2) and β-estradiol (E2) standards hormones were supplied by Santa Cruz Biotechnology, Texas, USA. HPLC grade methanol, acetonitrile and water (99.9% purity) were supplied by Sigma Aldrich, Germany, n-heptane (99%), acetone (99.8%) and hydrochloric acid (37%, 1.18M) were supplied by Carlo Erba Reagenti. Solid phase extraction C-18 cartridges (130 mg, 3 mL) by Varian and Chromabond, silica gel (3 ml/500 mg) from Macherey-Nagel in Germany were employed.

2.2 Preparation of Standard Solution and Calibration Standard Solution

Stock solution of 10,000 ng/ml in methanol was prepared for a mixture standard E2 and EE2, and then stored at 4^{o}C in a fridge. Serial dilution of the stock solution was carried out to obtain 1000, 750, 500, 250, 100, 50, 25, 10, 5, 2.5, 1, 0.5, and 0.1 ng/ml for the mixture of the two hormones. In addition, separate standard solutions of the two hormones were prepared at 100 ng/mL for determination of their retention time.

2.3 Spiking Standard Estrogens in Distilled Water

For determination of recoveries the estrogens standard solutions were spiked in 1 L of distilled water to make different concentrations for both E2 and EE2. The established concentrations were 1000, 750, 500, 250, 100, 50, 25, 10, 5, 2.5, 1, 0.5, and 0.1 ng/ml. Each solution was filtered twice using by GFCs, a procedure which could be applied for removal of debris from low quality water.

2.4 HPLC Conditions

Analyses were performed at Ecotoxocology and Natural Product Laboratory at the College of Veterinary and Medical Sciences, Sokoine University of Agriculture. The HPLC (Shimadzu 20AD) fitted with an auto sampler and a SPA-UV detector at 230 nm was used for analysis. A reversed phase phenomenex C-18 column (150 x 4.6 mm and particle size of 5µm) was used for separation with the oven temperature set at 35 ^{o}C. The sample injection volume was 10 µL and flow rate 0.7 mL/min. The mobile phases employed were A; water B; acetonitrile (50:50).

2.5 Method Development

With the theoretical background, detection, separation and quantification of the two estrogens hormones were achieved by manipulating factors such as wavelength, mobile phase composition, flow rate and temperature. Several trials were carried out to separate, identify and quantify a mixture of estradiol, and ethinylestradiol.

When the mobile phases were; A- water and B- methanol, the hormones were detected at shorter retention time but the resolution was very poor even after several trials upon changing column temperature, flow rate and gradient. When the

mobile phases were; A-water and B-acetonitrile, retention time increased with good resolution. It was observed that even when gradient elution was employed good resolution was obtained when equal proportions of the mobile phases run for longer time. Isocratic elution was found to be suitable over the gradient elution. Retention time for estradiol was 11.89 ± 0.03 minutes and for ethinylestradiol 14.79 ± 0.04 minutes while the method running time was 16 minutes.

2.6 Method Validation

Validation of method developed was carried out in accordance to ISO/IEC 17025:2005. Validation characteristics of the method such as precision, accuracy, linearity, specificity, limit of detection, quantification, and robustness were assessed. The procedures employed in assessment of validation characteristics were as stipulated in ICH (2005) document.

2.7 Collection of Water Samples from Wastewater Stabilization Ponds

Wastewater samples were collected from Mafisa WSPs owned by Morogoro Municipality in Tanzania. An untreated sewage wastewater samples were drawn using cleaned 2.5 liters glass bottle during dry season. Other samples were drawn from outlet of anaerobic and facultative ponds using cleaned 2.5 liters glass bottle. After sampling, the pH of the sampled wastewater samples was adjusted to about 3 by adding concentrated hydrochloric acid (1.18M) so as to fix the estrogens (Havens et al., 2010; Hansen et al., 2011). Then, the samples were carried in cool box packed with ice packs to the Ecotoxicology and Natural Products Research Laboratory in the College of Veterinary and Medical Sciences at Sokoine University of Agriculture. In the laboratory pretreatment and solid phase extraction of estrogens were conducted within 12 hours after sample collection.

2.8 Extraction of Estrogens from Water Samples

Extraction of estrogens from water samples was carried out according to the protocol described by (Hansen et al., 2011) with some modifications customized to our laboratory settings. Each water sample (1.5 litres) was first filtered twice using GFC filters papers to ensure removal of debris. The C-18 cartridges were conditioned with 2×3 mL heptane, 3 mL acetone, and lastly with 3 ml of distilled water. Thereafter, solid phase extraction (SPE) was performed with C-18 cartridges (Bond Elut 500 mg, 3cc reservoir, Varian Agilent Technologies, USA) facilitated by vacuum manifold. After extraction the cartridges were dried in air using vacuum manifold for about half an hour. Then, elution of the analyte was achieved by using 10 ml of heptane and acetone (65:35). Thereafter, the elute was air dried at 30 ^{o}C, followed by reconstitution using 5 ml methanol. The samples were stored at –20 ^{o}C, until analysis by HPLC-UV method.

2.9 Statistical Analysis

Microsoft excel 2007 with data analysis pack was used for statistical analysis. Descriptive statistics such as standard deviation, mean and relative standard deviation were computed.

3. Results and Discussion

3.1 Method Linearity and Range

Figure 1 and 2 demonstrate that the peak areas were directly proportional to the concentrations of E2 and EE2 respectively. Both at higher concentrations (from 100 to 1000 ng/mL) and lower concentrations (from 2.5 to 50 ng/mL) showed good linearity with linear regression coefficient being 0.9979 and 0.9973 for E2 and 0.9983 and 0.9976 for EE2. Those values of regression coefficient denote excellent linear relationship between the peak area and the concentrations of the two hormones (ICH 2005; Magnusson & Ornemark, 2014).

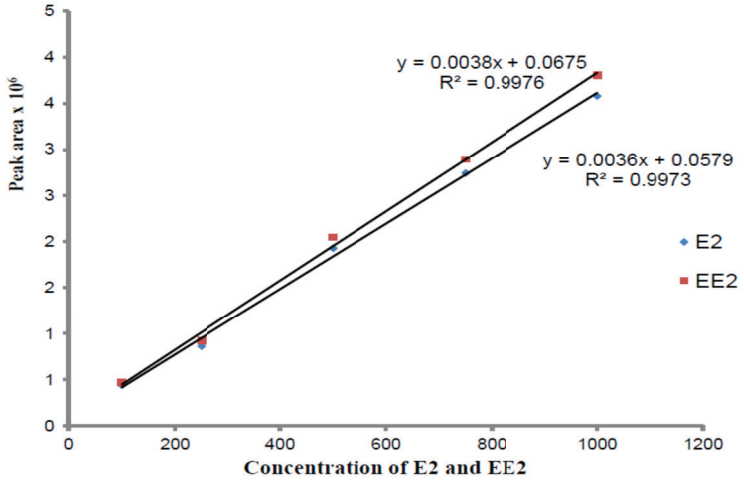

Figure 1. Calibration curves for standard E2 and EE2 at high concentrations

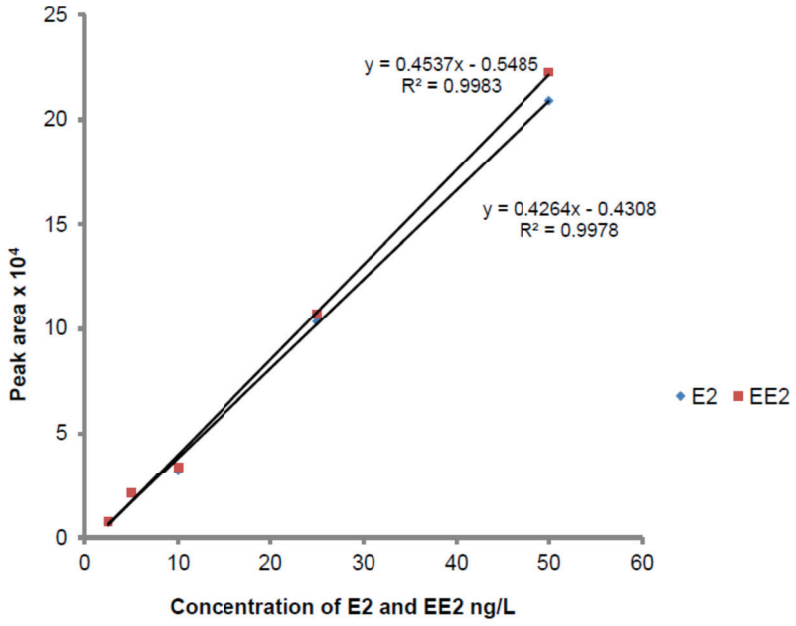

Figure 2. Calibration curves for standard E2 and EE2 at low concentrations

3.2 Method Precision

Table 1 and 2 display the method precision for detection and quantification of E2 and EE2 respectively. The relative standard deviations of peak area for both E2 and EE2 were below 2% except for the lowest concentrations which was above 2 % but below 10 %. Adebayo & Oduwaye (2015) stated that an effective HPLC method should have a relative standard deviation less than 10 % for 6 replicates. Figure 4 revealed good precision of this method when the standard solution at 100 and 250 ng/mL were analysed.

Table 1. Method Precision for detection and Quantification of E2 at Higher and Lower concentrations

	(250 ng/mL		100 ng/mL		5 ng/mL		0.1 ng/mL	
S/N	RT	PA	RT	PA	RT	PA	RT	PA
1	11.766	930,530	11.860	435,838	11.858	18,530	12.006	2,052
2	11.824	897,259	11.890	425,610	11.858	18,439	11.931	2,100
3	11.874	919,495	11.903	421,479	11.912	18,763	11.958	2,156
4	11.868	941,589	11.916	422,706	11.937	17,842	11.937	1,951
5	11.844	891,922	11.908	422,062	11.921	17,762	11.961	2,145
6	11.784	905,404	11.887	419,813	11.893	18,471	11.927	2,044
Mean	11.827	911033.17	11.894	424584.667	11.897	18,301.167	11.953	2,074.67
Std	0.044	15164.476	0.020	5830.884	0.033	403.740	0.029	76.094
RS (%)	0.374	1.665	0.167	1.373	0.278	2.206	0.246	3.668

Abbreviations: RT = retention time; PA= peak area; Std = standard deviation; RS = relative standard deviation

Table 2. Method Precision for detection and Quantification of EE2 at Higher and Lower concentrations

	250 ng/mL		100 ng/mL		5 ng/mL		0.1 ng/mL	
S/N	RT	PA	RT	PA	RT	PA	RT	PA
1	14.645	921,207	14.749	410,521	14.749	18,317	14.86	2,114
2	14.728	923,056	14.787	405,267	14.73	18,634	14.854	1,887
3	14.768	901,806	14.8	403,473	14.816	18,694	14.788	1,836
4	14.748	890,451	14.802	401,949	14.841	19,273	14.856	1,874
5	14.731	895,886	14.809	401,227	14.811	18,661	14.835	2,115
6	14.768	924,008	14.774	405,635	14.802	18,672	14.803	1,890
Mean	14.731	909,402.333	14.787	404678.667	14.792	18,708.5	14.8386	1952.667
Std	0.046	15,090.705	0.022	3352.977	0.043	310.252	0.030	126.822
RS(%)	0.310	1.659	0.151	0.829	0.289	1.658	0.201	6.495

Abbreviations: RT = retention time; PA= peak area; Std = standard deviation; RS = relative standard deviation

3.3 Method Accuracy

Table 3 and 4 display the method performance accuracy for quantification of E2 and EE2 respectively. For E2 recoveries ranged from 82.3 to 99.84 %, on the other hand recoveries for EE2 ranged from 84.6 to 103.52 %. The recoveries are within the recommended range for analytical method between 80 % to 120 % (Shabir, 2004).

Table 3. Method performance accuracy for quantification of E2 at Low & High Concentrations

Spiked Concentration ng/mL	Sample No.	Calculated amount ng/mL	% Recovery	Spiked Concentration ng/mL	Sample No.	Calculated amount ng/mL	% Recovery
50	1	49.61	99.22	1000	1	954.93	95.49
	2	49.90	99.80		2	987.00	98.70
25	1	24.74	98.96	750	1	748.83	99.84
	2	24.88	99.52		2	747.50	99.67
10	1	8.23	82.30	500	1	468.39	93.68
	2	8.97	89.70		2	480.00	96.00
5	1	4.93	98.60	250	1	239.62	95.85
	2	5.12	102.40		2	245.98	98.39
2.5	1	2.44	97.60	100	1	98.69	98.69
	2	2.49	99.60		2	99.45	99.45

Table 4. Method performance accuracy for quantification of EE2 at Low & High Concentrations

Spiked Concentration ng/mL	Sample No.	Calculated amount ng/mL	% Recovery	Spiked Concentration ng/mL	Sample No.	Calculated amount ng/mL	% Recovery
50	1	49.700	99.4	1000	1	960.46	96.046
	2	49.48	98.96		2	1002.00	100.2
25	1	24.057	96.23	750	1	753	100.4
	2	24.155	96.62		2	749.45	99.93
10	1	8.460	84.6	500	1	468.35	93.67
	2	8.860	88.6		2	485.10	97.02
5	1	5.176	103.52	250	1	240.13	96.05
	2	5.088	101.76		2	247.85	99.14
2.5	1	2.460	98.4	100	1	97.50	97.50
	2	2.478	99.12		2	99.98	99.98

3.4 Method Sensitivity

Limit of detection (LOD) and limit of quantification (LOQ) were determined using equation 1 and 2 respectively. The LOD and LOQ for E2 were found to be 0.054 ng/mL and 0.18 ng/mL respectively. The corresponding LOD and LOQ for EE2 were 0.084 ng/mL and 0.28 ng/mL respectively. This result implies that the method is suitable for moderate and higher extent of pollution of low quality water by estrogens. At low extent of pollution the method could be used in conjunction with ELISA technique. Huang & Sedlak (2001) used HPLC-UV method in conjunction with ELISA

technique for analysis of estrogens in wastewater; the results were comparable to those obtained by applying GC-MS/MS. In addition, the developed HPLC-UV method can be used in low extent pollution when standard addition technique would be applied in quantifying the estrogens. The sensitivity of this method could be comparable to HPLC-DAD method which allowed precise and accurate determination of estrogens in various environmental water at concentrations ranging between 0.025 ng/ml to 0.3 ng/ml, (Lopez and Alpha, 2001). On the other hand, this method demonstrated higher sensitivity than HPLC-UV method developed by Fonseca et al., 2013, in such method the detection limits were 0.25 ng/ml and 0.11 ng/ml for E2 and EE2 respectively. Contrary, LC-MS/MS method is more sensitive than this method, for instance Naldi *et al*., 2016 developed LC-MS/MS method for determination of free and conjugated steroids that had LOD ranging between 0.003 ng/mL to 0.015 ng/mL for surface water and 0.014 ng/mL to 0.076 ng/mL in wastewater samples.

$$LOD = \frac{standard\ deviation}{slope} * 3 \quad \ldots\ldots\ldots \ equation\ 1$$

$$LOQ = \frac{Standard\ deviation}{Slope} * 10 \ldots equation\ 2$$

3.5 Robustness

The method gave comparable results at different wavelengths such as at 215, 230, and 254 nm. Likewise when column temperature was varied from 35^{o} C to 40^{o} C no significant change of result occurred. Contrary to that retention time changed with change in flow rate for instance at flow rate 1 mL/min retention time was found to be 8.3 and 10.4 minutes for E2 and EE2 respectively. Whereas at a flow rate of 0.7 mL/min the retention time is 11.89 ± 0.03 and 14.79 ± 0.04 minutes for E2 and EE2 respectively.

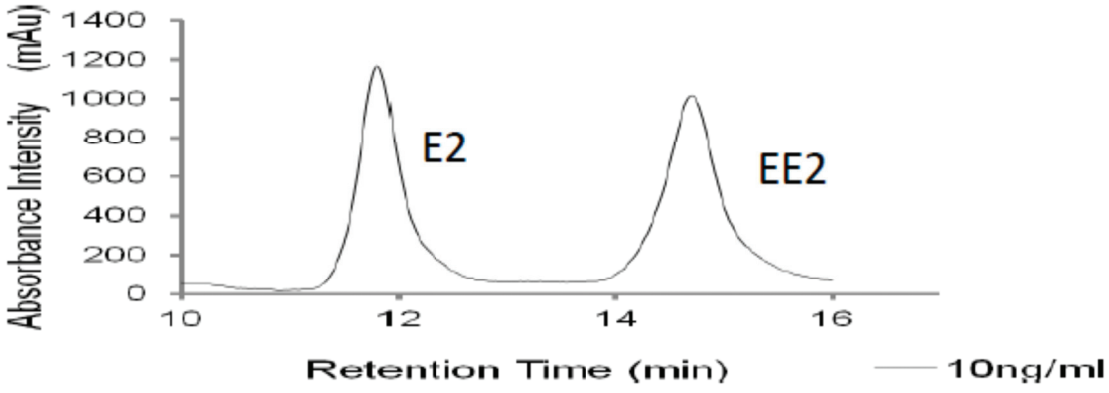

Figure 3. Chromatogram of E2 and EE2 when concentration was 10 ng/mL

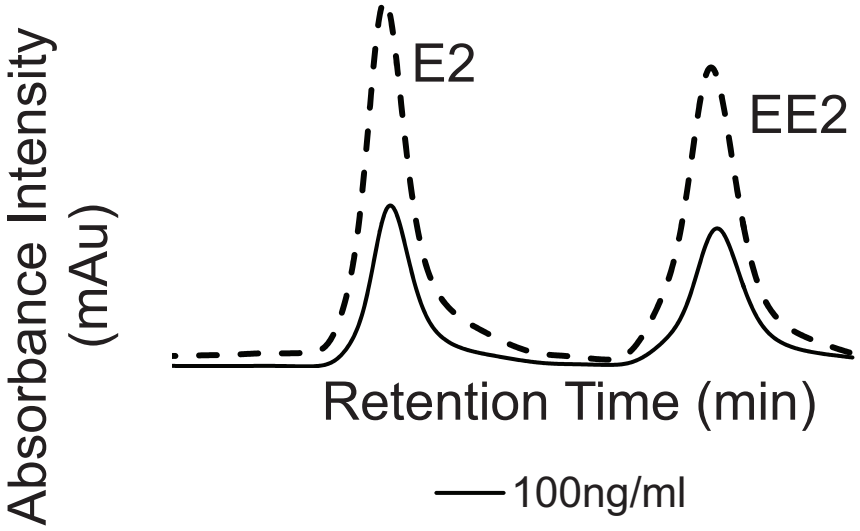

Figure 4. Chromatogram of E2 and EE2 at 100 ng/ml and 250 ng/ml

3.6 Levels of Estrogens in LQW Detected through HPLC-UV Method

Estrogens were detected in untreated sewage sample but in the outlets of anaerobic and facultative ponds were below the detection limit. The concentration of E2 and EE2 in untreated sewage was found to be 0.28 ng/ml and 0.18 ng/ml respectively. When ELISA competitive technique was employed revealed that the levels of estrogens in the study area were below the detection limit of the developed method. The concentrations EE2 and E2 at Mafisa WSPs ranged from 0.036 ng/ml to 0.0015 ng/ml and 0.086 ng/ml to 0.0044 ng/ml respectively (Msigala et al., 2017).

4. Conclusion

This paper presents a fast, linear, precise, accurate and robust HPLC-UV method for separation, detection and quantification of estrogens hormones from low quality water. The method can give precise and accurate results for moderate and higher extent of pollution of low quality water by estrogens. At lower extent of pollution (below 0.15 ng/mL) can be used in conjunction with ELISA technique, in such combination the HPLC method offset the shortcomings of the results which could be obtained through ELISA alone, on the other hand utilize the high sensitivity of ELISA technique.

Conflict of Interest

The authors declare that there are no conflicts of interest which could potentially influence this work

Acknowledgments

This research was funded by Danish Ministry of Foreign Affairs through Safe Water for Food (SaWaFo) project. We are very grateful to DANIDA for funding this research.

References

Adebayo, J. K., & Oduwaye, O. (2015). Effective HPLC method development. *Journal of Health, Medicine and Nursing*, *12*, 123–133. Retrieved from www.iiste.org

Belhaj, D., Turki, N., Kallel, M., Ayadi, H., & Zhou, J. L. (2014). Comparison of estrogen compounds removal efficiency in sample and alternating anoxic / aerobic activated sludge process. *Journal of Environmental Science, Toxicology And Food Technology*, *8*(1), 100–108.

Christiansen, L. B., Winther-Nielsen, M., & Helweg, C. (2002). Feminisation of fish. The effect of estrogenic compounds and their fate in sewage treatment plants and nature. Environmental Project no. 729 Scientific Report, 1-184.

Cui, C. W., Ji, S. L., & Ren, H. Y. (2006). Determination of steroid estrogens in wastewater treatment plant of a controceptives producing factory. *Environmental Monitoring and Assessment*, *121*(1–3), 407–417.

https://doi.org/10.1007/s10661-005-9139-8

Das, S. (2016). Vertebrate hormones in insects : the role of estrogen in silkworm – a review. *Turkish Journal of Zoology, 40*, 297–302. https://doi.org/10.3906/zoo-1507-37

Dong, W. M. (2013). The Essence of Modern HPLC: Advantages Limitation, Fundamentals and Opportunities. *LCGC North America*, *31*(6), 472–479.

Faqehi, A. M. M., Cobice, D. F., Naredo-gonzalez, G., Mak, T. C. S., Walker, B. R., Homer, N. Z. M., & Andrew, R. (2016). Derivatisation of estrogens enhances specificity and sensitivity of analysis of human plasma by liquid chromatography tandem mass spectrometry Analysis of estrogens Chromatographic separation. *Talanta*, *879*(4–5), 1748–1756. https://doi.org/10.1016/j.jchromb.2011.04.020

Fonseca, A. P., Cardoso, M., & Esteves, V. (2013). Determination of Estrogens in Raw and Treated Wastewater by High-Performance Liquid Chromatography-Ultraviolet Detection, *Journal Environmental & Analytical Toxicology 4*(1), 1-5. https://doi.org/10.4172/2161-0525.1000203

Hansen, M., Jacobsen, N. W., Nielsen, F. K., Björklund, E., Styrishave, B., & Halling-Sørensen, B. (2011). Determination of steroid hormones in blood by GC-MS/MS. *Analytical and Bioanalytical Chemistry*, *400*(10), 3409–3417. https://doi.org/10.1007/s00216-011-5038-8

Havens, M. S., Hedman, J. C., Hemming, C. D. J., Mieritz, G. M., Shafer, M. M., & Schauer, J. (2010). Sability, preservation, and quantification of hormones and estrogenic and androgenic activities in surface water runoff. *Environmental Toxicology and Chemistry*, *29*(11), 2481–2490. https://doi.org/10.1002/etc.307

Huang, C. H., & Sedlak, L. D. (2001). Analysis of estrogenic hormones in Municipal wastewater effluent and surface water using Enzyme-Linked Immunosorbent Assay and Gas Chromatography/Tandem Mass Spectrometry. *Environmental Toxicology and Chemistry*, *20*(1), 133–139. https://doi.org/10.1002/etc.5620200114

Huang, G., Liu, Y., Chen, X., Liang, Y., & Liu, S. (2016). Feminization and masculinization of western mosquitofish (Gambusia affinis) observed in rivers impacted by municipal wastewaters. *Nature Publishing Group*, (October 2015), 1–11. http://doi.org/10.1038/srep20884

ICH. (2005). International Conference on Harmonisation of Technical Requirements for Registration of Pharmaceuticals for Human Use (pp. 1–13).

Ingerslev & Halling-Sorensen, (2003). Evaluation of Analytical Chemical Methods for Detection of Estrogens in the Environment. *Danish Environmental Protection Agency*, (44), 1–69.

Ingrand, V., Herry, G., Beausse, J., & De Roubin, M. R. (2003). Analysis of steroid hormones in effluents of wastewater treatment plants by liquid chromatoraphy-tandem mass spectrometry. *Journal of Chromatography A*, *1020*(1), 99–104. https://doi.org/10.1016/S0021-9673(03)00770-2

ISO/IEC 17025:2005, I. (2005). *International Standard: General requirements for the competence of testing and calibration laboratory* (2nd Editio). ISO 2005. Retrieved from www.iso.org

Kumar , V., Johnson, C.A., Nakada, N., Yamashita, N., Tanaka, H. (2012). De-conjugation behavior of conjugated estrogens in the raw sewage, activated sludge and river water. Journal *of Hazardous Materials, 22*, 49–54. https://doi.org/10.1016/j.jhazmat.2012.04.078

Lopez, M. J., & Alda, D. (2001). Determination of steroid sex hormones and related synthetic compounds considered as endocrine disrupters in water by fully automated on-line solid-phase extraction – liquid chromatography – diode array detection. *Science*, *911*, 203–210.

Magnusson, B., & Ornemark, U. (2014). Eurachem Guide: The Fitness for Purpose of Analytical Methods-A Laboratory Guide to Method Validation and Related Topics (2nd Editio). Eurachem Analytical Chemistry in Europe. Retrieved from www.eurachem.org

Msigala, S. C., Mabiki, F. P., Styrishave, B., & Mdegela, R. H. (2017). Performance of wastewater stabilization ponds in treatment of endocrine disrupting estrogens in. *International Journal of Public Health and Epidemiology*, *6*(1), 305–317.

Naldi, A. C., Fayad, P. B., Prévost, M., & Sauvé, S. (2016). Analysis of steroid hormones and their conjugated forms in water and urine by on-line solid-phase extraction coupled to liquid chromatography tandem mass spectrometry. *Chemistry Central Journal*, *10*(30). https://doi.org/10.1186/s13065-016-0174-z

Schellinger, A. P., & Carr, P. W. (2006). Isocratic and gradient elution chromatography : A comparison in terms of speed , retention reproducibility and quantitation, *1109*, 253–266. http://doi.org/10.1016/j.chroma.2006.01.047

Settle, F. A. (2004). *Handbook of Instrumental Techniques for Analytical Chemistry* (1st Editio). Singapore: Pearson Education Inc., 147-160.

Shabir, G. (2004). A practical approach to validation of HPLC methods under current good manufacturing practices. *Journal of Validation Technology*, 29–37.

Shook, L. L. (2011). An update on hormone replacement therapy: Health and medicine for women: A multidisciplinary, evidence-based review of mid-life health concerns. *Yale Journal of Biology and Medicine, 84*, 39–42.

Sood, R., Faubion, S. S., Kuhle, C. L., Thielen, J. M., & Shuster, L. T. (2014). Prescribing menopausal hormone therapy: An evidence-based approach. *International Journal of Women's Health*, *6*(1), 47–57. https://doi.org/10.2147/IJWH.S38342

Swart, N., & Pool, E. (2007). Rapid detection of selected steroid hormone from sewage effluents using ELISA in the Kuils river water catchment area, South Africa. *Journal of Immunoassay Immunochem*, *28*(4), 395–408. https://doi.org/10.1080/15321810701603799

Yoon, S. M., Kim, J. W., Lee, S. J., Narumiya, M., Nakada, N., Han, I. S., & Tanaka, H. (2012). Fate of Estrogens Wastewater Treatment Plants in Korea, *35*, 62–65.

Zheng, W., Zou, Y., Li, X., & Machesky, M. L. (2013). Fate of estrogen conjugate 17α-estradiol-3-sulfate in dairy wastewater: Comparison of aerobic and anaerobic degradation and metabolite formation. *J. Hazard. Mater.*, 258−259. https://doi.org/10.1016/j.jhazmat.2013.04.038

International Journal of Chemistry; Vol. 9, No. 3; 2017
ISSN 1916-9698 E-ISSN 1916-9701
Published by Canadian Center of Science and Education

The Outstanding Applications of Skeletal Numbers to Chemical Clusters

Enos Masheija Rwantale Kiremire

Correspondence: Enos Masheija Rwantale Kiremire, Department of Chemistry and Biochemistry, University of Namibia, Private Bag 13301, Windhoek, Namibia. E-mail: kiremire15@yahoo.com

Received: April 17, 2017 Accepted: May 11, 2017 Online Published: June 1, 2017

doi:10.5539/ijc.v9n3p28 URL: https://doi.org/10.5539/ijc.v9n3p28

Abstract

The evolution of the use of the 14/4n series method has resulted in the discovery of skeletal numbers. The skeletal numbers have rendered the testing of the 18-and 8-electron rules much easier and faster. In the same way, they have been very useful in simplifying the categorization of clusters, the prediction of shapes, and the matching of isolobal fragments. Furthermore, the skeletal numbers have made it possible to tentatively assign ligands to individual skeletal elements in such way that the 18- or 8-electron rule is obeyed. Thus, skeletal numbers can be utilized as a simple guide in analyzing and understanding clusters.

Keywords: clusters, 14n/4n series, 18/8-electron-rule, isolobal, fragment, skeletal, categorization

1. Introduction

The Wade-Mingos rules (PSEPT) have been exceedingly helpful in analyzing and categorizing clusters for several decades (Wade, 1971; Mingos, 1972; Rudolph, 1976; Welch, 2013). In an attempt to understand these rules and the pattern within clusters especially the osmium carbonyls, the 14n and 4n rules were revealed for transition and main group elements (Kiremire, 2014; Kiremire, 2015a). On further scrutiny of the series and clusters, the skeletal numbers of transition and main group elements were recently discovered (Kiremire, 2016a). These skeletal numbers have made the analysis and characterization of clusters much easier (Kiremire, 2016b). The aim of this paper is to point out some of the applications to chemical clusters that have so far been found by the use of skeletal numbers. It is hoped that our readers will enjoy the rapidity and smooth flow of using skeletal numbers to analyze and study clusters and that they can be applied to other more complex cluster systems.

2. Results and Discussion

The **4n(14n) series method** developed in this work, in which n represents the number of skeletal elements in a cluster, can be used to categorize a wide range of clusters, among others, transition metal carbonyls, boranes, heteroboranes, metalloboranes, Zintl ions, and gold clusters (Kiremire, 2015a, 2015b,2016c,2016d, 2017). Using the series formula, the number of valence electrons of a given cluster can easily be calculated directly without counting the valence electrons of individual skeletal atoms and ligands. Furthermore, from the series formula a corresponding required cluster formula can also be derived. For instance, for the series S = 4n+2 and n = 6, a corresponding borane cluster can be illustrated by the formula F_B = [BH](6)+2H = B_6H_8 = $B_6H_6^{2-}$, while a for Zintl ion cluster, F_Z = [Pb](6)+2— = Pb_6^{2-}. However, for a corresponding transition metal carbonyl, say that of rhodium, F_R = 14n+2 = [Rh(H)$(CO)_2$](6)+CO =$Rh_6(H)_6(CO)_{12}$+CO = $Rh_6(CO)_3(CO)_{12}$+CO = $Rh_6(CO)_{16}$. On the other hand, a corresponding osmium cluster will be given by F_O = [Os$(CO)_3$](6)+CO = $Os_6(CO)_{19}$ = $Os_6(CO)_{18}^{2-}$. For all these clusters, the building block for transition metals is based on a cluster fragment of [14] electrons, and for main group elements it is [4] electrons.

In order to easily follow the applications of skeletal numbers (K values) in the areas to be briefly discussed, it is proposed that the assigned skeletal numbers (skeletal linkage values) of elements be provided for ease of reference, despite the fact that they have already appeared in print (Kiremire, 2016a). The K values are given in Tables 1 and 2. They are derived from applying the series formula to valence electrons of the elements (Kiremire, 2016a)**.** The numbers are positive for main group and transition metal elements. Also, from the study of series, the ligands were also given K values. This assignment is also based on the knowledge of the same series. It was found that for every one electron donated by a ligand, K = -0.5. Selected K values for ligands are given in Table 3.

2.1 Calculation of the K Value of a Cluster or Fragment

This is simply done by adding up the respective skeletal numbers (obtained from Tables 1, 2 and 3) of the skeletal elements and the ligands in a given chemical formula. Examples:

i. C_2, K = 2[2] = 4

ii. BN, K = 1[2.5] +1[1.5] = 4

iii. CB^-, K = 1[2]+1[2.5]+1(-0.5) = 4

iv. CN^+, K = 1[2] +1[1.5]+1(0.5) = 4 ;

All the above chemical species are expected to possess quadruple bonds, demonstrated as sketch S-1A, where E is a skeletal atom.

S-1A. The quadruple bond between two skeletal elements

This method can be used to calculate K values in other fragments or molecules.

v. C_2H_2, K =2[2]+2(-0.5) = 3 (triple bond)

vi. C_2H_4, K = 2[2]+4(-0.5) = 2 (double bond)

vii. C_2H_6, K = 2[2]+6(-0.5) = 1 (single bond)

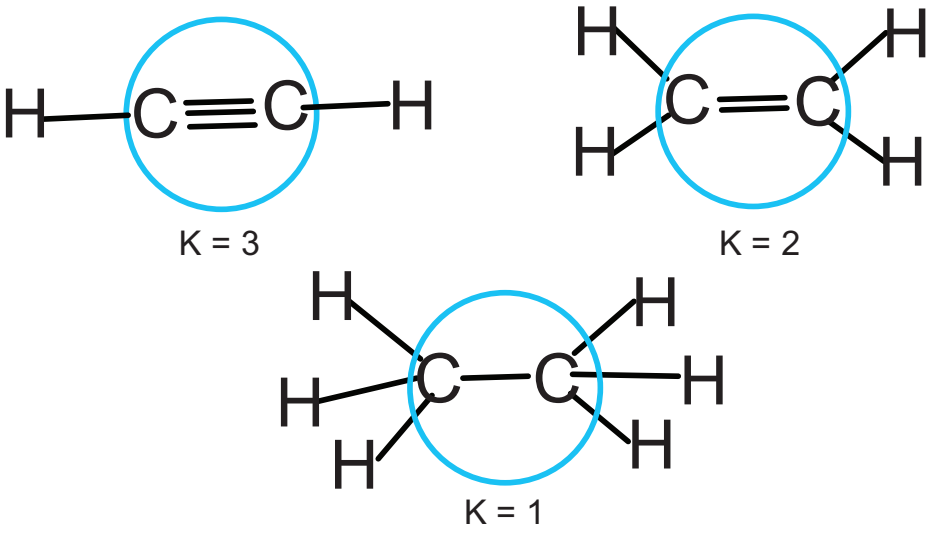

S-1B. The triple, double and single bonds derived from C_2.

The presence of a quadruple bond in C_2 sketched in S-1 A is still shrouded in controversy (de Sausa, et al, 2016). However, according to the 4n series method, the derived molecules from C_2 such as C_2H_2, C_2H_4 and C_2H_6 are well known and possess triple, double and single bonds respectively as sketched in S-1B. This implies that the existence of a quadruple bond in C_2 in support of the recent discovery (Shaik, S., et al, 2012) makes sense.

Table 1. Skeletal Numbers of Transition Metal Elements

Element	Representative Group	Valence electrons	Series, S = 14n+q(n = 1)	K value=2n-q/2
Sc, Y, La	3	3	14n-11	7.5
Ti, Zr, Hf	4	4	14n-10	7.0
V, Nb, Ta	5	5	14n-9	6.5
Cr, Mo, W	6	6	14n-8	6.0
Mn, Tc, Re	7	7	14n-7	5.5
Fe, Ru, Os	8	8	14n-6	5.0
Co, Rh, Ir	9	9	14n-5	4.5
Ni, Pd, Pt	10	10	14n-4	4.0
Cu, Ag, Au	11	11	14n-3	3.5
Zn, Cd, Hg	12	12	14n-2	3.0

Table 2. Skeletal Numbers of Main Group Elements

Element	Representative Group	Valence electrons	Series, S = 4n+q(n = 1)	K value =2n-q/2
Li, Na, K, Rb, Cs	1	1	4n-3	3.5
Be, Mg, Ca, Sr, Ba	2	2	4n-2	3.0
B, Al, Ga, In, Tl	3	3	4n-1	2.5
C, Si, Ge, Sn, Pb	4	4	4n+0	2.0
N,P, As, Sb, Bi	5	5	4n+1	1.5
O, S, Se, Te	6	6	4n+2	1.0
F, Cl, Br, I	7	7	4n+3	0.5
Ne, Ar, Kr, Xe	8	8	4n+4	0.0

The K value is defined as K = 2n- ½ q where q is a variable of the series S = 4n+ q for main group elements or 14n+q for transition elements.

Table 3. Skeletal Numbers of Selected Ligands

NUMBER OF ELECTRONS DONATED BY LIGAND	K VALUE	EXAMPLES(NEUTRAL)
1	-0.5	H, X = F, Cl, Br, I, R(alkyl, aryl)
2	-1	CO, PPh_3,N_2, C_2H_4, NH_3, H_2O
3	-1.5	η^3-C_3H_5, NO,CR
4	-2	η^4-C_4H_4
5	-2.5	η^5-C_5H_5
6	-3	η^6-C_6H_6

2.2 Effect on the K Value by Adding an Electron to or Removing an Electron from a Fragment

In order to shed more light on the effect of adding an electron to or removing an electron from a fragment, some brief explanation is necessary. In this regard, Scheme 1 has been developed as an illustration. According to the series method, a set of four [4] electrons forms the basis of the 4n series approach. In this regard, suitable candidates for the 4n series are carbon [C] and [BH] skeletal fragments. The development of the 4n series was discussed amply in previous work (Kiremire, 2015a)**.** For the purposes of this paper, a brief of outline of the method will be given below in order for the readers to appreciate the applications of the skeletal numbers explained in this paper. Let us consider a carbon skeletal element, [C]. The carbon atom has 4 valence electrons. This means it belongs to the series S = 4n+0 = V (valence electrons). For n =1, S = V = 4(1) +0 = 4. The K value is defined as K = 2n- ½ q where q is a variable of the series S = 4n+ q for main group elements or 14n+q for transition elements. For the carbon skeletal element with S = 4n+0, K = 2n- ½ q = 2(1) - ½ (0) = 2. This is the value indicated in Table 2 for C element and its family members (congeners). Let us consider adding a hydrogen atom [H] as a 'ligand' to the carbon[C] atom to produce a fragment [CH], or a negative charge to produce [C^{-}] fragment. In so doing, we will increase the valence electron environment of the carbon atom by 1 unit and hence V =S = 4n+1. The corresponding K value will be given by K = 2n- ½ q = 2(1) - ½ (1) = 1.5. In terms of valence electrons, the [CH] or [C^{-}] fragment will correspond to the [N] skeletal element or any of the family members of group V elements. In other words, these are isolobal fragments, that is, [CH]⇔[C^{-}]⇔[N]⇔[P]⇔[As]⇔[Sb]⇔[Bi]. Similarly, CH_2⇔C^{2-}⇔O ⇔S ⇔Se ⇔ Te with S = V = 4n+2 = 4(1) +2 = 6 and K =2n – ½ q = 2(1)- ½ (2) = 1 as given in Table 2. It is not difficult to see that with CH_3⇔C^{3-}⇔F⇔ Cl ⇔ Br ⇔I, S = 4n+3, and K = 0.5. Let us start from a C skeletal element as a 4n series reference and move to the left in the second period of the periodic table by removing one electron from the carbon [C] atom. Then we will get a [C^{+}] fragment. This fragment has 3 valence electrons and corresponds to a boron [B] skeletal element. Also the corresponding series will be given by S = 4n-1 = V = 4(1)-1 = 3. The K value for the series will be K = 2n- ½ q = 2(1) – ½ (-1) = 2.5. This corresponds to the K value of boron as shown in Table 2. Clearly going from [C] to [C^{+}], the K value increases from 2 to 2.5 by 0.5. Similarly, for [C] to become [C^{2+}] {[C]→[C^{2+}]}, K goes from 2.0 to 3.0, so the increase is 1.0. On the other hand for [C] → [C^{-}], K goes from 2.0to 1.5 and thus there is a decrease of 0.5. For [C]→[C^{2-}], the decrease will be 1.0. Some of the isolobal fragments corresponding to C^{+} are B, Al, Ga, In, and Tl, while those of C^{2+} are Be, Mg, Ca, Sr and Ba. The isolobal relationship is illustrated in Scheme 1.

S = 4n+q	4n-3	4n-2	4n-1	4n+0	4n+1	4n+2	4n+3	4n+4
				C	C^{-}	C^{2-}	C^{3-}	C^{4-}
	C^{3+}	C^{2+}	C^{+}	C	CH	CH_2	CH_3	CH_4
	Li	Be	B	C	N	O	F	Ne
V	1	2	3	4	5	6	7	8
K = 2n- ½ q	3.5	3.0	2.5	2.0	1.5	1.0	0.5	0.0

K = Skeletal number, V = valence electrons, S = Series

Scheme 1. Influence on K value of adding or removing an electron from a fragment

We can also illustrate the significance of the skeletal numbers by calculating the K values of a few clusters. Consider $B_6H_6^{2-}$ cluster: using the knowledge of skeletal numbers, its K value is given by K = 6[2.5] +6[-0.5]+2[-0.5] = 15-3-1

=11. Similarly, for $Rh_6(CO)_{16}$, K = 6[4.5]+16[-1] = 27-16 = 11. Also, for $Os_6(CO)_{18}^{2-}$, K = 6[5]+18[-1]+2[-0.5] = 30-18-1 = 11. This implies that the skeletal structures of $B_6H_6^{2-}$, $Rh_6(CO)_{16}$, and $Os_6(CO)_{18}^{2-}$ are similar or identical. In actual fact, all the above clusters have an octahedral geometry (O_h). Let us consider a few more clusters. First, Bi_5^{3+}, K = 5[1.5] +3[0.5] = 9; K(n) = 9(5). Since K = 2n- ½ q, then q = 2[2n-K], q = 2[2(5)-9] =2 and S = 4n+ q = 4n+2 (closo series). Similarly, for Sn_5^{2-}, K = 5[2]+2[-0.5] = 9; K(n) = 9(5), and S = 4n+2 (closo series). Another good example is $Os_5(CO)_{15}^{2-}$, for which K = 5[5]+15[-1]+2[-0.5] = 25-15-1 = 9; K(n) = 9(5) , and S = 4n+2 (closo series). This means that we expect the clusters, Bi_5^{3+}, Sn_5^{2-} and $Os_5(CO)_{15}^{2-}$ to have similar skeletal geometry. All these clusters have a trigonal bipyramid shape as predicted (King and Schleyer, 2004; Teo, et al, 1984). Furthermore, according to the series method in terms of ligand electron donation to skeletal elements, H• ≡ 1e ≡ -1 charge, for which the K value is -0.5. A :CO ligand may be regarded as equivalent to a -2 charge or ligand(:L), for which K = -1; For cyclopentadienyl ligand, C_5H_5 with five electron donation 5e, K= -2.5. One positive charge (+1) corresponding to the removal of one electron, results in the increase of K value by 0.5.This is similar to removing an electron from carbon in Scheme 1 above, so C (K = 2.0) becomes C^+(K = 2.5), an increase ΔK = 0.5. A charge of two units (+2) on a skeletal system corresponds to an increase in K value by + 1, similar to C losing two electrons to become C^{2+} in Scheme 1. Likewise, N (K = 1.5) + O (K = 1.0)→NO(K = 2.5); also NO(K =2.5) becomes NO^+(K =2.5+0.5 = 3.0) by losing an electron, and NO(K =2.5)+1e →NO^-(K = 2.5-0.5 = 2.0). These simple results correspond to what is derived from the molecular orbital energy level diagrams of diatomic species (Cotton and Wilkinson, 1980; Meissler, Fischer and Tarr, 2014). The skeletal elements have positive K values. As indicated in Tables 1 and 2, the K values depend upon the valence electrons of the skeletal elements. The standard is four valence electrons [4] for the main group elements and [14] for the transition metal atoms.

2.3 The Test for the 18- and 8- Electron Rules

The 18 and 8 electron rules have been used in chemistry since the beginning of the 20th century (Langmuir, 1921; Lewis, 1916)**.** As we are aware, the 18-electron rule involves adding up the number of the electrons in the d atomic orbitals of the central metal atom and those donated by the ligands. If the counting gives 18, then the complex obeys the 18-electron rule. In the same manner, in the case of main group elements, if the addition gives 8, then the molecule or ion obeys the 8-electron rule.

2.3.1 Using Skeletal Numbers to Test The 18-Electron Rule

The groups of transition elements were assigned positive skeletal numbers using series (Kiremire, 2016b). In addition, ligands were also assigned negative skeletal numbers based upon series. For a ligand that donates one electron such as a hydrogen atom, H•, K = -0.5, while a for a carbonyl ligand that donates 2 electrons, :CO is assigned K = -1. The skeletal element provides the skeletal linkages which get reduced when ligands are added to it. The ligand K value depends upon the number of electrons donated. The method of calculating the K value for a given cluster using skeletal numbers is straight- forward, and worked out examples are given in Table 4 below. Nonetheless, it is important to clarify the meaning of K values and how they are obtained, in the same table. Consider the cluster, $Fe(CO)_5$: the K value of iron (Fe) is 5 as shown in Table 4. If we carefully reflect, the K = 5 for Fe represents 8 valence electrons as obtained from the formula S = 14n-6 (where n = 1) and K = 2n- ½ q = 2(1)- ½ (-6) =5. So if we add a :CO ligand we get a fragment [Fe(CO)], and the series becomes, S =14n-6+2 = 14n-4 (n =1) = 14(1)-4 = 10 and K = 2n- ½ q = 2(1)- ½ (-4) = 4. This is the same as adding 8+2 = 10 for the [Fe(CO)] fragment. If we continue adding :CO ligands to the Fe skeletal atom to finally get a $Fe(CO)_5$ fragment, the series becomes S = 14n+4 (where n =1), so S = 18 which is the same as V (total valence electrons). However the K value will be given by K = 2n- ½ q = 2(1) - ½ (+4) = 0. Thus, the 18-electron rule is obeyed for a mono-skeletal cluster when K = **0.** This value is the same as calculated from the formula $Fe(CO)_5$, K = 1[5]+5[-1] = 0 using K = 5 for Fe and K = -1 for the :CO ligand. This means the K = 5 takes into account the valence electrons for the Fe skeletal element and K = -5 for the 5 CO ligands takes into account the 10 electrons donated by the 5 CO ligands. Therefore the overall K = 0 value embodies the 18 gross valence electrons of Fe and those donated by the 5 CO ligands. If one gets familiar with the use of skeletal numbers, it will be discerned that the calculations are much simpler and easier than the electron counting based upon using the valence electrons of the skeletal elements and ligands. Let us consider one more example: Does the complex, $Mo(CO)_4^{4-}$ obey the 18-electron rule? We then perform a simple calculation: K = 1[6] +4[-1]+4[-0.5] = 6-4-2 = 0. This means the complex obeys the 18-electron rule. More mono-skeletal cluster examples are given in Table 4.

Table 4. Skeletal Numbers of Selected Mono-skeletal Clusters

CLUSTER	CALCULATION OF K VALUE	n VALUE	K(n)	SERIES	VALENCE ELECTRONS
$Ni(CO)_4$	1[4]-4 = 0	1	0(1)	4n+4	14(1)+4 = 18
$Fe(CO)_5$	1[5]-5 =0	1	0(1)	4n+4	14(1)+4 = 18
$Cr(CO)_6$	1[6]-6 = 0	1	0(1)	4n+4	14(1)+4 = 18
η^6-$C_6H_6CrCO)_3$	1[6]-3-3 = 0	1	0(1)	4n+4	14(1)+4 = 18
$H_2Fe(CO)_4$	1[5]-1-4 = 0	1	0(1)	4n+4	14(1)+4 = 18
$CpFe(CO)_2^-$	1[5]-2.5-2-0.5 =0	1	0(1)	4n+4	14(1)+4 = 18
$Fe(CO)_4^{2-}$	1[5]-4-1 =0	1	0(1)	4n+4	14(1)+4 = 18
$Mo(CO)_4^{4-}$	1[6]-4-2 =0	1	0(1)	4n+4	14(1)+4 = 18
$HFe(CO)_4^-$	1[5]-4-0.5-0.5=0	1	0(1)	4n+4	14(1)+4 = 18
$HMn(CO)_5$	1[5.5]-0.5-5 =0	1	0(1)	4n+4	14(1)+4 = 18
$(\eta^6$-$C_6H_6)_2Cr$	1[6]-2(3)=0	1	0(1)	4n+4	14(1)+4 = 18
$(\eta^7$-$C_7H_7)Mo(CO)_3^+$	1[6]-3.5-3+0.5 =0	1	0(1)	4n+4	14(1)+4 = 18
$(\eta^4$-$C_4H_4)Fe(CO)_3$	1[5]-2-3=0	1	0(1)	4n+4	14(1)+4 = 18
$CpFe(CO)_2Cl$	1[5]-2.5-2-0.5 =0	1	0(1)	4n+4	14(1)+4 = 18
$Mn(CO)_5Cl$	1[5.5]-5-0.5 =0	1	0(1)	4n+4	14(1)+4 = 18
$(Cp)_2Fe$	1[5]-2(2.5)=0	1	0(1)	4n+4	14(1)+4 = 18
$Ti(CO)_6^{2-}$	1[7]-6-1=0	1	0(1)	4n+4	14(1)+4 = 18
$(Cp)_2Co^+$	1[4.5]-2(2.5)+0.5 = 0	1	0(1)	4n+4	14(1)+4 = 18
$(\eta^5$-$C_5H_5)(\eta^3$-$C_5H_5)Fe(CO)$	1[5]-2.5-1.5-1 =0	1	0(1)	4n+4	14(1)+4 = 18
$V(CO)_6^-$	1[6.5]-6-0.5 = 0	1	0(1)	4n+4	14(1)+4 = 18
$Ti(CO)_6^{2-}$	1[7]-6-1 =0	1	0(1)	4n+4	14(1)+4 = 18
$Mn(CO)_6^+$	1[5.5]-6+0.5 = 0	1	0(1)	4n+4	14(1)+4 = 18
$Fe(CO)_6^{2+}$	1[5]-6+1=0	1	0(1)	4n+4	14(1)+4 = 18
$Co(CO)_4^-$	1[4.5]-4-0.5=0	1	0(1)	4n+4	14(1)+4 = 18
(Cp)Ni(NO)	1[4]-2.5-1.5 =0	1	0(1)	4n+4	14(1)+4 = 18
$HCo(CO)_4$	1[4.5]-0.5-4=0	1	0(1)	4n+4	14(1)+4 = 18
ReH_9^{2-}	1[5.5]-4.5-1 =0	1	0(1)	4n+4	14(1)+4 = 18
FeH_6^{4-}	1[5]-3-2 = 0	1	0(1)	4n+4	14(1)+4 = 18
NiH_4^{4-}	1[4]-2-2 = 0	1	0(1)	4n+4	14(1)+4 = 18
CuH_4^{3-}	1[3.5]-2-1.5 = 0	1	0(1)	4n+4	14(1)+4 = 18
$RhClL_3$, L =PPh_3	1[4.5]-0.5-3 = 1	1	1(1)	4n+2	14(1)+2 =16
$Rh(CO)_2I_2^-$	1[4.5]-2-1-0.5 =1	1	1(1)	4n+2	14(1)+2 =16
$HCo(CO)_4$	1[4.5]-0.5-4 = 0	1	0(1)	4n+4	14(1)+4 = 18
$HRh(CO)_4$	1[4.5]-0.5-4 = 0	1	0(1)	4n+4	14(1)+4 = 18
$HRh(CO)L_3$	1[4.5]-0.5-1-3 = 0	1	0(1)	4n+4	14(1)+4 = 18
$Ru(CO)_2I_3^-$	1[5]-2-1.5-0.5 = 1	1	1(1)	4n+2	14(1)+2 =16
$(Cp)_2TiMe_2$	1[7]-2(2.5)-1 = 1	1	1(1)	4n+2	14(1)+2 =16
$(Cp)_2ZrH_2$	1[7]-5-1 = 1	1	1(1)	4n+2	14(1)+2 =16

2.3.2 Using Skeletal Numbers to Test the 8-Electron Rule

The procedure used for main group elements is the same as in the case of transition metals. The worked out examples are given in Table 5. The 8-electron rule is obeyed when K = 0 for a mono-skeletal cluster.

Table 5. Skeletal Numbers of Selected Mono-skeletal Main group Elements

FRAGMENT/MOLECULE	K VALUE	n VALUE	K(n)	SERIES	VALENCE ELECTRONS
H_2O	1[1]-2(0.5) = 0	1	0(1)	4n+4	4(1)+4 = 8
NH_4^+	1[1.5]-4(0.5)+0.5 = 0	1	0(1)	4n+4	4(1)+4 = 8
CH_4	1[2]-4(0.5) = 0	1	0(1)	4n+4	4(1)+4 = 8
NH_3	1[1.5]-3(0.5) = 0	1	0(1)	4n+4	4(1)+4 = 8
NH_2^-	1[1.5]-2(0.5)-0.5 = 0	1	0(1)	4n+4	4(1)+4 = 8
HCl	1[0.5]-0.5 = 0	1	0(1)	4n+4	4(1)+4 = 8
Cl^-	1[0.5]-0.5 = 0	1	0(1)	4n+4	4(1)+4 = 8
O^{2-}	1[1]-1 = 0	1	0(1)	4n+4	4(1)+4 = 8
N^{3-}	1[1.5]-1.5 = 0	1	0(1)	4n+4	4(1)+4 = 8
OH^-	1[1]-1(0.5)-0.5 = 0	1	0(1)	4n+4	4(1)+4 = 8

2.4 USING Skeletal Numbers to Categorize and Predict Shapes for Clusters

2.4.1 Categorization of Clusters

The use of skeletal numbers to categorize clusters has been done (Kiremire, 2017). This is yet another area where skeletal numbers are extremely useful. Nonetheless, let us take a few more examples for illustrations.

Let us consider the nickel complex, $Ni_5(CO)_{12}^{2-}$. From Table 1, nickel skeletal element was assigned a K value of 4 according to the series method, and for each :CO ligand, K = -1 for the donation of two electrons to the skeletal element. The negative charge of two (—2) of the complex, also has a K value -1 just like each of the CO ligands. Hence the K

value of the cluster, will be given by K = 5[4] +12[-1] +2[-0.5] = 20-12-1 = 7. The K value of the cluster is given by K = 2n- ½ q, and n = 5. Therefore, 7 = 2(5)- ½ q , and ½ q = 10-7 = 3 and hence q = 6. The $Ni_5(CO)_{12}^{2-}$ cluster belongs to the series, S = 4n+6. The K values can be calculated in the same way and series determined. The similar clusters are given in examples 1 to 7. The clusters with K = 7 and n =5 are expressed as K(n) = 7(5) and their shapes have been described as elongated trigonal bipyramid while those with K(n) = 9(5) have been described as regular trigonal bipyramid (Teo, et al, 1984).

1. $Ni_3Cr_2(CO)_{16}^{2-}$; K = 3[4]+2[6]-16-1 = 7, K(n) = 7(5)→S = 4n+6
2. $RuIr_4(CO)_{15}^{2-}$; K = 1[5]+4[4.5]-15-1 = 7, K(n) = 7(5)→S = 4n+6
3. $PtRh_4(CO)_{14}^{2-}$; K = 1[4]+4[4.5]-14-1 = 7, K(n) = 7(5)→S = 4n+6
4. B_5H_{11}; K = 5[2.5]-5.5 = 7, K(n) = 7(5)→S = 4n+6

The possible ideal shape of the above examples (1 to 4) is shown as sketch S-2.

Elongated Trigonal Bipyramid

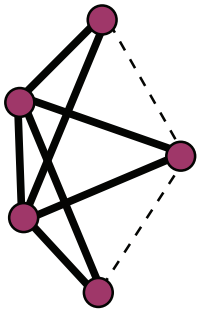

K(n) = 7(5)

S-2

For the examples 5 to 7 below, the ideal shape is shown in sketch S-3.

5. $Os_5(CO)_{16}$; K = 5[5]-16 = 9, K(n) = 9(5)→S = 4n+2
6. $PtRh_4(CO)_{12}^{2-}$; K = 1[4]+4[4.5]-12-1 = 9, K(n) = 9(5)→S = 4n+2
7. $B_5H_5^{2-}$; K = 5[2.5]-2.5-1 = 9, K(n) = 9(5)→S = 4n+2

Regular Trigonal Bipyramid

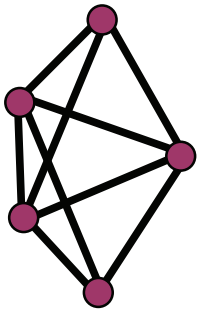

K(n) = 9(5)

S-3

8. $Ru_6(B)(CO)_{16}(AuL)_3$

The above is an example of a heterometal nanocluster (Ciabatti, 2015).

Using the skeletal numbers and the series, as simple as they look, we are able to predict the geometry of some clusters with seemingly formidable formulas. For instance, we know that Ru (K = 5), B (K= -1.5 taken as a ligand), CO (K= -1), Au (K= 3.5), and L (K = -1). Hence the K value of the cluster is given by: K = 6[5] +1[-1.5]+16[-1]+3[3.5-1] = 20. Since n = 9(6 Ru + 3 Au), then we have the parameter K(n) = 20(9). We can derive the cluster series from K(n) as follows: K = 2n- ½ q: K= 20 = 2(9)- ½ q; ½ q = 18-20 = -2, and hence q = -4. Therefore the S = 4n+q = 4n-4; Cp = C^3C[M-6].

2.4.2 The Capping and Capping Symbol

The symbol Cp = C^3C[M-6] derived from the cluster series in example 8 was introduced in earlier work(Kiremire,2015d). Since many readers are not familiar with the Capping Symbol (Cp) and its relationship with series, it is important to explain it briefly. Let us look at the following set of series: S = 4n+10(Klado), 4n+8(Hypho), 4n+6(Arachno), 4n+4(Nido), 4n+2(Closo), 4n+0(Mono-cap), 4n-2(Bi-cap), 4n-4(Tri-cap), 4n-6(Tetra-cap),

4n-8(Penta-cap) and 4n-10(Hexa-cap); cap = capping. Boranes, heteroboranes, Zintyl ions and hydrocarbons normally belong to members of the series 4n+q where q > 0. A large number of transition metal carbonyl clusters, metalloboranes and golden clusters belong to the series S = 4n+q, where q≤ 0. This means that a good percentage of these clusters are highly capped (Kiremire, 2017). A series symbol for these was created, S = 4n+q as well as its corresponding K value given by K = 2n- ½ q. Since all the clusters which belong to the series S = 4n+q (q≤ 0) are capped, it was important to find a symbol for it. When we take a closer look at the sequence of the series S = 4n+0(Mono-cap, C^1), 4n-2(Bi-cap, C^2), 4n-4(Tri-cap, C^3), and 4n-6(Tetra-cap, C^4), etc a beautiful pattern emerges. Thus, for q = 0, we have a mono-capped cluster, C^1, q = -2, C^2, a bi-capped cluster, q = -4, C^3, a tri-capped cluster, and so on. A Capping Symbol, Cp = $C^nC[M\text{-}x]$ where n is the number of skeletal atoms capping , x is the number of skeletal elements around which the capping takes place, and M stands for skeletal element, was introduced (Kiremire, 2015b, 2015d,2017). It is quite clear that the number of capping elements correspond to the multiple of (-2) in the series. Hence, for the cluster $Ru_6(B)(CO)_{16}(AuL)_3$ the series is S = 4n-4 = 4n+2(-2). This could be translated as 4n+0, 1 capping atom, and 2(-2) which represents 2 other capping elements. This gives a total of 1+2 = 3 capping skeletal elements out of a total of 9 skeletal elements. The remaining 6 un-capped elements belong to the S = 4n+2 series and constitute an octahedral inner cluster nucleus. This is what is observed in sketch S-4, which has been previously identified (Ciabatti,2015). It is found that all the 3 gold skeletal elements are capping around the 6 nickel skeletal elements which constitute an octahedral geometry, O_h. What is interesting is that all the three gold skeletal atoms are capping around the octahedral ruthenium skeletal elements.

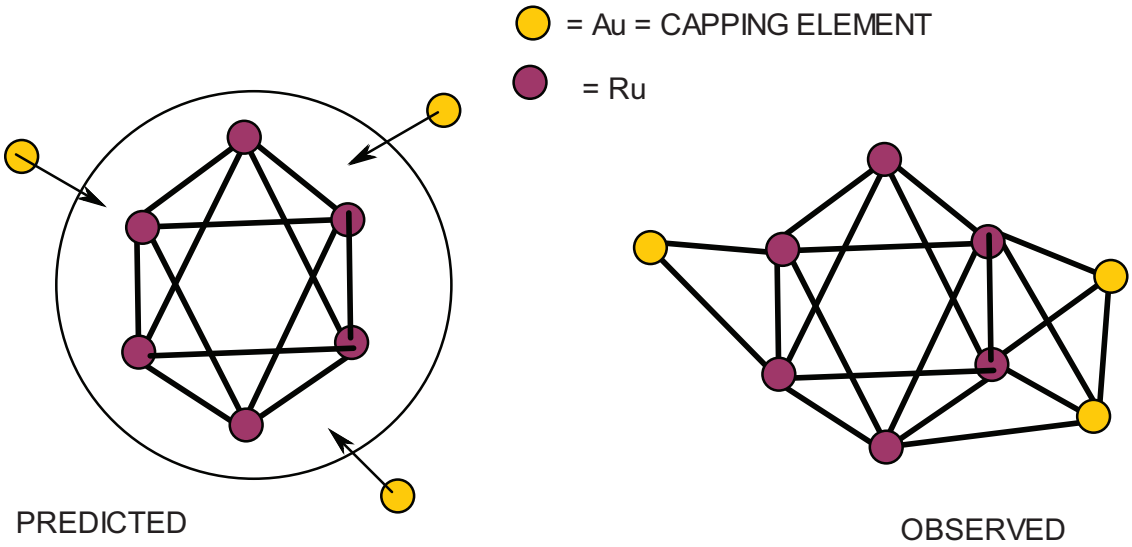

$Ru_6(B)(CO)_{16}(AuL)_3$, L = PPh_3

S-4

$K = 2n - 1/2\ q; \quad q = 2[2n-K]$

K(n), K = cluster number, n = number of identified skeletal elements

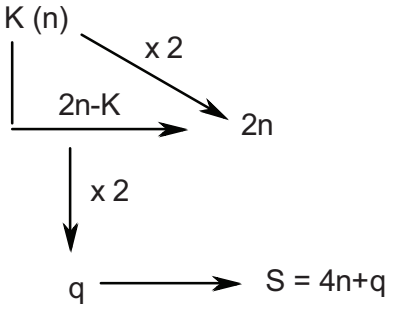

Scheme 2. Derivation of Series Formula from K(n) Parameter

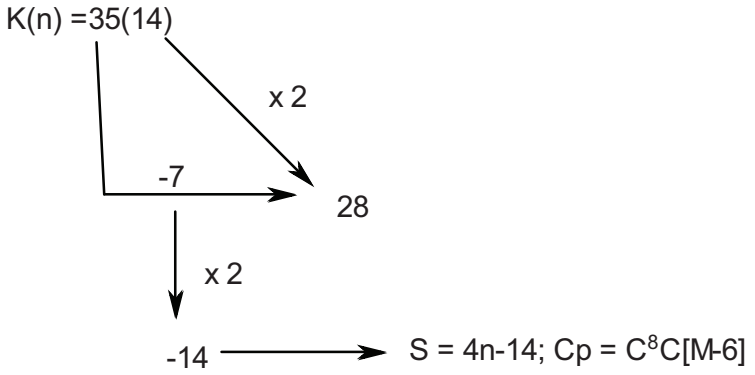

Scheme 3. Example illustrating the derivation of the Cluster Series Formula

From the capping symbol Cp = $C^8C[M-6]$, we know that the cluster has an octahedral nucleus capped by 8 skeletal elements. This is what is observed in sketch S-5 which was previously identified (Ciabatti, 2015). It is found that all the 8 gold skeletal elements are capping around the nickel skeletal elements which constitute an octahedral geometry, O_h. This is a clear testimony of the power of the series method for categorizing clusters.

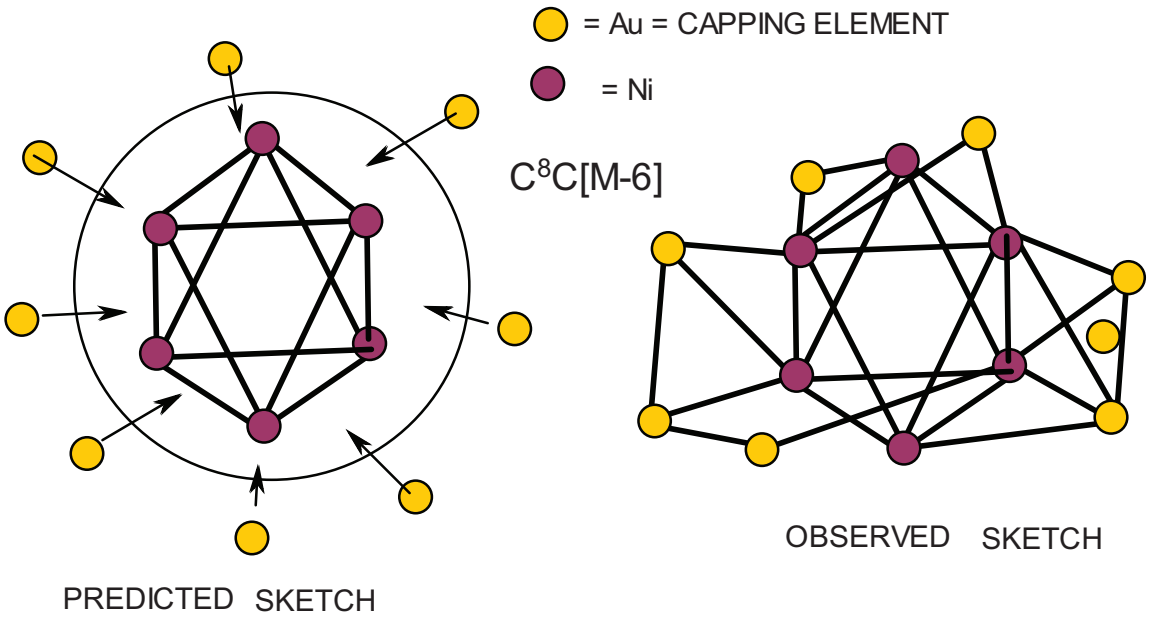

$Ni_6(C)(CO)_8(AuL)_8^{2+}$, L = PPh_3

S-5

10. $Au_8L_7^{2+}$, L = PPh_3

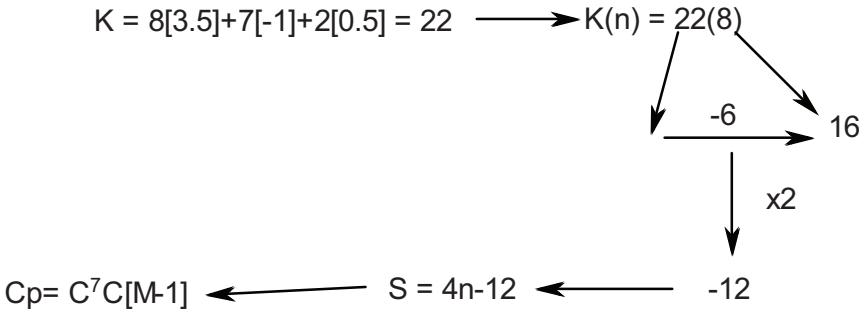

This implies that the golden cluster has ONE skeletal atom at the cluster nucleus with the rest of the skeletal elements surrounding it(capping). This is found to be the case. This is sketched in S-6.

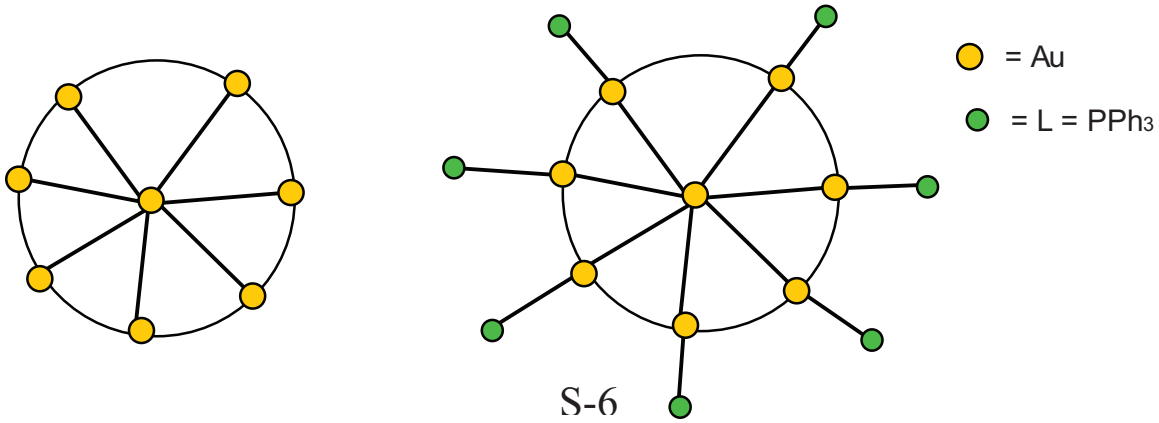

S-6

In this golden cluster, the 7 capping golden skeletal elements each possess a ligand while the one in the nucleus has no ligand.

11. $Pt_5(CO)_6L_4$

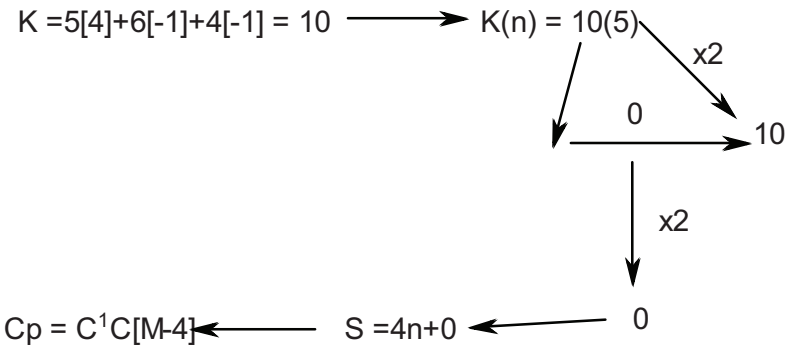

The capping symbol, Cp = $C^1C[M-4]$ means that the cluster comprized of 4 platinum skeletal elements which form a tetrahedral shape, T_d, while one of the five platinum skeletal element sits in a capping position.

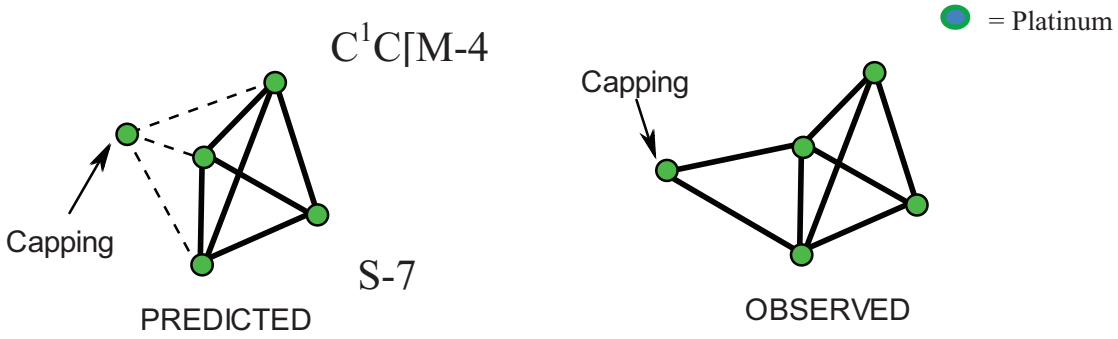

Sketch S-7 shows the predicated and observed geometry of the above cluster (Ciabatti, 2015). Not only is the 4n series method easy to work with, but is also quite precise in predicting the skeletal shape of a cluster.

More examples to demonstrate the power of skeletal numbers to categorize clusters are given in Table 6.

Table 6. Examples of Categorized Clusters

CLUSTER	CALCULATION OF K VALUE	n VALUE	K(n)	SERIES	VALENCE ELECTRONS	CATEGORY
B_4H_{10}	4[2.5]-5 = 5	4	5(4)	4n+6	4(4)+6 =22	ARACHNO
$Os_5(CO)_{16}$	5[5]-16 = 9	5	9(5)	4n+2	14(5)+2 =72	CLOSO
B_5H_9	5[2.5]-4.5 = 8	5	8(5)	4n+4	4(5)+4 =24	NIDO
$B_4H_8Fe(CO)_3$	4[2.5]+1[5]-4-3=8	5	8(5)	4n+4	4(5)+4+1(10) =34	NIDO
B_5H_{11}	5[2.5]-5.5 = 7	5	7(5)	4n+6	4(5)+6 = 26	ARACHNO
$Co_4Ni_2(CO)_{14}^{2-}$	4[4.5]+2[4]-14-1 =11	6	11(6)	4n+2	14(6)+2 =86	CLOSO
B_6H_{10}	6[2.5]-5 = 10	6	10(6)	4n+4	4(6)+4 =28	NIDO
CB_5H_9	1[2]+5[2.5]-4.5=10	6	10(6)	4n+4	4(6)+4 =28	NIDO
$B_7H_7^{2-}$	7[2.5]-3.5-1 = 13	7	13(7)	4n+2	4(7)+2 = 30	CLOSO
$C_2B_6H_{10}$	2[2]+6[2.5]-5 =14	8	14(8)	4n+4	4(8)+4=36	NIDO
B_8H_{14}	8[2.5]-7=13	8	13(8)	4n+6	4(8)+6 =38	ARACHNO
$Rh_9(P)(CO)_{21}^{2-}$	9[4.5]-2.5-21-1 =16	9	16(9)	4n+4	14(9)+4 = 130	NIDO
B_9H_{15}	9[2.5]-7.5 = 15	9	15(9)	4n+6	4(9)+6 =42	ARACHNO
$B_{10}H_{12}$	10[2.5]-6 =19	10	19(10)	4n+2	4(10)+2 = 42	CLOSO
$B_{10}H_{10}^{6-}$	10[2.5]-5-3 =17	10	17(10)	4n+6	4(10)+6 = 46	ARACHNO
$B_{10}H_{15}^{-}$	10[2.5]-7.5-0.5 = 17	10	17(10)	4n+6	4(10)+6 = 46	ARACHNO
$B_{10}H_{14}$	10[2.5]-7 =18	10	18(10)	4n+4	4(10)+4 =44	NIDO
$B_9H_{11}S$	9[2.5]+1[1]-5.5 = 18	10	18(10)	4n+4	4(10)+4 =44	NIDO
$(CpCo)C_2B_7H_{11}$	1[4.5]+2[2]+7[2.5]-2.5-5.5 =18	10	18(10)	4n+4	4(10)+4+1(10) =54	NIDO
$C_2B_9H_{11}$	2[2]+9[2.5]-5.5 =21	11	21(11)	4n+2	4(11)+2 =46	CLOSO
$B_{11}H_{11}^{4-}$	11[2.5]-5.5-2 = 20	11	20(11)	4n+4	4(11)+4 =48	NIDO
$B_{11}H_{13}^{2-}$	11[2.5]-6.5-1 =20	11	20(11)	4n+4	4(11)+4 =48	NIDO
$B_{10}CPH_{11}$	10[2.5]+1[2]+1[1.5]-5.5=23	12	23(12)	4n+2	4(12)+2 =50	CLOSO
$B_{12}H_{12}^{2-}$	12[2.5]-6-1 = 23	12	23(12)	4n+2	4(12)+2 =50	CLOSO
$Fe_5(C)(CO)_{15}$	5[5]-2-15 =8	5	8(5)	4n+4	14(5)+4 =74	NIDO
$Ru_6(C)(CO)_{17}$	6[5]-2-17 = 11	6	11(6)	4n+2	14(6)+2 = 86	CLOSO
$Co_4(PPh)_2(CO)_{10}$	4[4.5]+2[1.5]-1-11=9	6	9(6)	4n+6	4(6)+6 +4(10) =70	ARACHNO
$Sn_9Cr(CO)_3$	9[2]+1[6]-3 = 21	10	21(10)	4n-2	4(10)-2+1(10) = 48	C^1C[M-9]

2.5 Using Skeletal Numbers to identify a Selected Common Geometry Within Clusters

The examples below have been selected to demonstrate the method of calculating K(n) and the categorization of a cluster according to 4n Series. For the same examples, the linkage to symmetry is shown in sketch S-8. These are given in Table 7.

Table 7. Identification of Clusters with Ideal Tetrahedral Skeletal Shape Using K(n) Parameter

CLUSTER	CALCULATION OF K VALUE	n VALUE	K(n)	SERIES, S	VALENCE ELECTRONS
$Os_4(CO)_{14}$	4[5]-14 = 6	4	6(4)	4n+4	14(4)+4 =60
P_4	4[1.5] = 6	4	6(4)	4n+4	4(4)+4 = 20
$Ir_4(CO)_{12}$	4[4.5]-12 = 6	4	6(4)	4n+4	14(4)+4 =60
$Re_4H_4(CO)_{13}^{2-}$	4[5.5]-2-13-1 = 6	4	6(4)	4n+4	14(4)+4 =60
$Rh_4(CO)_{11}^{2-}$	4[4.5]-11-1 = 6	4	6(4)	4n+4	14(4)+4 =60
$S_2Fe_2(CO)_6$	2[1]+2[5]-6 = 6	4	6(4)	4n+4	4(4)+4+2(10) =40
$SeFe_3(CO)_9^{2-}$	1[1]+3[5]-9-1 =6	4	6(4)	4n+4	4(4)+4+3(10) =50
$Fe_4(CO)_4(Cp)_4$	4[5]-4-4(2.5) = 6	4	6(4)	4n+4	14(4)+4 =60
$InBi_3^{2-}$	1[2.5]+3[1.5]-1= 6	4	6(4)	4n+4	4(4)+4 = 20
$GaBi_3^{2-}$	1[2.5]+3[1.5]-1 = 6	4	6(4)	4n+4	4(4)+4 = 20
$FeIr_3(CO)_{12}^{-}$	1[5]+3[4.5]-12-0.5 =6	4	6(4)	4n+4	14(4)+4 =60
$Fe_2Ir_2(CO)_{12}^{2-}$	2[5]+2[4.5]-12-1 = 6	4	6(4)	4n+4	14(4)+4 =60

The ideal shape corresponding to the parameter K(n) = 6(4) is tetrahedral as shown in sketch S-8.

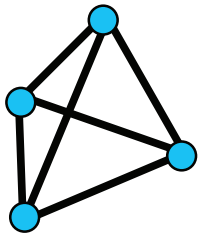

K(n) = 6(4)

S-8

2.6 Using Skeletal Numbers to Match Isolobal Fragments

Isolobal fragments are extremely important in linking inorganic chemistry with organic chemistry (Hoffmann, 1982).

Using skeletal numbers, isolobal fragments can easily be identified by calculating the K value of the fragments. Categorization of isolobal fragments using 14n and 4n series was done earlier (Kiremire, 2015c). The isolobal fragments with their corresponding K values are given in Table 8. From this table, we can readily pick out the following selected isolobal relationships.

Table 8. Identification of Isolobal Fragments Using Skeletal Numbers

FRAGMENT	CALCULATION OF K VALUE	K(n)	SERIES , S
CH_2^{2-}	1[2]-1-1=0	0(1)	4n+4
CH_3^-	1[2]-1.5-0.5 = 0	0(1)	4n+4
NH_2^-	1[1.5]-1-0.5 = 0	0(1)	4n+4
CH_3	1[2]-1.5 =0.5	0.5(1)	4n+3
CH_2^-	1[2]-1-0.5 = 0.5	0.5(1)	4n+3
$Co(CO)_4$	1[4.5]-4 = 0.5	0.5(1)	4n+3
$Mn(CO)_5$	1[5.5]-5 = 0.5	0.5(1)	4n+3
CpNi(CO)	1[4]-2.5-1 =0.5	0.5(1)	4n+3
$Cu(CO)_3$	1[3.5]-3 = 0.5	0.5(1)	4n+3
F	1[0.5] =0.5	0.5(1)	4n+3
MnL_5	1[5.5]-5 = 0.5	0.5(1)	4n+3
$CpFe(CO)_2$	1[5]-2.5-2=0.5	0.5(1)	4n+3
$Fe(CO)_5^+$	1[5]-5+0.5 =0.5	0.5(1)	4n+3
$CpCr(CO)_3$	1[6]-2.5-3=0.5	0.5(1)	4n+3
$AsMe_2$	1[1.5]-1=0.5	0.5(1)	4n+3
CH_3^+	1[2]-1.5+0.5 = 1	1(1)	4n+2
$Mn(CO)_5^+$	1[5.5]-5+0.5 = 1	1(1)	4n+2
CH_2	1[2]-1 = 1	1(1)	4n+2
CR_2	1[2]-1 = 1	1(1)	4n+2
SnR_2	1[2]-1 = 1	1(1)	4n+2
$Fe(CO)_4$	1[5]-4 = 1	1(1)	4n+2
$Ru(CO)_4$	1[5]-4 = 1	1(1)	4n+2
$Os(CO)_4$	1[5]-4 = 1	1(1)	4n+2
$Cr(CO)_5$	1[6]-5 =1	1(1)	4n+2
CpCo(CO)	1[4.5]-2.5-1=1	1(1)	4n+2
$CpMn(CO)_2$	1[5.5]-2.5-2=1	1(1)	4n+2
$Re(CO)_4^-$	1[5.5]-4-0.5 =1	1(1)	4n+2
$CpFe(CO)^-$	1[5]-2.5-1-0.5 =1	1(1)	4n+2
CH_3^+	1[2]-1.5+0.5 =1	1(1)	4n+2
$Cr(CO)_5$	1[6]-5 = 1	1(1)	4n+2
CH	1[2]-0.5 = 1.5	1.5(1)	4n+1
CR	1[2]-0.5 = 1.5	1.5(1)	4n+1
$Co(CO)_3$	1[4.5]-3 = 1.5	1.5(1)	4n+1
$Mn(CO)_4$	1[5.5]-4 =1.5	1.5(1)	4n+1
CpNi	I[4]-2.5 = 1.5	1.5(1)	4n+1
CpFe(CO)	1[5]-2.5-1 =1.5	1.5(1)	4n+1
$Rh(CO)_3$	1[4.5]-3 = 1.5	1.5(1)	4n+1
$Ir(CO)_3$	1[4.5]-3 = 1.5	1.5(1)	4n+1
$Fe(H)(CO)_3$	1[5]-0.5-3 = 1.5	1.5(1)	4n+1
$CpW(CO)_2$	1[6]-2.5-2 = 1.5	1.5(1)	4n+1
$CpCr(CO)_2$	1[6]-2.5-2 = 1.5	1.5(1)	4n+1
$Cr(CO)_5^+$	1[6]-5+0.5 =1.5	1.5(1)	4n+1
CH_2^+	1[2]-1+0.5 =1.5	1.5(1)	4n+1
P	1[1.5] = 1.5	1.5(1)	4n+1
BH^-	1[2.5]-0.5-0.5 = 1.5	1.5(1)	4n+1
BH	1[2.5]-0.5 = 2	2(1)	4n+0
$CpFe^-$	1[5]-2.5-0.5 = 2	2(1)	4n+0
CpCo	1[4.5]-2.5 = 2	2(1)	4n+0
C	1[2] = 2	2(1)	4n+0
CH^+	1[2]-0.5+0.5 = 2	2(1)	4n+0
$Fe(CO)_3$	1[5]-3 = 2	2(1)	4n+0
$Cr(CO)_4$	1[6]-4 = 2	2(1)	4n+0
CpCo	1[4.5]-2.5 = 2	2(1)	4n+0
CpMn(CO)	1[5.5]-2.5-1 = 2	2(1)	4n+0

A simple illustration of the isolobal relationship of P, CH and $Co(CO)_3$ is given in sketch S-9.

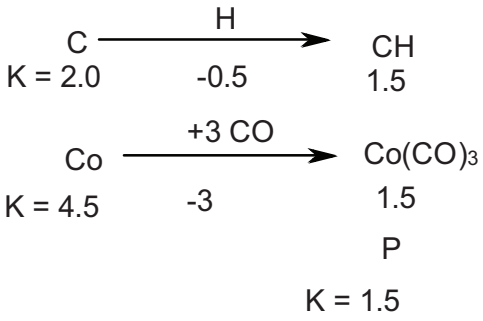

P⇔ CH ⇔$Co(CO)_3$

S-9

Some more examples of isolobal relationships are given blow.

i. CH_2^{2-} ⇔ CH_3—⇔NH_2^-, K = 0

ii. CH_3⇔$Mn(CO)_5$⇔$Co(CO)_4$⇔(Cp)Ni(CO), K = 0.5

iii. CH_2⇔$Fe(CO)_4$⇔$Cr(CO)_5$⇔O, K = 1

iv. CH⇔ CR ⇔$Co(CO)_3$⇔$Mn(CO)_4$⇔(Cp)Ni ⇔P, K = 1.5

v. C⇔ $Fe(CO)_3$⇔$Ru(CO)_3$⇔$Os(CO)_3$⇔$Cr(CO)_4$⇔(Cp)Co⇔(Cp)Mn(CO), K = 2

2.7 Using Skeletal Numbers to Distribute Ligands onto Skeletal Elements in a Cluster

The shapes of skeletal elements and the ligands distributed around them are very important. The x-ray crystal structure analysis has been crucial in providing such information (Cotton and Wilkinson, 1980; Greenwood and Earnshaw, 1998; Housecroft and Sharpe, 2005; Miessler, Fischer and Tarr, 2014).It has been found that the use of skeletal numbers helps immensely in distributing ligands around skeletal elements in such a way that the 18-or 8-electron rule is obeyed. In this way, hypothetical shapes of clusters can be obtained. The actual shapes can only be deduced from experimental determinations. The first step in distributing the ligands around skeletal elements is to determine the possible skeletal shape of the cluster from the cluster formula. The second one is to assign and determine the K value of each skeletal element in the assigned geometry using the skeletal numbers. Let us illustrate this by a few examples, starting with the cobalt complex in Figure (F-1).

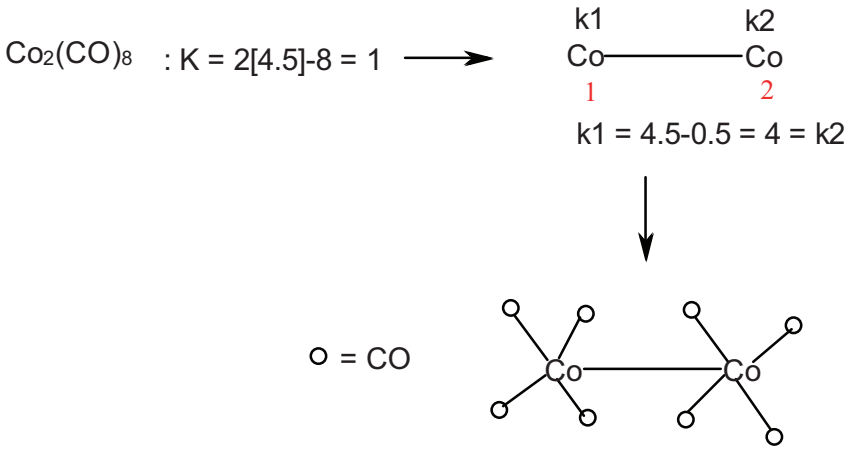

F-1

From Table 1, the cobalt atom is assigned a K value of 5. The above calculation shows that the complex, $Co_2(CO)_8$ has a K value of 1. This means there is one Co-Co metal-metal bond. In this metal-metal bond, one of the electrons comes from cobalt 1 while the other comes from cobalt 2. This concept is simply represented in diagram D-1.

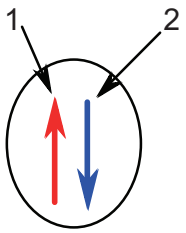

D-1

If we regard the electron from cobalt 2 as being donated to cobalt 1 like a one electron donor ligand, then k1 = 4.5-0.5 = 4.0. In order for cobalt 1 to obey the 18-electron rule, 4 carbonyl ligands must be added to cobalt 1. Similarly, 4 other carbonyls must be added to cobalt 2. This gives rise to figure F-1. The same explanations can be extended to figures F-2 to F-9.

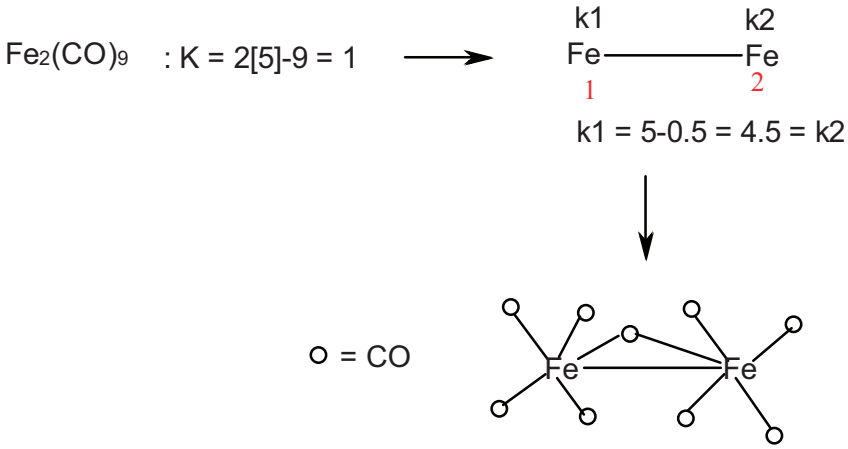

F-2

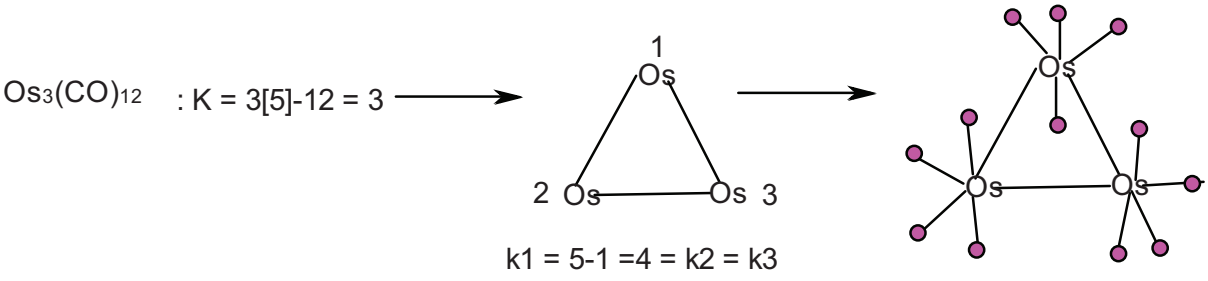

F-3

$Os_4(CO)_{14}$: K = 4[5]-14 = 6

k1 = 5-1.5 = 3.5 = k2 = k3 = k4

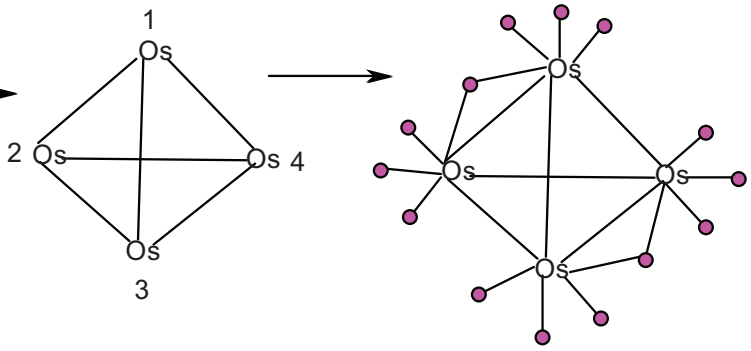

F-4

$Os_5(CO)_{18}$: K = 5[5]-18 =7

k1 = 5-1 =4

k2 = 5-2 = 3

k3 = 5-1 = 4

k4 = 5-1.5 = 3.5

k5 = k4 = 3.5

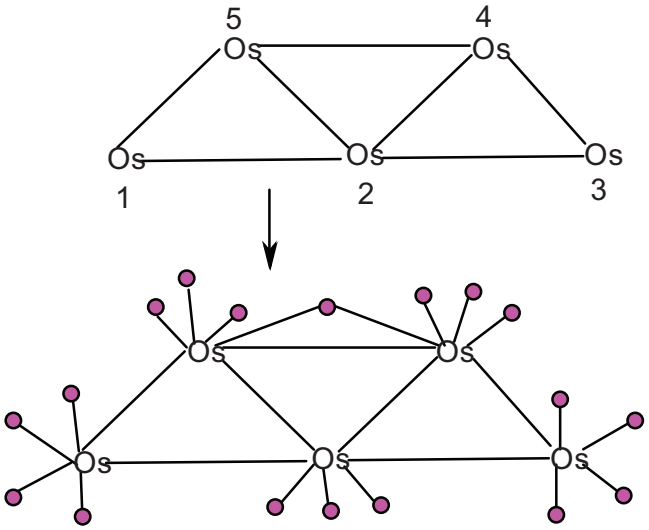

F-5

$Os_5(CO)_{16}$: K = 5[5]-16 =9

k1 = 5-1.5 =3.5

k2 = 5-2 = 3

k3 = 5-2 = 3

k4 = 5-2 = 3

k5 = 5-1.5 = 3.5

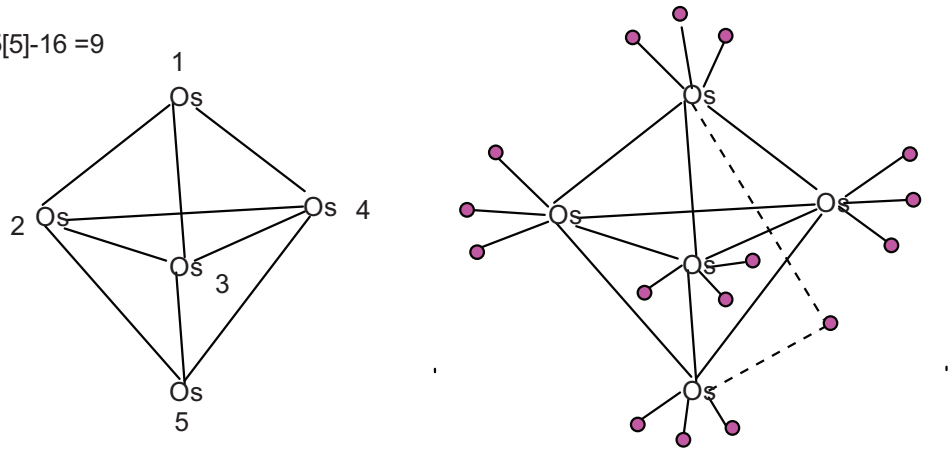

F-6

$Os_6(CO)_{18}^{2-}$: K = 6[5]-18-1 = 11

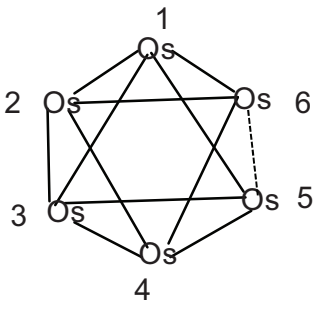

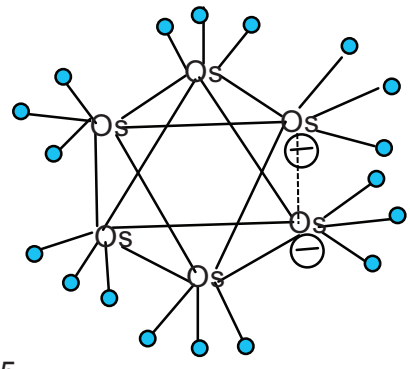

k1 = 5-2 = 3

k2 = 5-2 = 3

k3 = 5-2 = 3

k4 = 5-2 = 3

k5 = 5-1.5 = 3.5

k6 = 5-1.5 = 3.5

F-7

$Re_4H_5(CO)_{14}^{-}$; K = 4[5.5]-2.5-14-0.5 =5

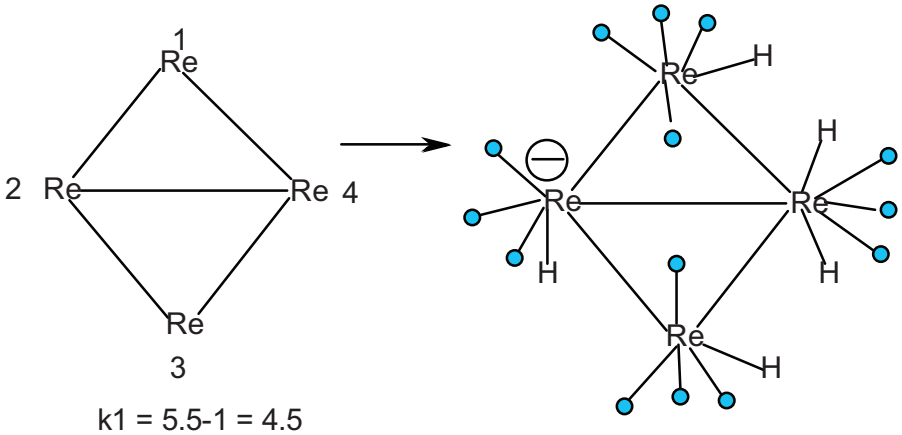

k1 = 5.5-1 = 4.5

k2 =5.5-1.5 = 4

k3 = k1 = 4.5

k4 = k2 = 4

F-8

$Re_6H_5(CO)_{24}^-$; K = 6[5.5]-2.5-24-0.5 = 6

k1 = 5.5-1 =4.5
k2 = k3 = k4 = k5 = k6 = k1 = 4.5

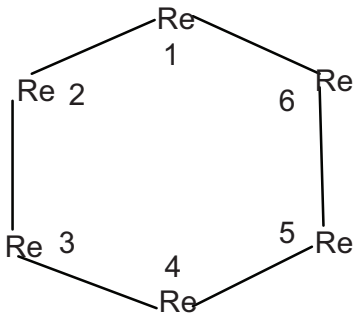

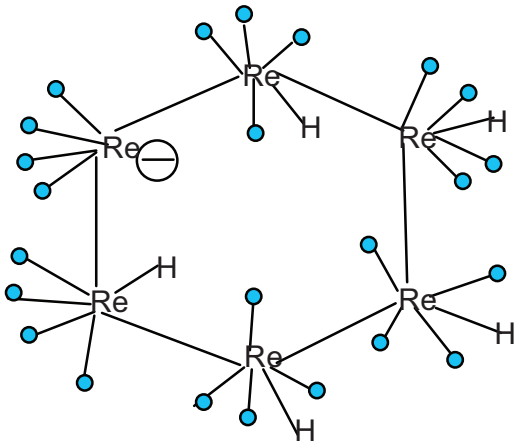

K(n) = 6(6) S = 4n+12 ⟶ $F_{CH} = C_6H_{12}$

F-9

2.8 Using Skeletal Numbers to Test the 18-Electron Rule in Multi-skeletal Clusters

Let us consider a few examples (Meissler, 2014) given below. The details of the method are also explained for each of the sketches (F-1 to F-9 and F-10 to F-12). The K values were calculated using the appropriate skeletal numbers presented in Tables 1 to 3.

1. $Re_2(Cp)_2(CO)_5$ ⟶

K =2[5.5]+2[-2.5]+5[-1]
= 11-5-5 = 1

k1 = k2 = 1[5.5]+1[-0.5] = 5.5-0.5 = 5

If we divide the ligands between the 2 Re skeletal atoms we get, [2Cp+5CO]/2 = 1Cp+2.5CO.
In terms of K values = 1[-2.5]+2.5[-1] = -5.0. This clearly means that if we evenly distribule the ligands around the 2 Re skeletal elements, the overall K value on each rhenium atom will be 0. In that way, each Re skeletal element wil obey the 18 electron rule. On this basis, the sketch of the complex will be as shown in F-10.

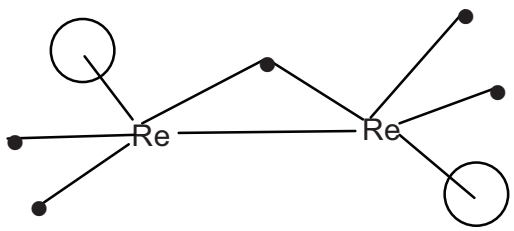

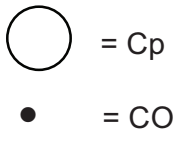

Cp = cyclopentadienyl ligand, η^5-C_5H_5

F-10

2. $Mo_2(Cp)_2(CO)_4$ → k1 Mo 1 ≡ k2 Mo 2

K = 2[6]+2[-2.5]+4[-1] = 12-5-4 = 3

k1 = k2 = 1[6]+3[-0.5] = 4.5

Let us divide the ligands among the 2 Mo skeletal elements we get, [2Cp+4CO]/2 = Cp+2CO. The K value of 1 Cp + 2CO = 1[-2.5]+2[-1] = -4.5. This means that if we add 1Cp and 2 CO ligands to each Mo skeletal element the net K value on the Mo atom will be 0. This implies the skeletal atom obeys the 18 electron rule. A sketch of the complex is given in F-11.

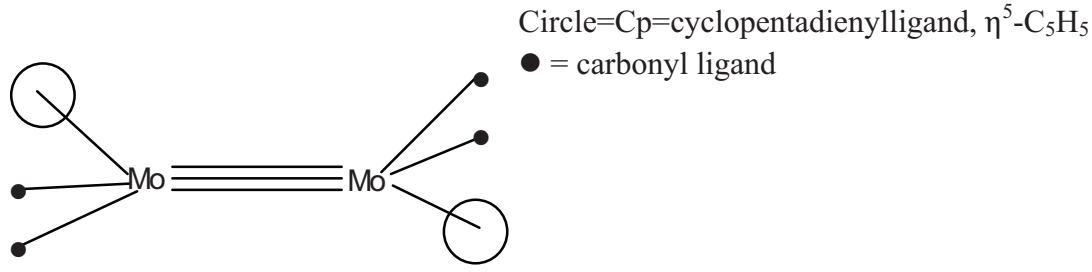

F-11

3. $Ir_4(CO)_{12}$

The K value is given by K = 4[4.5]+12[-1] = 18-12 = 6. The skeletal sketch is given in F-12.

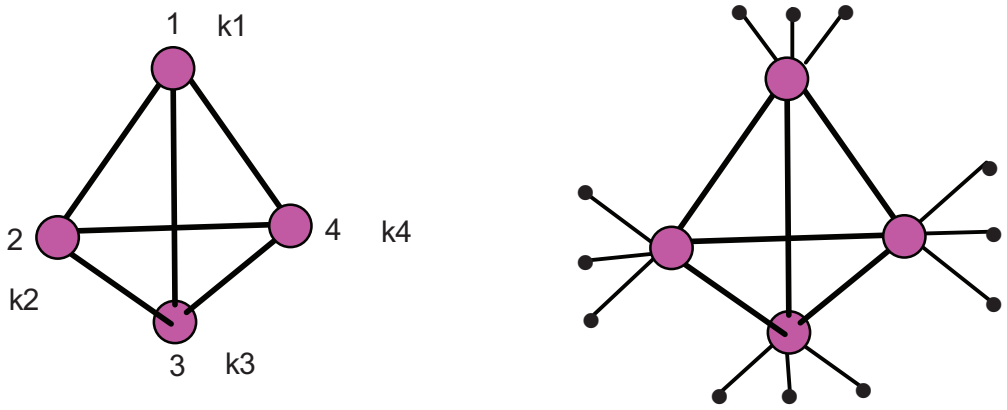

k1 = k2 = k3 = k4 = 1[4.5]+3[-0.5] =3.

If we divide the ligands among the 4 skeletal elements we get 3 CO.

The K value of 3 CO = 3[-1] = -3. This means that adding 3 CO ligands to each skeletal element the net K value of the skeletal atom = 0. Ideally, this means that the skeletal atom obeys the 18 electron rule. The sketch of the cluster is given in F-12.

F-12

3. Conclusion

The various areas in which skeletal numbers can be utilized in categorizing fragments and clusters have been presented. These include predicting whether a cluster obeys the 8 or 18 electron rule, categorization of a given cluster and predicting its possible geometry, the linkage of the cluster number K(n) with a possible specific geometry, and the

matching of fragments which are isolobal. More importantly, the skeletal numbers can be used as a guide to distribute ligands to skeletal geometries of clusters in order to generate possible cluster isomers. The method has been found to be easy and rapid in categorizing a cluster into its series and generally precise in predicting the geometrical shape of a cluster.

Acknowledgement

The University of Namibia is greatly acknowledged for providing the enabling environment and facilities to support this work and Dr. P. E. T. Kiremire and Mrs M.K. Kiremire for proof-reading the draft.

References

Ciabatti, I. (2015). Homo-and Heterometal carbonyl Nanoclusters. PhD Thesis. Universita Di Bologna.

Cotton, F. A., & Wilkinson, G. (1980). *Advanced Inorganic Chemistry, 4th Ed.*, John Wiley and Sons, New York, 1980.

de Sausa, D. W. O., & Nascimanto, M. A. C. (2016). Is There a Quadruple Bond in C_2? *J. Chem. Theory Comput., 12*(5), 2234-2241. https://doi.org/10.1021/acs.jctc.6b00055

Greenwood, N. N., & Earnshaw, A. (1998). *Chemistry of the Elements, 2nd Ed.*,Butterworth, Oxford.

Hoffmann, R. (1982). Building Bridges Between Inorganic and Organic Chemistry. *Angew. Chem. Int. Ed. Engl., 21*, 711-724. https://doi.org/10.1002/anie.198207113

Housecroft, C. E., & Sharpe, A. G. (2005). *Inorganic Chemistry, 2nd Ed.*, Pearson, Prentice Hall, Harlow, England

King, R. B., & Schleyer, P. V. R. (2004). Molecular Clusters of the Main Group Elements, Edited by M. Driess and H. NÖth, Wiley-VCH: Heppenheim, Germany.

Kiremire, E. M. (2014). Validation and verification of the Expanded Table for Transition Metal Carbonyl and Main Group Element Cluster Series which obey the 18-Electron and the 8-Electron Rules Respectively. *Orient. J. Chem., 30*(4), 1475-1495. https://doi.org/10.13005/ojc/300404

Kiremire, E. M. (2015a). Classification of Transition Metal Carbonyl Clusters Using the 14n Rule Derived from Number Theory. *Orient. J. Chem., 31*(2), 605-618. https://doi.org/10.13005/ojc/310201

Kiremire, E. M. (2015b). Categorization and Structural Determination of Simple and More Complex Carbonyl Clusters of Rhenium and Osmium Using k values and the Cluster Table. *Orient. J. Chem., 31*(1), 293-302. https://doi.org/10.13005/ojc/310133

Kiremire, E. M. (2015c). Isolobal Series of Chemical Fragments. *Orient. J. Chem. ,31*(spl. Edn), 59-70.

Kiremire, E. M. (2015d). A Unique Bypass to the Carbonyl Cluster Nucleus Using the 4n Series. *Orient. J. Chem., 31*(3), 1469-1476. https://doi.org/10.13005/ojc/310326

Kiremire, E. M. R. (2016b). Clusters of Gold containing p-Block Elements. *Am. J. Chem., 6*(5), 126-144.

Kiremire, E. M. R. (2016c). The Application of the 4n Series Method to Categorize Metalloboranes. *Int. J. Chem., 8*(3), 62-73. https://doi.org/10.5539/ijc.v8n3p62

Kiremire, E. M. R. (2016d). Classification of Zintl Ion Clusters Using 4n Series Approach. *Orient. J. Chem., 32*(4), 1731-1738. https://doi.org/10.13005/ojc/320401

Kiremire, E. M. R. (2017). The Golden Series and Clusters of Gold-unique Shapes and Bonding. *Int. J. Chem., 9(*1), 38-57. https://doi.org/10.5539/ijc.v9n1p38

Langmuir, I. (1921). Types of Valence. *Science, 54*, 59-67. https://doi.org/10.1126/science.54.1386.59

Lewis, G. N. (1916). The Atom and the Molecules. *J. Am. Chem. Soc., 38*(4), 762-785. https://doi.org/10.1021/ja02261a002

Miessler, G., Fischer, P., & Tarr, D. (2014). *Inorganic Chemistry, 5th Edition*, Pearson Education, Inc., Upper Saddle River

Mingos, D. M. P. (1972). A General Theory for Cluster and Ring Compounds of the Main Group and Transition Elements. *Nature (London), Phys. Sci., 236*, 99-102. https://doi.org/10.1038/physci236099a0

Rudolph, R. W. (1976). Boranes and heteroboranes: a paradigm for the electron requirements of clusters? *Acc. Chem. Res., 9*(12), 446-452. https://doi.org/10.1021/ar50108a004

Shaik, S., Danovich, D., Wu, W., Su, P., Rzepa, H. S., & Hiberty, P. C. (2012). Quadruple bonding in C_2 and analogous eight valence electron species. *Nature Chemistry, 4*, 195-200. https://doi.org/10.1038/nchem.1263

Teo, B. K., Longoni, G., & Chung, F. R. K.(1984). Applications of Topological Electron-Counting Theory to Polyhedral

Metal Clusters. *Inorg. Chem., 23*(9), 1257. https://doi.org/10.1021/ic00177a018

Wade, K. (1971). The structural significance of the number of skeletal bonding electron-pairs in carboranes, the higher boranes and borane ions and various transition metal carbonyl cluster compounds. *Chem. Commun.,* 792-793. https://doi.org/10.1039/c29710000792

Welch, A. J. (2013). The significance of Wade's rules. *Chem. Commun., 49*, 3615-3616. https://doi.org/10.1039/c3cc00069a

International Journal of Chemistry; Vol. 9, No. 3; 2017
ISSN 1916-9698 E-ISSN 1916-9701
Published by Canadian Center of Science and Education

Synthesis, Characterization and Biological Activity of Novel Zirconium, Zinc and Cadmium Complexes Derived from Substituted Tetramethyl Guanidine

Hoda Pasdar[1], Naser Foroughifar[1], Bahare Hedayati Saghavaz[1], Mehran Davallo[1]

[1]Department of Chemistry, Tehran North Branch, Islamic Azad University, Tehran, Iran

Correspondence: Hoda Pasdar, Department of Chemistry, Tehran North Branch, Islamic Azad University, Tehran, Iran. E-mail: H_pasdar@iau-tnb.ac.ir

Received: May 23, 2017 Accepted: June 15, 2017 Online Published: June 20, 2017

doi:10.5539/ijc.v9n3p49 URL: https://doi.org/10.5539/ijc.v9n3p49

Abstract

A novel series of metal complexes of guanidine ligand derived from condensation of 1,1,3,3-tetramethylurea and 2-aminopyridine in present of $POCl_3$ have been synthesized. The complexes are characterized using FTIR, UV-Vis and also molar conductance was measured. These spectroscopic studies confirmed that the ligand bonded to the metals through the nitrogen atoms. The suggested structures of the metal complexes are square planner. The ligand and its metal complexes were tested against Gram-negative bacteria; *Escherichia coli, Serratia marcescens* and Gram-positive bacteria; *Bacillus sabtilis and Staphylococcus aureus* by applying disc diffusion method. The most antibacterial activity of synthesized compounds belongs to CdL_2 complex. The results of this study showed that the metal complexes have more antibacterial activity against species when compared to the parent ligand.

Keywords: Guanidine, $POCl_3$, disc diffusion method, antibacterial activity

1. Introduction

Bacterial infections and bacteria drug resistance are very common all around the world. Also modern life and working conditions afford an encouraging environment for rapid evolution of microorganisms (Afradi et al., 2017). Therefore, in order to solve this important issue, it is necessary to improve effective antimicrobial agents to control the bacterial infection. As a result, antibacterial compounds that can efficiently inhibit the growth of microorganism with limited cytotoxicity have stimulated considerable attention in research fields (Behmaram et al., 2017). In recent years, the application of inorganic antibacterial agents has attracted much attention for the control of pathogenic microorganisms (Hedayati Saghavaz et al., 2017).

Guanidine, has already gained excessive attention since its discovery, due to their chemical and biological properties (Manetti et al., 2009). They also appear in a number of important antibiotic drugs including: Streptomycin, Trimethoprim, Chlorhexidine, Polyhexamethylene bi guanidine, Pyrrplidine bis-cyclic guanidine and others (Ghulam Murtaza, 2012). They can be used for urinary tract infection and disinfectant for swimming pools and wound care. In 2008 L.Qian et al. reported the synthesis of a novel guanidine polymer which has high antimicrobial activity against *Escherichia coli* and *Staphylococcus aureus*. In the present of 1 wt. % of this compound in wood fibers, the growing inhabitation reached nearly 100% (L. Qian et al., 2008).

In addition, transition metal complexes derived from guanidines have been found to exhibit some biological properties like antibacterial and antifungal activities (Cesme et al., 2015). The important pathogens such as *Escherichia coli, Serratia marcescen, Bacillus sabtilis,* and *Staphylococcus aureus* have wildly caused many diseases, so antibacterial activity of these complexes against four kinds of bacteria have been established. Present work describe the synthesis and antibacterial activity of metal complexes derived from 1,1,3,3-tetramethyl-2-(pyridin-2-yl)guanidine. The antibacterial activity of synthesized compounds compared to standard antibiotic drugs against gram-negative and gram-positive bacterial strains.

2. Experimental

2.1 Material and Equipment

All chemical and solvents purchased from Merck and Aldrich Company and used without further purification. ZnI_2, $CdCl_2.2H_2O$ and $ZrO(NO_3)_2.9H_2O$ were used as metal salts. The IR spectra were taken with a Shimidzo 300

spectrometer using potassium bromide pellets. ^{1}HNMR (nuclear magnetic resonance) spectra of ligand were recorded on a Brucker AMX 250 MHz spectrometer in DMS-d_6 solvent using tetramethyl silan as an internal reference. Melting points of compounds were measured with an electrothermal melting point apparatus and were not corrected. The molar conductance of the complexes in DMSO (1×10^{-3} M solution) was performed at 25 °C using oakton ECTestr 11 dual-range, conductivity tester. The Mass spectra for metal complexes were run at 70 eV at 230 °C with Agilent technologies. The progress of the reactions was monitored by thin-layer chromatography (TLC) on silica gel polygram precoated TLC sheets.

2.2 Procedure for Synthesis of 1,1,3,3-Tetramethyl-2-(Pyridin-2-yl)Guanidine (L)

The corresponding ligand (L) prepared according to the previously published procedure (Foroughifar et al., 1993). To a solution of 1,1,3,3 tetramethyl urea (1 m mol) in 10 ml dry benzene was added drop-wise to a solution of $POCl_3$ (4 m mol) in 20 ml dry benzene. The reaction mixture stirred for 12h at ambient temperature, then the solution of 2-aminopyridin(1 m mol) in 50 ml dry benzene added in several portions. The resulting mixture refluxed for 44 h at 75 ºC. The precipitate dissolved in water and NaOH 25% to bring the solution pH to about 14, followed by extraction with benzene. The organic layer evaporated in vacuum.

pale brown. Yield :(0.167 g, 87%); m.p. 120-122 °C. Selected IR data (KBr, υ_{max} [cm^{-1}]:3421, 3170, 2927, 1632, 1567, 1386; ^{1}H- NMR (250 MHz, DMSO-d_6) δ : 8.11-8.09 ppm (1H, t, Ar-H), 7.50-7.43 ppm (2H, m, Ar-H), 6.69-6.54 ppm (m, 3H, Ar-H), 2.95-2.51 ppm (m, 18H, CH_3), UV-Vis (DMSO): λ_{Max}=280, 310 nm.

2.3 General Preparation of Metal Complexes

The metal complexes were prepared by the addition of a hot methanol solution of the appropriate metal salt (1 mmol) to the hot solution of the guanidine ligand (2 mmol) in the same solvent (25 mL) under inert atmosphere of nitrogen. The resulting mixture was refluxed for 2-3 h. The solid product was filtered, washed with methanol and dried in vacuum desiccator.

Bis(1,1,3,3-tetramethyl-2-(pyridin-2-yl)guanidine) zirconium (ZrL_2)

White solid; Yield: (0.305 g, 70%); m.p.>300 °C. Molar conductance in DMSO: 10. Selected IR data (KBr, cm^{-1}): 3430, 2998, 2913, 1659, 1437, 703, 670. UV-vis (DMSO): λ_{Max}= 240, 300 nm.

Bis(1,1,3,3-tetramethyl-2-(pyridin-2-yl)guanidine)Zinc (ZnL_2)

Pale yellow solid; Yield: (0.267 g, 75%); m.p.>300 °C. Molar conductance in DMSO: 12. Selected IR data (KBr, cm-1): 3437, 2996, 2913, 1660, 1437, 700, 669. UV-vis (DMSO): λ_{Max}= 360, 310, 350 nm.

Bis(1,1,3,3-tetramethyl-2-(pyridin-2-yl)guanidine)cadmium (CdL_2)

Creamy solid; Yield: (0.343 g, 65%); m.p.>300 °C. Molar conductance in DMSO: 8. Selected IR data (KBr, cm^{-1}): 3425, 2999, 2915, 1657, 1437, 705, 609. UV-vis (DMSO): λ_{Max}= 250-300 nm.

2.4 Antibacterial Screening

Escherichia coli (ATCC: 25922), *Serratia marcescens* (ATCC: 13880) as gram negative bacteria as well as, *Bacillus sabtilis* (ATCC: 6633) and *Staphylococcus aureus* (ATCC: 6838) as gram positive bacteria were used for the test of antibacterial activity of synthesized compounds. All bacteria strains were maintained as stock strains in Microbank cryovials and kept at -80 °C until used. Microorganisms were cultured onto Muller Hinton Agar (MHA) plate and incubated for 18-24 h at 35 °C. The density of bacteria cultures required for the test was adjusted to 0.5 McFarland. Disk diffusion method according to standard method was applied for the antibacterial activity (Shahi et al., 2015). Tetracycline, impeneme and cephradine were used as standards drugs for antibacterial measurements. The compounds (0.02 g) were dissolved in 1 mL DMSO. A bacterial culture (which has been adjusted to 0.5 McFarland) was used to lawn Hinton agar plates using a sterile swab. The discs had been impregnated with synthesized compounds were placed on the Muller-Hinton agar surface. DMSO showed no activity against any bacterial strains. After incubation for 18-24 h at 35 °C, the diameter of each zone of inhabitation was measured (mm). The results are presented in Figure 1.

3. Results

In this research work Zirconium(II), Zinc(II) and Cadmium(II) metal complexes of 1,1,3,3-tetramethyl-2-(pyridin-2-yl) guanidine have been prepared to explore their antibacterial properties. The complexes were prepared by adding methanol solution of metal salts to methanol solution of guanidine ligand in stoichiometric ratio 1:2. Table 1 shows the physical properties of ligand and its metal complexes. The molar conductivity of complexes was also calculated.The molar conductance values of all the complexes were in the range 8-12 siemens, which indicate the complexes are non-electrolytes. The method for synthesis of ligand and its complexes and their proposed structures is illustrated in Scheme 1.

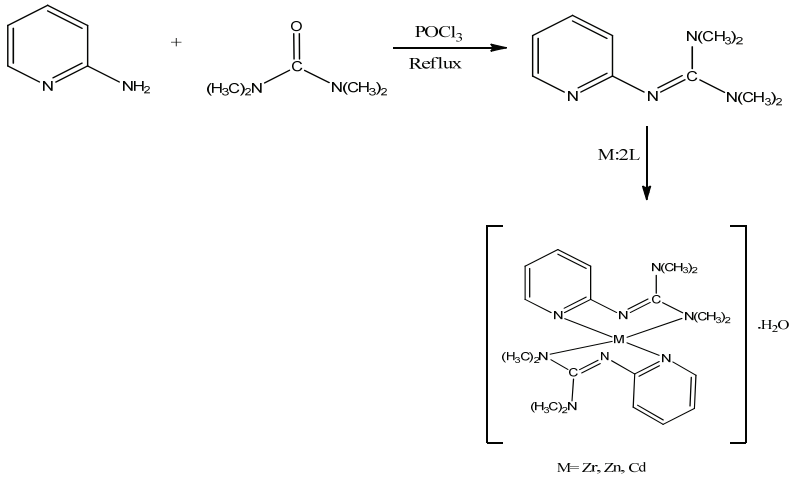

Scheme 1. Method for synthesis of guanidine ligand and its metal complexes

Table 1. Physical properties of ligand and its metal complexes

Compounds	Molecular formula	Color	Yield%	Molar conductance	Melting point °C
L	$C_{10}H_{16}N_4$	Pale brown	87	-	120-122
ZrL_2	Zr $C_{20}H_{34}N_4O$	white	70	10	> 300
ZnL_2	Zn $C_{20}H_{34}N_4O$	Pale yellow	65	12	> 300
CdL_2	Cd $C_{20}H_{34}N_4O$	creamy	75	8	> 300

3.1 Spectral Studies

In the ^{1}H-NMR spectrum of guanidine ligand, aromatic protons are appeared at 8.11-6.54 ppm as multiples and CH_3 aliphatic protons are observed as multiples in 2.95-2.51 ppm.

In the FTIR spectrum of parent ligand, C-H (aromatic) and C-H (aliphatic) bands are observed in 3100 and 2927 cm^{-1} respectively. The C=N frequency appear in 1632 cm^{-1} which confirm the formation of guanidine ligand. The FTIR spectra of ligand and its metal complexes were compared to characterize the metal complexes. In all the complexes C-H (aromatic) and C-H (aliphatic) bands are shifted to lower wavenumbers. The C=N peaks in complexes appear in the range 1657-1660 cm^{-1}. In the FTIR spectrum of parent ligand, the C-N groups are observed in the range 1386-1220 cm^{-1} and these peaks shifted to the lower wavenumbers in all the metal complexes, which confirm the ligand is bonded to the metal ions through the nitrogen atoms. Also the Zr-N, Zn-N and Cd-N frequencies appear in 670, 669 and 669 cm^{-1} respectively. The appearance of broad peaks in the range 34372-3430 cm^{-1} in all the complexes indicate the presence of H_2O in the structure of all the compounds.

The electronic absorption spectra of the parent ligand and its metal complexes were recorded at ambient temperature using DMSO as the solvent. Electronic absorption of the free ligand shows bands at 280 and 310 nm which is assigned to $\pi \rightarrow \pi^*$ and $n \rightarrow \pi^*$ transitions, respectively. In the electronic spectra of all the metal complexes slight shifts are observed in these transition to the lower wavelength compared to the parent ligand. The Cadmium (Ⅱ) complex shows a broad band in the range 250-300 nm , Zirconium (Ⅱ) complex shows peaks in the range 240 and 300 nm and Zinc (Ⅱ) complex shows absorptions in the regions of 260, 310 and 350 nm.

The mass spectra of the complexes are in good agreement with the proposed structures. The molecular ion peaks for the Cadmium(II), Zirconium(II) and Zinc(II) complexes observed at m/z= 514, 499 and 467 respectively, are equal to their molecular mass. The other peaks in the mass spectrum were attributed to the fragmentation of the complex obtained from the rupture of different bonds inside the molecule.

3.2 Biological Screening

The antibacterial activity of synthesized compounds were evaluated against two gram positive (*Bacillus sabtilis, Staphylococcus aureus*) and two gram negative (*Escherichia coli, Serratia marcescens*) bacterial strains using disc diffusion method. All the synthesized compounds dissolved in DMSO to evaluate their antibacterial activity. DMSO showed no antibacterial activity against the species. The susceptibility of ligand and its metal complexes compared to tetracycline, imipenem and cephradine as standard antibiotic drugs. The results are shown in Figure 1. The results indicate that the metal complexes have higher antibacterial activity when compared to the parent ligand. This phenomenon can be explained on the basis of chelation theory (Pasdar et al., 2017). As can be seen in Figure 1 the

guanidine ligand has moderate antibacterial activity. The diameter inhabitation zones of ligand are in the range 10-12 mm. Among the studied metal complexes the CdL_2 has higher antibacterial activity. The metal complexes showed more effective activity on *S. marcescens* compared to other pathogens.

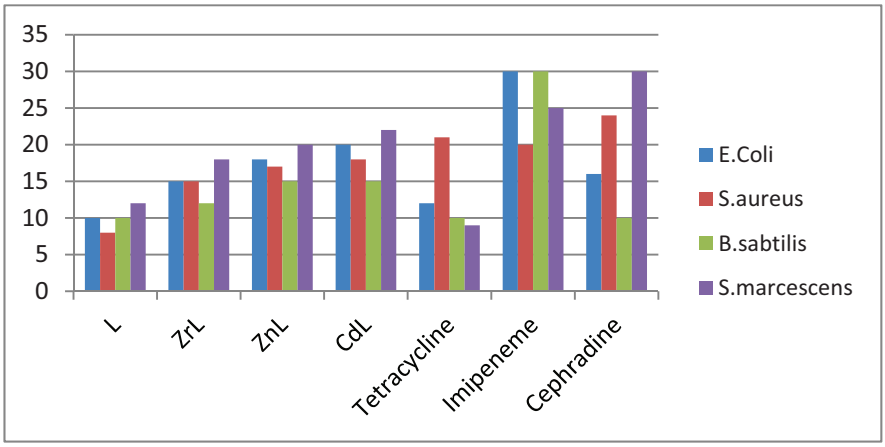

Figure 1. Graphical presentation of inhabitation zone diameter (mm) of ligand and its metal complexes

4. Conclusion

In this paper, we report on the synthesis of Cadmium (II), Zirconium (II), and Zinc (II) complexes with 1,1,3,3-tetramethyl-2-(pyridin-2-yl) guanidine ligand. They were characterized by several spectroscopic methods. Square planner geometry was assigned for all the complexes. The antibacterial activities were screened for all the compounds by disc diffusion method. The Cadmium complex demonstrated higher antibacterial activity compared to other compounds.

References

Bahareh, B., Naser, F., Neda, F., & Sara, H. (2017). Synthesis of some derivatives of 4-phenyl-1,3-dihydro-2H-imidazle-2-thion using ionic liquid as catalyst and evaluation of their antimivrobial activity. *Inter. J. Chem*., *9*, 45-51. https://doi.org/10.5539/ijc.v9n2p45

Cesme, M., Golcu, A., & Demirtas, I. (2015). New metal based drugs: Spectral, electrochemical, DNA-binding, surface morphology and anticancer activity properties. *Spectrochim. Acta. A*., *135*, 887-993. https://doi.org/10.1016/j.saa.2014.06.144

Foroughifar, N., Leffek, K. T., & Lee, Y. G. (1993). Synthesis and basicity of 2-N-quinolyl-and 2-N-isoquinolys-1,1,3,3-tetramethylguanidines, *Can. J. Chem.*, *71*, 164-169. https://doi.org/10.1139/v93-023

Ghulam, M., Muhammad, K. R., Amin, B., Masahiro, E., Muhammad, S., Marcel, G., … Bushra, M. (2012). *Eur. J. Med. Chem*., *48*, 26. https://doi.org/10.1016/j.ejmech.2011.11.029

Hedayati, B., Pasdar H., & Foroughifar, H. N. (2016). Novel dinuclear metal complexes of guanidine –pyridine hybrid ligand: synthesis, structural characterization and biological activity. *Biointerface Res. Appl. Chem*., *6*, 1842-1846.

Manetti, F., Castagnolo, D., Raffi, F., Zizzari, A. T., Rajamäki, S., Arezzo, S. D., … Botta, M. (2009). Synthesis of new linear guanidines and macrocyclic amidinourea derivatives endowed with high antifungal activity against Candida spp. And Aspergillus spp, *J. Med. Chem., 52*, 73-76. https://doi.org/10.1021/jm900760k

Mojgan, A., Naser, F., Hoda, P., & Hassan, M. (2016). Facile green one-pot synthesis of novel thiazolo[3,2-a] pyrimidine derivatives using Fe3O4@L-arginine and their biological investigation as potent antimicrobial agents. *Appl. Organomet. Chem*. https://doi.org/10.1002/aoc.3683

Pasdar, H., Foroughifar, N., & Hedayati, B. (2017). synthesis, characterization and antibacterial activity of Co(II), Ni(II), Mn(II), Cu(II) and Zn(II) complexes with 2-amino, 7,7-dimethyl-5-oxo-4-chlorobenzen 5,6,7,8-tetrahydro-4H-chromone3-carbonitrile. *Biotechnology and Biopharma*, *1*, 63-70.

Qian, L., Guan, Y., He, B., & Xiao, H. (2008). *Polymer, 49*, 2471. https://doi.org/10.1016/j.polymer.2008.03.042

Shahi, M., Foroughifar, N., & Mobinkhaledi, A. (2015) Synthesis and antimicrobial of some tetrahydro quinolone and pyrano[2,3-d] pyrimidine derivatives. *Iran J. Pharm. Res*., *14*, 757-763.

Copyrights

International Journal of Chemistry; Vol. 9, No. 3; 2017
ISSN 1916-9698 E-ISSN 1916-9701
Published by Canadian Center of Science and Education

Comparative Structural Modeling of Vitamin D_3 Containing Sulfur, Selenium and Tellurium

Petr Melnikov[1], Ana Nogueira Gaúna[1], Lourdes Z. Zanoni[1], Lincoln C.S. de Oliveira[2], Valter A. Nascimento[1]

[1]School of Medicine of the Federal University of Mato Grosso do Sul/UFMS, Brazil

[2]Institute of Chemistry of the Federal University of Mato Grosso do Sul/UFMS, Brazil

Correspondence: Valter A. Nascimento, School of Medicine, Federal University of Mato Grosso do Sul/UFMS, Caixa Postal 549, Campo Grande/MS, Brazil. E-mail: aragao60@hotmail.com

Received: May 24, 2017 Accepted: June 11, 2017 Online Published: June 22, 2017

doi:10.5539/ijc.v9n3p53 URL: https://doi.org/10.5539/ijc.v9n3p53

Abstract

The comparative structural modeling of vitamins D_3 containing sulfur, selenium and tellurium in oxygen site has provided detailed information about the bond lengths and bond angles, filling the gap in the structural characteristics of virtual VD_3 variants. The investigation using the molecular mechanics technique with good approximation confirmed the information available on X-ray refinements for the natural VD_3. It was shown that Ch-H and Ch-C bond lengths grow in parallel with the increasing chalcogen ionic radii and practically insensitive to the presence of the organic moiety. These findings demonstrate a higher polarity of VD_3S-H, VD_3Se-H and VD_3Te-H as compared to VD_3. It maybe suggested that enhanced polarity can have a positive impact on hydroxylation processes.

Keywords: vitamin D_3, sulfur, selenium, tellurium, modeling

1. Introduction

Vitamin D_3 or VD_3 [cholecalciferol; 9,10-Secocholeasta-5,7,10(19) – trien-3β-ol)] is a truly remarkable compound as it is both an essential nutrient and steroid prohormone that has a wide variety of biologic effects on the human body as its receptors are present practically in every tissue and cell (Burtis, Ashwood, & Bruns, 2006). This is the parent member of the naturally occurring family of vitamins D, which are lipophilic molecules with low aqueous solubility that must be transported in the circulation bound to plasma proteins. VD_3 is produced in the skin on exposure of its precursors to the ultraviolet B portion of sunlight.

The complex network of roles, functions and effects makes this family a fascinating subject for protein chemists, biochemists, nutritionists and pathologists (Holick, 2010). Schematic representation of VD_3 molecular formula is given in Fig. 1

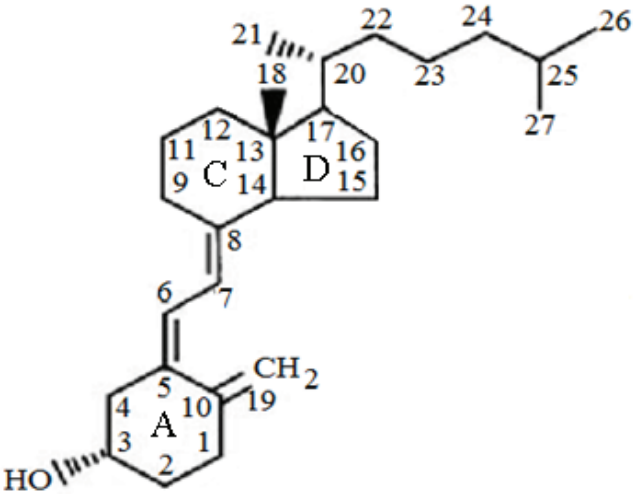

Figure 1. Schematic representation of VD_3 molecular formula (from (Holick, 2010) with modifications)

The structural formula of VD_3 contains four distinct moieties within the molecule: ring A (where a single O-H group is located), rings C and D, side chain and triene. In both the solid state and the solution the molecules are flexible and can

exist in many conformations at room temperature. In particular, ring A chair conformations are crucial for biological activity and mechanism of action of all D vitamins (Novak & Potts, 1997).

It is known that VD_3 exists as a dynamically equilibrating mixture of α and β chair conformers, the former with an equatorial disposition of the hydroxyl group and the latter with an axial orientation (Fig.2). The ratio between them was reported to be solvent and temperature dependent (Novak & Potts, 1997; Walsh et al., 2003).

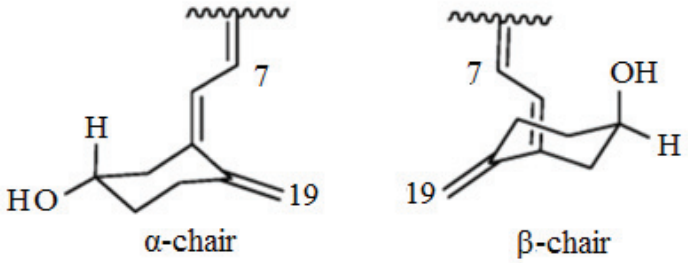

Figure 2. Two chairs conformations (from (Wang, Chun, Yu, & Mei, 2014) with modifications)

Although VD_2 has been known for almost ninety years (Blaner W. S.J Lipid Res. 2013; 54(7): 1716–1718, references therein), the structure of this important compound is not comprehensively characterized As for the crystal arrangement, it was concluded (Toan, Deluca, & Dahl., 1976) that VD_3 crystallizes in the orthorhombic system with the parameters given as ***a*** = 19.730Å; ***b*** = 7.340 Å and ***c*** = 35.716 Å. This crystalline compound exists in the form of a pseudo-homodimer and comprises a 1:1 complex of α- and β chairs. This modification has a close structural relationship with vitamin VD_2 (Hull, Leban, White, & Woolfson, 1976). In a recent structural studies (Wang, Zho, Qihui, & Mei, 2016), the hexagonal cell was proposed with the parameters given as ***a*** = ***b*** = 28.280Å and ***c*** = 5.932Å. The analysis of crystal structure data allowed suggesting that this polymorph contains exclusively α-chair conformation which is much prone to photo- or thermo-induced cyclization reactions than β conformer, and consequently it is more promising from the biochemical point of view (Wang, Chun, Yu, & Mei., 2014;). It should be born in mind that the value of the R factor that characterizes these investigations is of moderate accuracy, that is, 6.42 and 8.70%, respectively, and quite high even for large molecules.

At the same time, virtually nothing is known about VD_3 analogs containing the Ch-H group in which the oxygen analogs (Ch = sulfur, selenium and tellurium) replace this element in the classic hydroxyl group. Actually it was suggested elsewhere that such substitution may lead to uncommon biochemical and physico-chemical properties (Soriano-Garcia, 2004; Tiekink, 2012). In particular, selenium incorporated into natural bioactive compounds can act as an effective radiosensitizer to enhance the anticancer efficacy through induction of cancer cell apoptosis (Xie, He, Lai, & Zheng, 2014). Motivated by the potential utility of sulfur, selenium and tellurium against a number of diseases and pathological conditions, we have undertaken this study in order to fill the gap in structural characteristics of the two vitamins D. Such an approach enabled us in particular to perform modeling of glutathiones containing selenium and tellurium.

The purpose of this publication is to perform the structural simulations using the modern molecular modeling software to elucidate the similarities and differences between the substituted derivatives and natural compounds. All methods use empirical data to determine individual force constants, in particular, bond lengths and bond angles. Herein we consider VD_3 as an independent unit, and not as a part of numerous final metabolites like 25(OH) D_3 or $1,25(OH)_2D_3$ which act as circulating hormones.

2. Methods

A number of techniques exist for computerized modeling and calculating the potential energy of molecular systems as a function of coordinates of their atomic nuclei, neglecting explicit treatment of electrons. In this work, the structure of VD_3 was simulated using the standard SPARTAN ‘14 for Windows, Macintosh and Cinox software package which employ MMFF force field (Halgren, 1996). In vacuo calculations would bring out most of the underlying conformations without being side-tracked by the solvent used in the study or the limitations imposed by the densest packing. Strictly speaking, no conformational search routine guarantees that all conformers have been found, so the strategy chosen in this work was to study a reasonably representative set of the optimized geometries, in particular related to the ring A.

The geometry optimization was carried out in Cartesian coordinates using the Berny optimization algorithm, and adjusting the parameters until a stationary point on the potential surface was found. That means that for a small displacement the energy does not change within a certain amount, and the placements are successfully converged. It should be pointed out that we did not perform any systematic energy sampling for searching conformational energy

space. Angles and interatomic distances were evaluated by using special features of the program. The experimental parameters used for the comparisons were taken from databases and publications on X-ray structural refinements of VD_3 molecule.

3. Results and Discussion

To the best of our knowledge, VD_3 containing sulfur (VD_3S-H), selenium (VD_3Se-H) or tellurium (VD_3Te-H) have never been described. As a result, the reference compounds with the structural data available for comparisons are limited to the orthorhombic and hexagonal polymorphs of VD_3 (Wang, Zho, Qihui, & Mei, 2016), orthorhombic VD_2 (Hull, Leban, White, & Woolfson, 1976) and, to some extent, to the simplest chalcogen hydrides H_2S, H_2Se and H_2Te (NIST, 2014). Three structurally similar conformers, one for each chalcogen, were constructed and oriented in a comparable manner, ie, a longitudinal view and a view allowing visualization at 45º. The corresponding models are represented in Figures 3 – 6.

The geometries can be analyzed using the set of interatomic distances and angles listed in Table 1. Although the carbon atoms are connected in three "fused" rings, the interatomic distances for both single and double bonds are close to those calculated for the orthorhombic and hexagonal DV_3 from X-ray measurements (Wang, Zho, Qihui, & Mei, 2016; Toan, Deluca, & Dahl, 1976), which are our reference data. At the same time, and according to the Atlas of steroid structures (Griffin, Duax, & Weeks, 1984), they are also very similar to the distances found for a number of steroid arrangements with the group O-H attached to the ring A.

Figures 3-6 show that the main difference between the conformers containing O, S, Se and T is the torsion angle C (3) - Ch - H, thus reflecting the variety of distortions of the chairs A. At the same time, the angles in the main chain do not appear to be sensitive to the chalcogen nature, although the coincidences are not very precise. This feature can be easily explained by the existence of a number of conformational isomers with slightly different values of potential energy. In the solution and in the solid state, the degree of freedom may be to some extent limited due to the demands imposed by the formation of pseudo-homodimers. For example, for the orthorhombic form it was shown that the two conformers are alternately connected by a set of intermolecular O – H O – H interactions to form a one-dimensional chain arrangement [Wang, Chun, Yu, & Mei, 2014].

As concerns the key bonds Ch- H and Ch – C(3), they grow linearly with the Ch H distances in the simplest sulfides, selenides and tellurides (1.35, 1.46 and 1.69 Å, respectively) (Macyntyre, 1999), that is, are practically insensitive to the presence of the organic moiety. On the other hand, if the distances Ch – C(3) are arranged in a row S – Se – Te, there is a net linear dependence on this parameter (Fig. 7). These findings unequivocally demonstrate a higher polarity of VD_3S-H, VD_3Se-H and VD_3Te-H as compared to VD_3. So we can suggest that the improvement of polarity may have a positive impact on the processes of further hydroxylation, which culminate in the water soluble form suitable for the uptake by peripheral tissues (Quinn & Kagan, 1998; Jovičić, Ignjatović, & Majkić-Singh, 2012). Hence, selenium and tellurium analogs might enhance metabolic functions of natural VD_3.

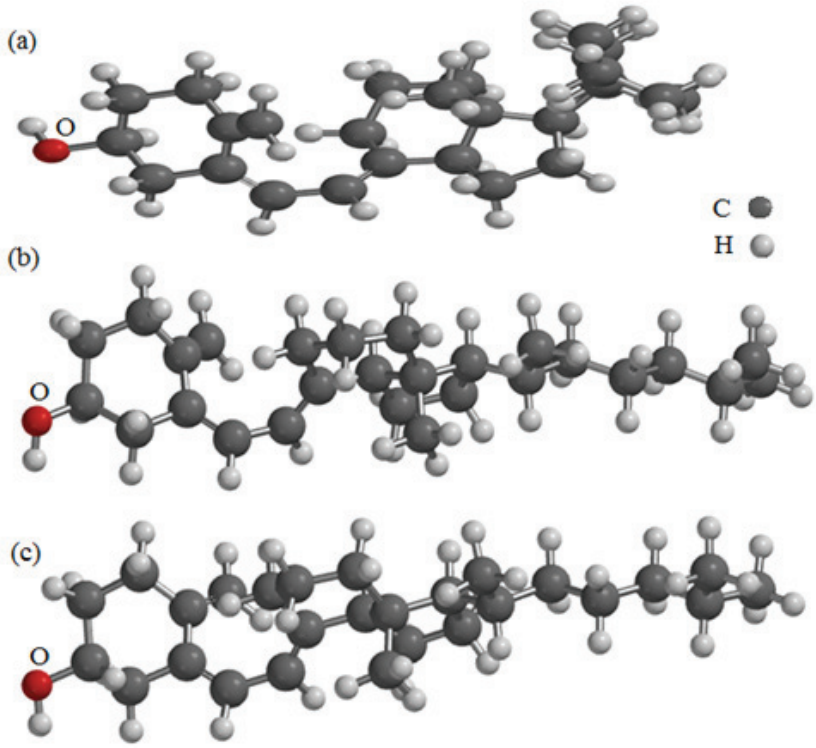

Figure 3. Structural models proposed for VD_3O-H, a – conformer 1, longitudinal view; b – conformer 2; longitudinal view; c – conformer 1, view permitting visualization at 45º

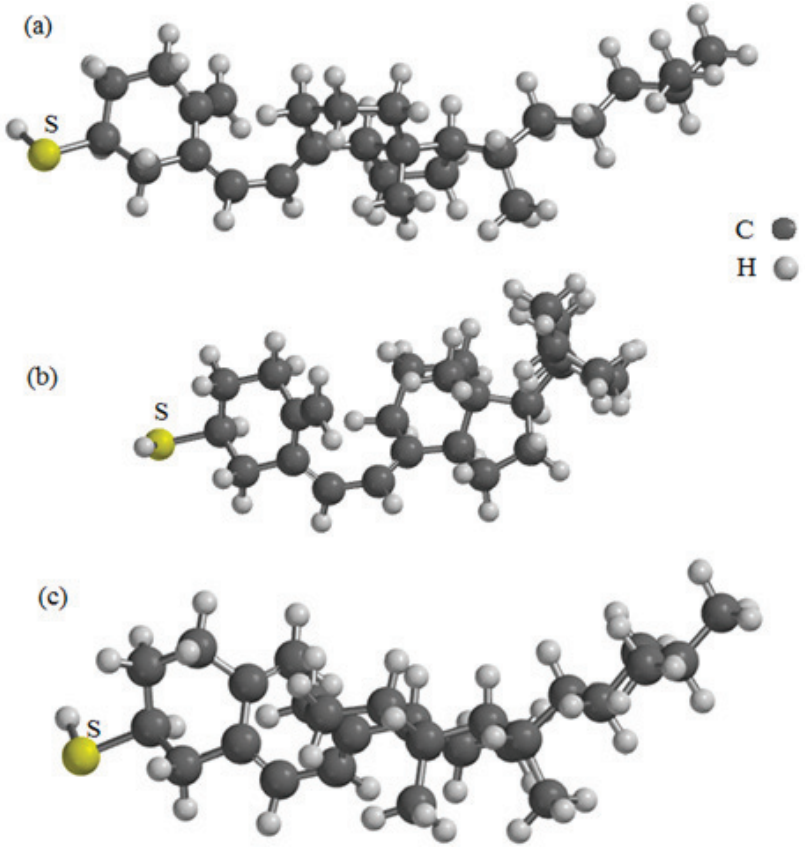

Figure 4. Structural models proposed for VD_3S-H, a – conformer 1, longitudinal view; b – conformer 2; longitudinal view; c – conformer 1, view permitting visualization at 45º

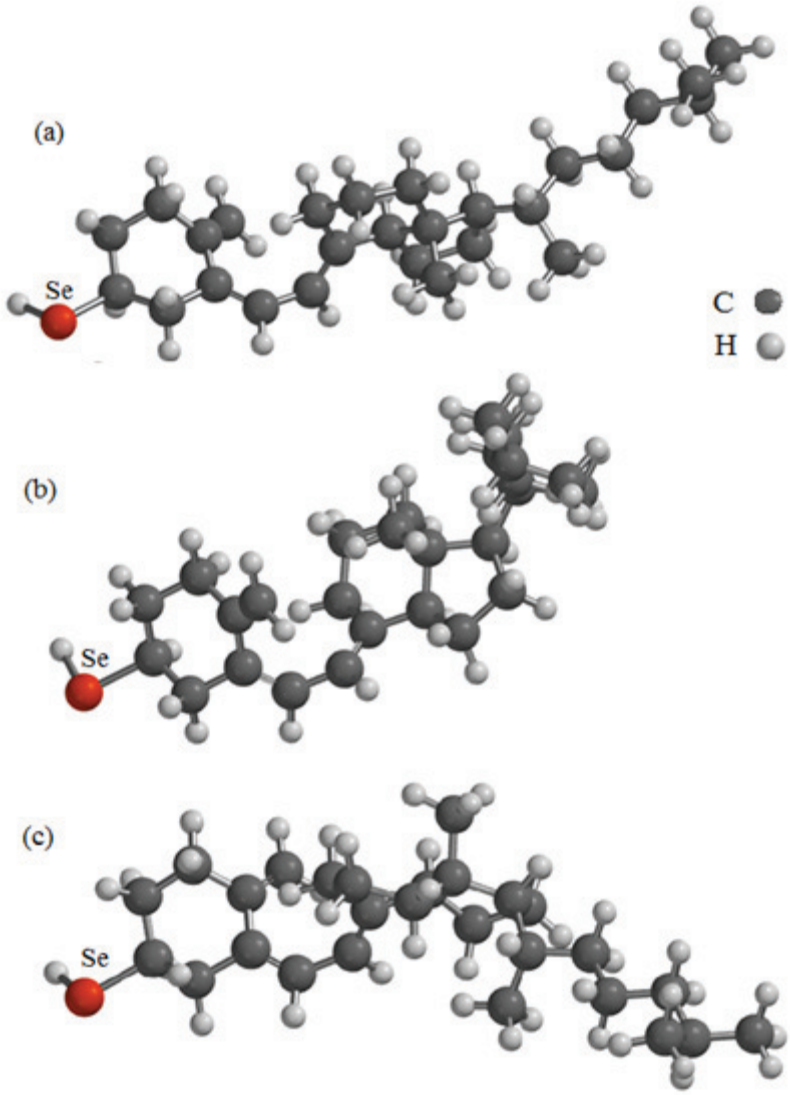

Figure 5. Structural models proposed for VD_3Se-H, a – conformer 1, longitudinal view; b – conformer 2; longitudinal view; c – conformer 1, view permitting visualization at 45º

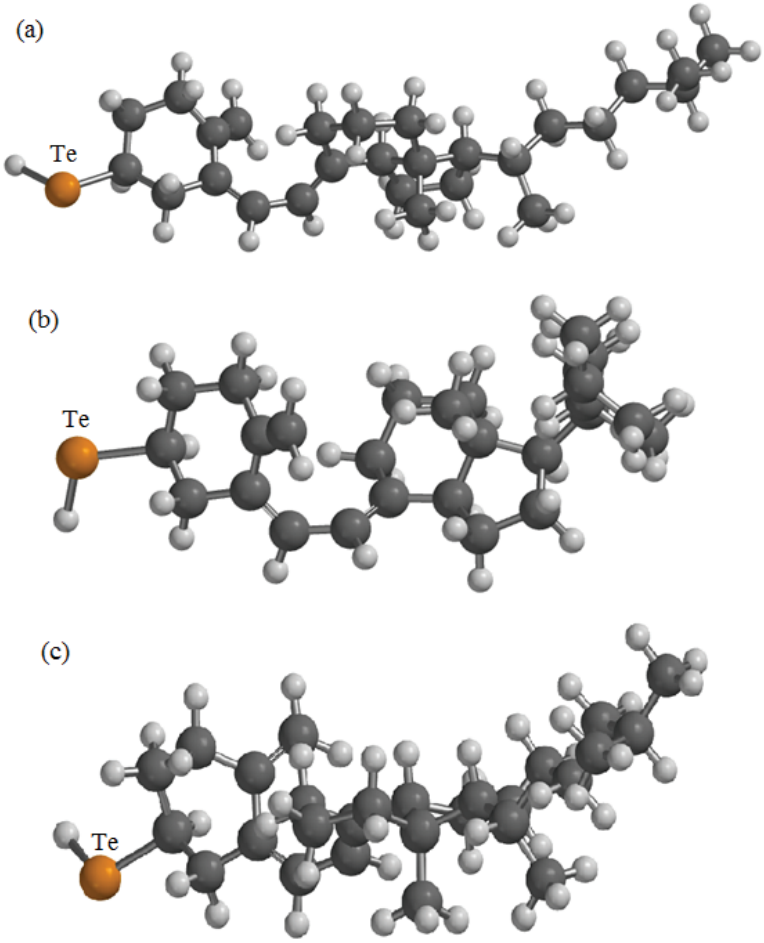

Figure 6. Structural models proposed for VD_3Te-H, a – conformer 1, longitudinal view; b – conformer 2; longitudinal view; c – conformer 1, view permitting visualization at 45º

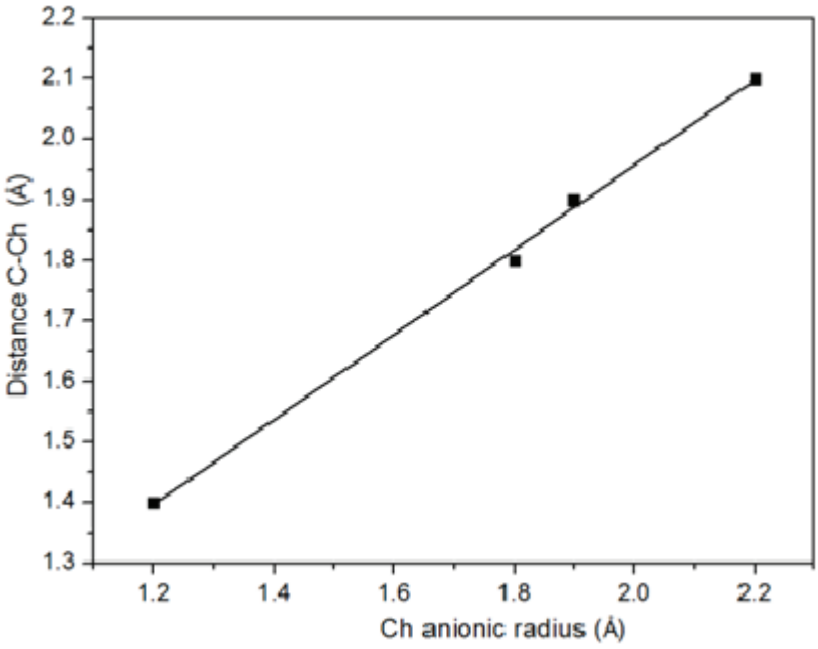

Figure 7. Dependence of the distances Ch-H on the chalcogen ionic radii

Table 1. Interatomic distances (Å) and potential energies (ua) calculated for substituted VD_3Ch-H

Distance	Ch					
	O	S	Se	Te	O [6]	O [7]
Ch - H	0.973	1.341	1.507	1.692	0.840	0.961
Ch-C3	1.427	1.828	1.937	2.103	1.433	416
C3-C2	1.533	1.537	1.530	1.530	1.503	1.564
C2-C1	1.532	1.535	1.532	1.532	1.540	1.527
C1-C10	1.509	1.508	1.509	1.509	1.496	1.479
C10-C19	1.342	1.342	1.342	1.342	1.339	1.329
C10-C5	1.466	1.465	1.466	1.466	1.483	1.448
C3-C4	1.533	1.536	1.529	1.528	1.519	1.508
C4-C5	1.521	1.524	1.520	1.320	1.515	1.506
C5-C6	1.349	1.349	1.349	1.349	1.341	1.338
C6-C7	1.447	1.447	1.447	1.447	1.454	1.436
C7-C8	1.347	1.347	1.347	1.348	1.325	1.336
C8-C9	1.519	1.519	1.519	1.513	1.515	1.572
C9-C11	1.534	1.534	1.534	1.532	1.526	1.518
C11-C12	1.537	1.538	1.538	1.532	1.522	1.559
C12-C13	1.546	1.546	1.546	1.543	1.530	1.532
C13-C17	1.563	1.563	1.563	1.577	1.554	1.523
C13-C18	1.548	1.548	1.548	1.555	1.520	1.537
C13-C14	1.556	1.556	1.556	1.570	1.557	1.518
C14-C8	1.513	1.513	1.513	1.525	1.550	1.548
C14-C15	1.525	1.525	1.525	1.533	1.525	1.502
C15-C16	1.532	1.532	1.532	1.518	1.538	1.533
C16-C17	1.558	1.558	1.558	1.536	1.550	1.572
C17-C20	1.559	1.559	1.559	1.564	1.546	1.512
C20-C21	1.532	1.532	1.532	1.533	1.530	1.547
C20-C22	1.554	1.554	1.554	1.554	1.520	1.522
C22-C23	1.535	1.535	1.535	1.534	1.610	1.514
C23-C24	1.534	1.534	1.534	1.533	1.415	1.533
C24-C25	1.540	1.540	1.540	1.540	1.514	1.258
C25-C26	1.531	1.531	1.531	1.531	1.516	1.569
C25-C27	1.529	1.529	1.529	1.529	1.518	1.489
C7-C19	3.232	3.230	3.226	3.322	3.232	3212
Energy	353.51	347.28	329.30	358.53		

Modeling is increasingly used in all aspects of drug candidates' with desired properties. Naturally, its results make available a large population of intermediate conformers. However, it is not the aim of this article to give an overview of their geometry and stabilities. Its objective is to draw attention to the possibility of changing the properties of vitamin D by means of the substitution of S, Se and Te for oxygen. Thus our data appear to be appropriate to fill the gap in structural characteristics of virtual VD_3 variants for further research.

4. Conclusions

For the first time, the comparative structural modeling of vitamin D_3 containing sulfur, selenium and tellurium in oxygen site has been carried out. It provided detailed information about the bond lengths and bond angles, filling the gap in the structural characteristics of virtual VD_3 variants. The investigation using the molecular mechanics technique with good approximation confirmed the information previously available on X-ray refinements for the natural VD_3. It was shown that Ch-H and Ch-C bond lengths grow in parallel with the increasing chalcogen ionic radii and practically insensitive to the presence of the organic moiety. These findings demonstrated a higher polarity of VD_3S-H, VD_3Se-H and VD_3Te-H as compared to VD_3. The main difference between the derivatives containing O, S, Se and T is the angle C (3) - Ch - H, thus reflecting a variety of distortions of α and β chairs. It may be suggested that increased polarity could significantly improve the metabolic functions of natural VD_3.

Acknowledgments

The authors are indebted to PROPP (Federal University of Mato Grosso do Sul, Brazil) for financial support and to Prof. Elizabeth Warner for useful discussions.

References

Blaner W. S. (2013). The fat-soluble vitamins 100 years later: where are we now? *Journal of Lipid Research*, *54,* 1716–1718. (and references therein). https://doi.org/10.1194/jlr.E039891

Burtis, C. A., Ashwood, E. R., & Bruns, D. E. (2006). Titzt Texbook of Clinical Chemistry and Diagnostics. Elsevier.

Griffin, J. F., Duax W. L., & Weeks, C. M. (Eds). (1984). Atlas of Steroid Structure, Vol. 2. Plenum Publishing Corp., New York.

Halgren, T. A. (1996). Merck molecular force field. I. Basis, form, scope, parameterization, and performance of MMFF94. *J. Comput. Chem., 17*, 490–519. https://doi.org/10.1002/(SICI)1096-987X(199604)17:5/6<490::AID-JCC1>3.0.CO;2-P

Holick, M. F. (2010). Vitamin D, Physiology, Molecular Biology and Clinical Applications. New York: Humana Press.

Hull, S. E., Leban, I., White, P. S., & Woolfson, M. M. (1976). The crystal and molecular structure of ergocalciferol (vitamin D_2), *Acta Crystallographica Section B, 32*, 2374–2381. https://doi.org/10.1107/S0567740876007796

Jovičić, S., Ignjatović, S., & Majkić-Singh, N. (2012). Biochemistry and metabolism of vitamin D / Biohemija i metabolizam vitamina D. *Journal of Medical Biochemistry*, *31*(4), 309-315. https://doi.org/10.2478/v10011-012-0028-8

Macyntyre, J. E. (Ed). (1999). Dictionary of Inorganic Compounds, CRC Press, Lomdon, Glasgow, New York.

National Institute of Standards and Technology [NIST], 2014.

Novak, I., & Potts, A. W. (1997). Electronic structure of vitamins D_2 and D_3. *Biochimica et Biophysica Acta (BBA) – Bioenergetics, 1319*. 86–90. https://doi.org/10.1016/S0005-2728(96)00118-1

Quinn, P. J., & Kagan, V. T. (Eds.). (1998). *Subcellular Biochemistry, 30*, Fat-Soluble Vitamins,., Plenum Press, N.Y.

Soriano-Garcia, M. (2004). Organoselenium compounds as potential therapeutic and chemopreventive agents: a review. *Current Medical Chemistry, 11*, 1657–1669. https://doi.org/10.2174/0929867043365053

Tiekink, E. R. (2012). Therapeutic potential of selenium and tellurium compounds: opportunities yet unrealized. *Dalton Transactions, 41,* 6390–6395. https://doi.org/10.1039/c2dt12225a

Toan, T., Deluca, H. F., & Dahl, L. F. (1976). Solid-state conformations of vitamin D3. *The Journal of Organic. Chemistry, 41*, 3476–3478. https://doi.org/10.1021/jo00883a035

Walsh, R. D. B., Bradner, M. W., Fleischman, S., Morales, L. A., Moulton, B., Rodríguez-Hornedo, N., & Zaworotko, M. J. (2003). Crystal Engineering of the compositions of pharmaceutical phases, *Chemical Communications,* 186–187. https://doi.org/10.1039/b208574g

Wang, J. R., Chun, Z., Yu, X. P., & Mei, X. F. (2014). Stabilizing vitamin D_3 by conformationally selective co-crystallization. *Chemical Communications, 50*, 855–858. https://doi.org/10.1039/C3CC47747A

Wang, J. R., Zho, B. Q., Yu, Q. H., & Mei, X. F. (2016). Selective crystallization of vitamin D3 to prepare novel conformational polymorphs with distinctive chemical stability. *Cryst. Eng. Commun., 18*, 1101–1104.

Xie, Q., He, L., Lai, H., Zheng, W., & Chen, T. (2014). Selenium substitution endows cysteine with radiosensitization activity against cervical cancer cells. *RSC Advances, 4*, 34210-34216. https://doi.org/10.1039/C4RA07031C

International Journal of Chemistry; Vol. 9, No. 3; 2017
ISSN 1916-9698 E-ISSN 1916-9701
Published by Canadian Center of Science and Education

The Mass Spectra Analysis for α-Ionone and β-Ionone

Abdalla Mustafa Walwil

Correspondence: Abdalla Mustafa Walwil, Arab American University, Department of Chemistry, Palestine.

Received: May 4, 2017 Accepted: May 30, 2017 Online Published: June 22, 2017

doi:10.5539/ijc.v9n3p61 URL: https://doi.org/10.5539/ijc.v9n3p61

Abstract

The presented work of this paper will be the first of a series of MS spectral analysis for some selected well-known compounds. In here the target molecules to have their MS spectra analyzed are α-Ionone and β-Ionone. The analysis will be in detail and show the mechanism of how the major fragments are formed in the mass spectrophotometer; hence, this paper is for educational purposes that could serve both students and instructors.

Keywords: α-cleavage, β-cleavage, Retro Diels-Alder, base peak, α-Ionone, MS spectrophotometer

1. Introduction

The Ionones, Damascones, and Damascenones are groups of compounds known as rose ketones. Ionones (α, ɤ) are aroma compounds found in some essential oils, a volatile oil of the plants from which they were extracted, such as rose oil. α-Ionone, (3*E*)-4-(2,6,6-trimethyl-2-cyclohexeneyl)-3-butene-2-one and ɤ -ionone, (3*E*)-4-(2,2-dimethyl-6-methylenecyclohexyl)-3-butene-2-one, are the main contributors to the aroma of roses and it is an important fragrance used in perfumery (Diez, Maros, Apesteguia, & Cosimo, 2009); whereas, β –Ionone, 3*E*)-4-(2,6,6-trimethyl-1-cyclohexenyl)-3-buten-2-one, is used in vitamin A synthesis. α-Ionone and β-Ionone combined are considered characteristic of the scent of violets (Leffingwell, 2005., Aiyeloagle, & Ekundayu, (2005).

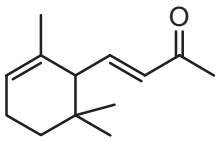

α-Ionone:

(3*E*)-4-(2,6,6-trimethyl-2-cyclohexeneyl)-3-butene-2-one

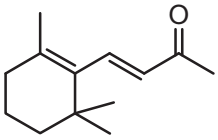

β-Ionone:

3*E*)-4-(2,6,6-trimethyl-1-cyclohexenyl)-3-buten-2-one

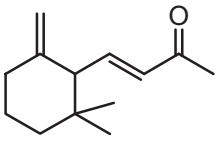

γ-Ionone:

3*E*)-4-(2,2-dimethyl-6-methylenecyclohexyl)-3-butene-2-one

Mass spectrometry is not a form of spectroscopy in the conventional sense, because no radiation is absorbed or released; however, mass spectrophotometer is considered by many chemists as the second most useful machine regarding structural elucidation of organic compounds. It is a high sensitive technique (I ng) of sample and contrary to the spectrophotometric techniques it is a destructive method.

A sample being studied will be vaporized once injected into the machine, then ionized, analyzed, detected, and recorded as MS spectrum respectfully (Solomons, Fundamentals of Organic Chemistry).

Each one of the five steps mentioned above takes place in the mass spectrometer in its five parts: sample inlet, ion source, mass analyzer, detector, and signal recorder.

The two major sources of ionization methods, converting the vaporized sample to ions, are Electron Ionization (EI) and Chemical Ionization (CI). The mass analyzer separates the ions based on their mass-to-charge ratio (m/z). The first and most used analyzer is called quadruple mass analyzer.

Upon the ions separation, the detector reads and counts them, and then a PC records and process the signals to give the mass spectrum (Vollhardt, & Schore, Organic Chemistry; Pavia, Lampman, Kriz, & Vyvyan, Introduction to Spectroscopy).

2. Spectral Analysis

As shown in Figure 1, the characteristic fragments of α-Ionone are the ones where the numbers are indicated on the signals. These signals represent the mass-to-charge ratio for the fragments. The method used in the ionization for the sample being studied is the EI Pavia, Lampman, Kriz, & Vyvyan, Introduction to Spectroscopy). Electron-impact-induced ionization of α-ionone involves loss of an electron from the lone pair, an unshared pair of electrons, or from the π bond leads to the formation of molecular ion plus the rest of fragments.

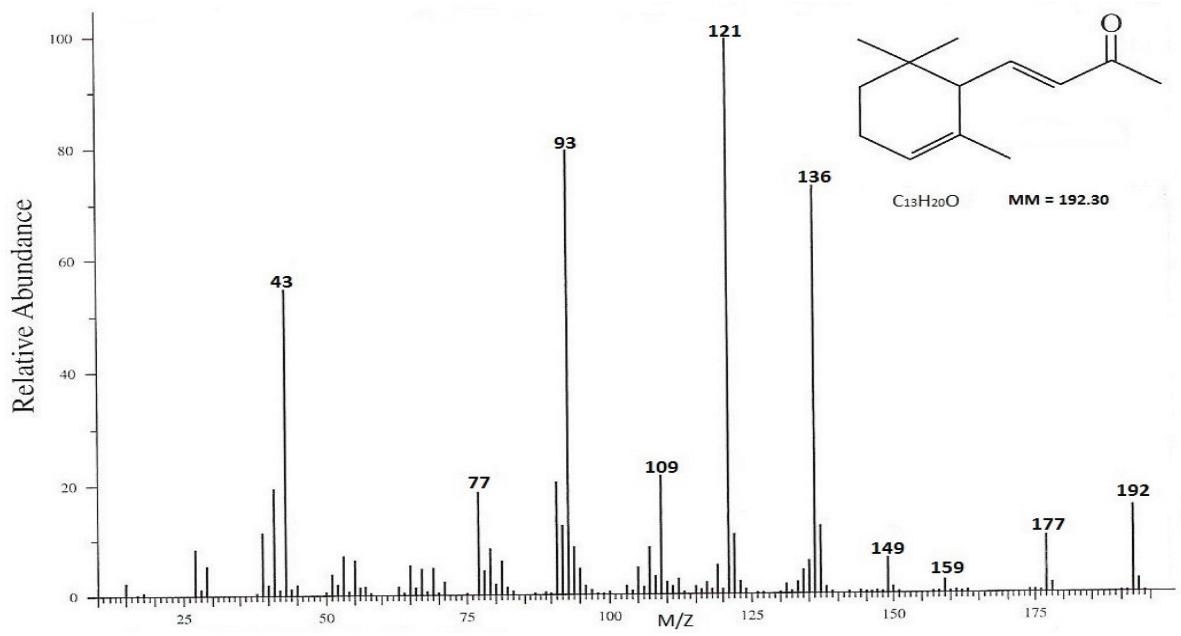

Figure 1. EI-MS of alpha-Ionone

3. The Structures of the Major Fragment Ions

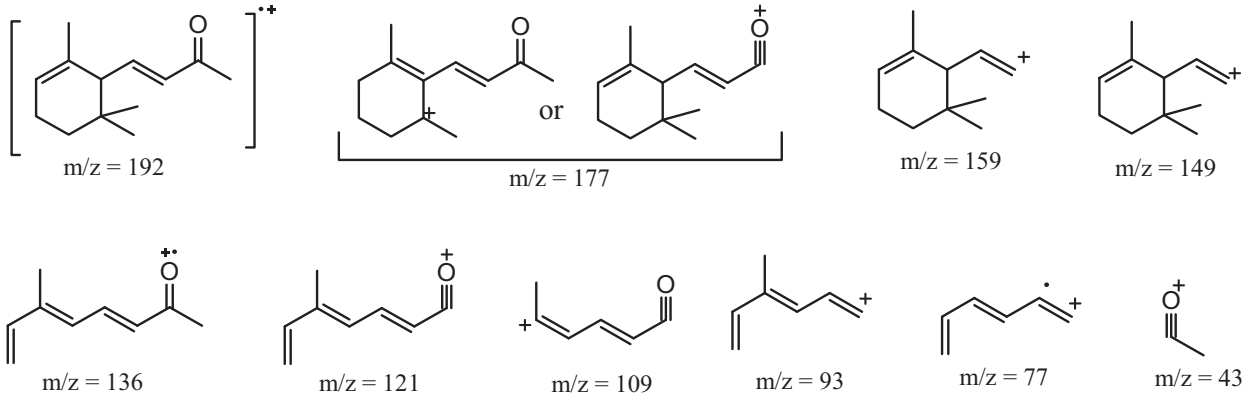

4. Fragmentation Mechanism

A. α-Ionone Fragmentation:

Once a sample of Ionone is introduced to the machine, it will be vaporized and then bombarded with a beam of high-energetic electrons (usually 70 eV, or about 1600 Kcal/mol) in the ionization chamber, an electron will be knocked off of the molecule leading to the formation of a positively charged ion called the molecular ion, $M^{+\cdot}$, as shown below

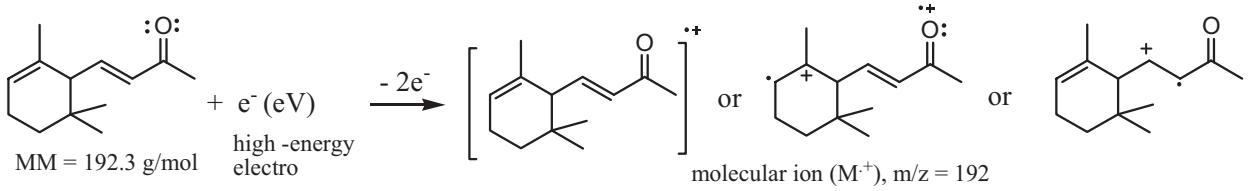

The molecular ions, and due to the high energy imparted in the ionization chamber, may break into smaller pieces (fragments). The Ionone ions may fractionate in various characteristic ways, where one fragment carry the charge and the other one remains uncharged. The following fragments are considered characteristic ones that are formed through α-cleavage, or β-cleavage, or Retro Diels-Alder Rearrangements.

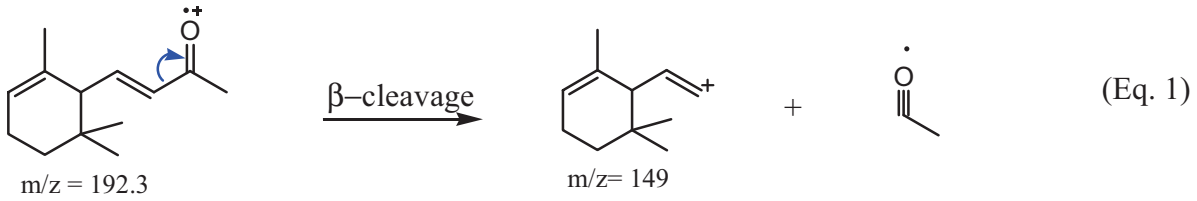

(Eq. 1)

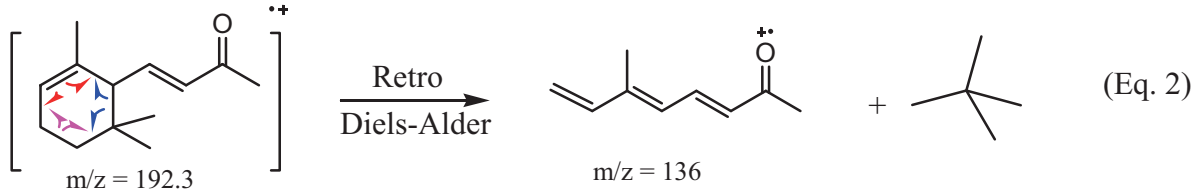

(Eq. 2)

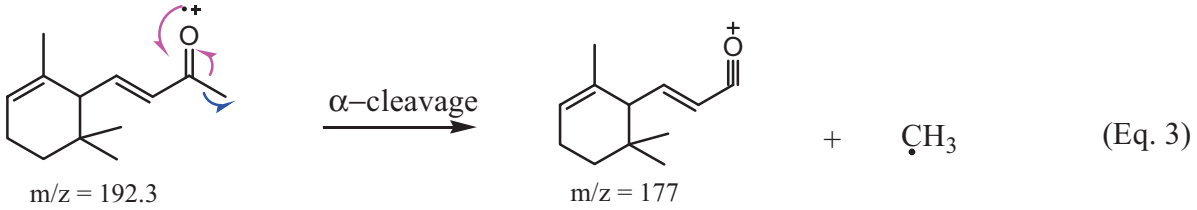

(Eq. 3)

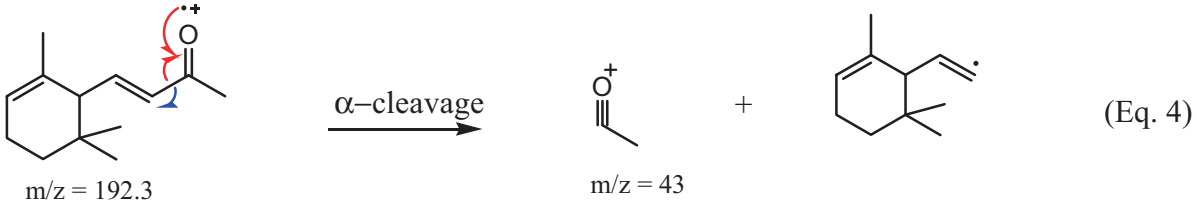

(Eq. 4)

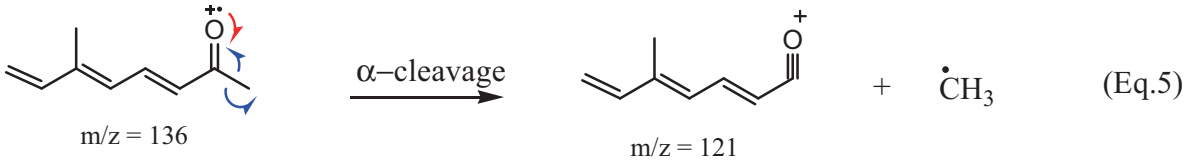

(Eq.5)

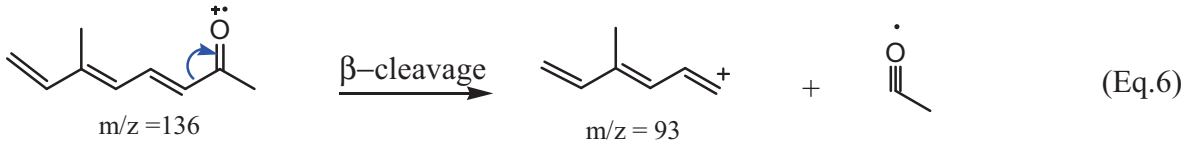

(Eq.6)

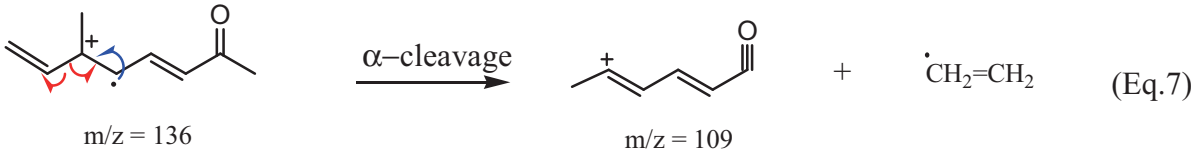

(Eq.7)

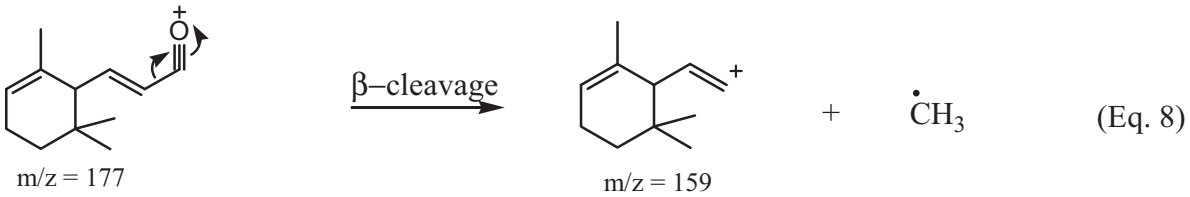

(Eq. 8)

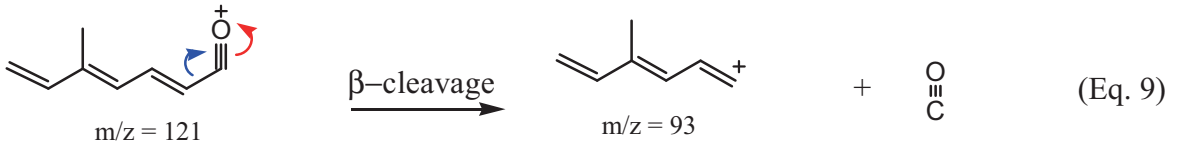

(Eq. 9)

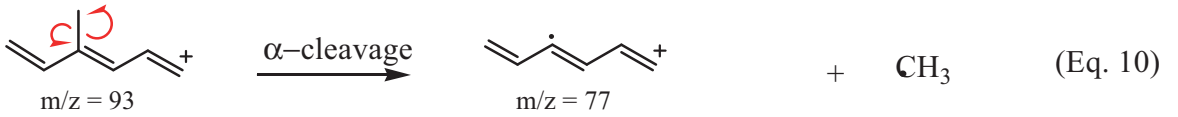

(Eq. 10)

B. β –Ionone Fractionation

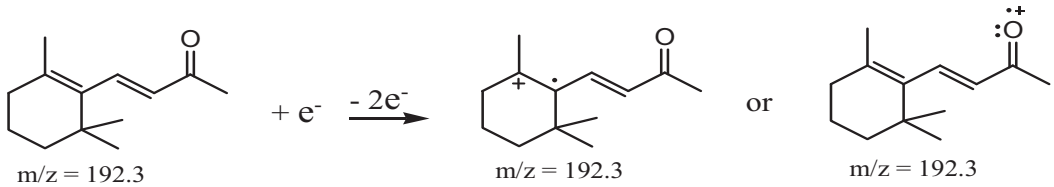

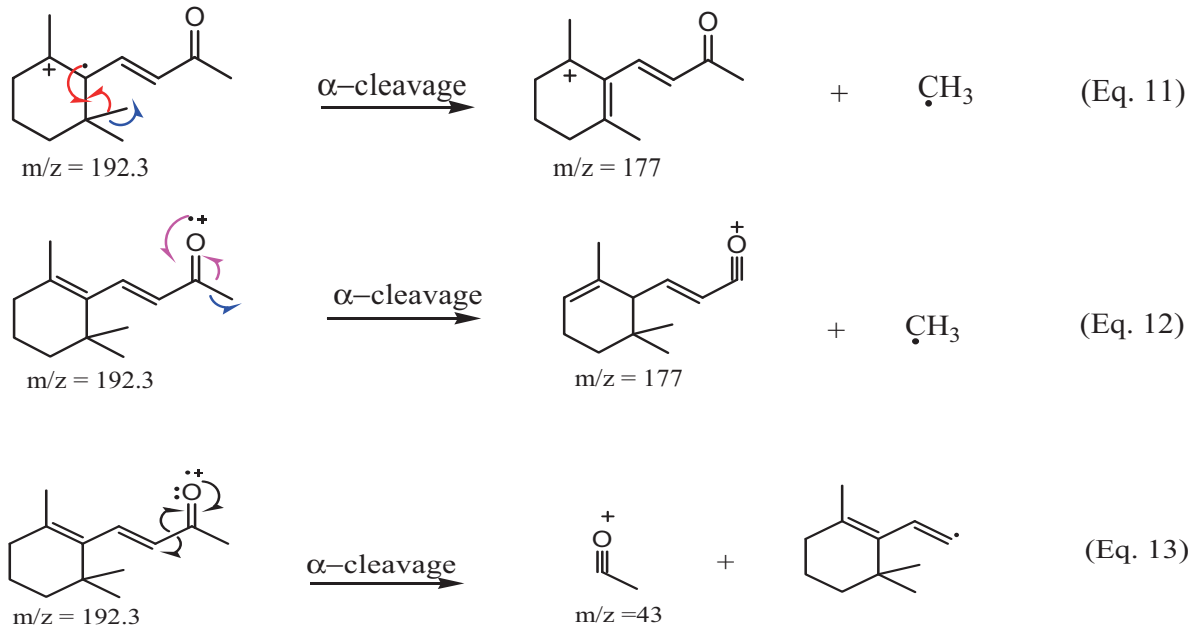

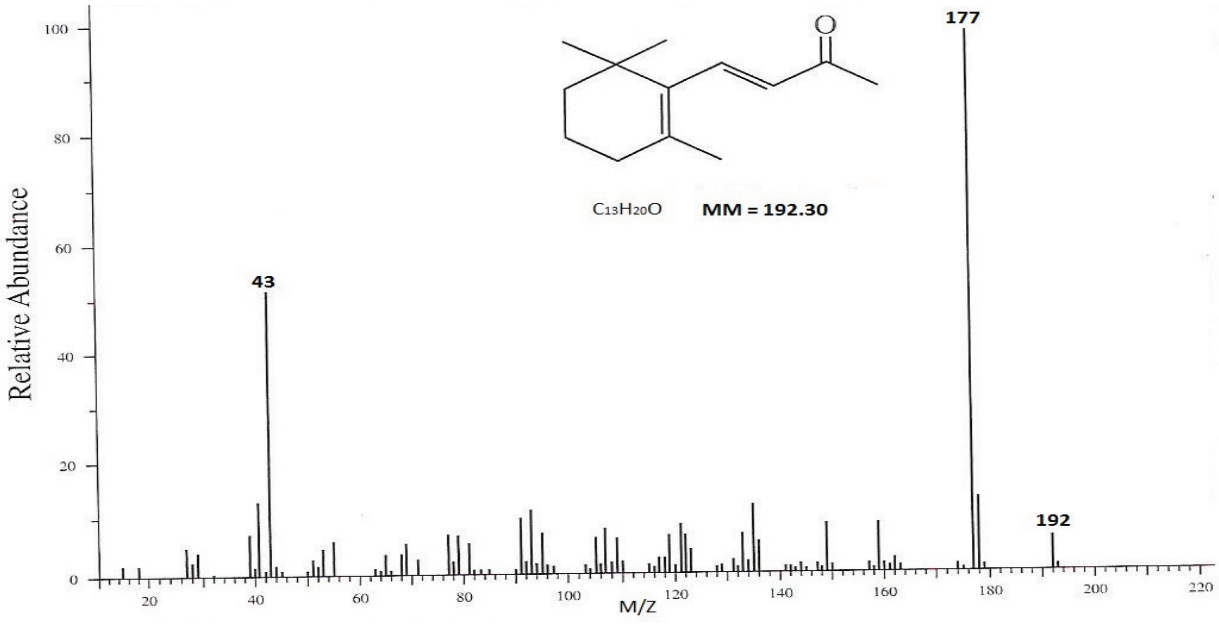

Figure 2. EI-MS of beta-Ionone

5. Discussion

Cleavage of molecular bonds in the EI-Mass Spectrometer will lead to charged and neutral fractions. There are well-known five characteristic cleavages that take place, such as, α-cleavage, β-cleavage (known as inductive cleavage), Retro Diels-Alder cleavage, Two-bond cleavage, and McLafferty cleavage (Rearrangement). Some or all of these characteristic fragmentations might take place depending on the compounds being fragmented.

Only the ionized fractions, usually carry one positive charge, can be detected and leads to singlet peaks as a function of their m/z ratio. The peak intensity depends on its number of ions formed; the most abundant ions will give rise to the tallest peak in the mass spectrum, called the base peak. The signal of molecular ion, M^+, if appears will be the highest m/z ratio of the spectrum not to confuse with M + 1 and M + 2 isotopic peaks.

Regarding α-Ionone's mass spectrum, the peak of weight m/z = 192 is the molecular ion peak and the smaller peak of weight m/z = 193 is the isotopic peak of M + 1.

The α-Ionone molecular ions undergo two major cleavages to lose the methyl acylium radical due to β-cleavage and 2,2-dimethyl propane due to Retro Diels-Alder cleavages respectively and form two fractions of the positively charged vinylcyclohexyl ion at m/z = 177 and 6-methyl-3,5,7-octatrienone ion at 136 respectively. (Eq. 1 & 2)

Furthermore, two α-cleavages of the molecular ion break into a methyl radical and the corresponding positively charged ion of weight m/z = 177 as well as the methyl acylium cation at m/z = 43 with the corresponding radical vinylcyclohexenyl moiety. (Eq. 3 & 4)

Usually, fragmentations take place not only on the molecular ion, $M^{\cdot +}$, level but also on the level of other fragments that might go a second or a third mode of fragmentations. The fragments at m/z = 136 undergo α- and β-cleavages to lose a methyl and acylium radicals respectively and form two fragments at m/z = 121 (the base peak, the most abundance fragment) and 93 respectively. (Eq. 5 & 6)

Besides the α- and β-cleavages of fragments at m/z = 136, it also loses a vinyl radical through α-cleavages to form fragments at m/z = 109. (Eq. 7)

The fragments at m/z = 177 undergo β-cleavages to lose a methyl radical and to form the vinylcyclohenium ion at m/z = 159. (Eq. 8)

Furthermore, the commonest fragment ion, m/z = 121, undergo β-cleavages to lose carbon monoxide and form another characteristic peak of weight m/z = 93. (Eq. 9)

Further cleavage of m/z = 93 leads to the loss of a methyl radical and the formation of the ionized fraction at m/z = 77 fraction. (Eq. 10)

The β –Ionone molecular ions undergo three major α-cleavages to lose methyl radical, methyl radical, and the radical moiety at m/z = 149 respectively and form the positively charged fragments at m/z = 177 & 177 & 43 respectively. (Eq. 9, 10, & 11)

For β-Ionone spectrum, only two major peaks are present at m/z = 177 and 43 comparing to several major ones for α-Ionone. Due to the absence of the fragment ions of weight m/z = 136, Retro Diels-Alder Rearrangement is prohibited which contributes to this low of fragmentations, hence, several peaks at m/z = 77, 93, 121, and 149 are missing or in low abundance. Also, and based on the MS-spectrum of β-Ionone, and since many of the fragmentation processes in mass spectrometry proceeds so as to form a stable carbocation, it indicates that the fraction moiety at ms/z = 177 is somewhat stable and it is the most abundance, hence, it is considered as the base peak.

6. Conclusion

In conclusion, I find it vital to make more MS-spectral analysis for more organic compounds and touch on all kinds of mechanisms that lead to various fragmentations. As you can see, the presented work only covered three typed includes alpha, beta, and Retro Diels Alder fragmentations. There are others such as McLafferty Rearrangements, Two-Bond Cleavage, and other special cleavages for alcohols and some compounds-containing carbonyl groups.

References

Aiyeloagle, O. O., & Ekundayu, O. (2005). *J. Essential Oil Bearing Plant, 8*(1), 360-369.

Diez, V. K., Maros., B. J., Apesteguia, C. R., & Cosimo, J. I. (2009). *Applied Catalysis A: General, 358*(1), 6700-6704.

Leffingwell, J. C. (2005). "Rosa damascena" Aroma from Carotenoinds – Rose. Leffingwell &Associates, 2014.

Pavia, D. L., Lampman, G. M., Kriz, G. S., & Vyvyan, J. R. Introduction to Spectroscopy, 4th Ed.Brooks/Cole, 484-458.

Solomons, T. W. Fundamentals of Organic Chemistry. 4th Ed. *Wiley & Sons,* 589-608.

Vollhardt, K. P., & Schore, N. E. Organic Chemistry/Structure and Function, 3rd Ed. W. H. Freeman and Company, 907-918.

International Journal of Chemistry; Vol. 9, No. 3; 2017
ISSN 1916-9698 E-ISSN 1916-9701
Published by Canadian Center of Science and Education

Determination of the Point of Zero Charge pH of Borosilicate Glass Surface Using Capillary Imbibition Method

Mumuni Amadu[1], Adango Miadonye[2]

[1]Dalhousie University, Department of Process Engineering and Applied Science (PEAS), Halifax Nova Scotia, Canada

[2]Chemical Engineering/Industrial Chemistry, Department of Chemistry, Cape Breton University, Nova Scotia, Canada

Correspondence: Mumuni Amadu, Dalhousie University, (PEAS), Halifax Nova Scotia, Canada. E−mail: mumuniamadu@hotmail.com; mm846771@dal.ca

Received: December 30, 2016 Accepted: June 5, 2017 Online Published: June 25, 2017

doi:10.5539/ijc.v9n3p67 URL: https://doi.org/10.5539/ijc.v9n3p67

Abstract

The point of zero charge pH of an oxide surface is a fundamental surface chemistry property or solids or metal oxides that determine the nature of interaction at the solid-aqueous solution interface. In colloid chemistry this physical parameter controls the evolution of the electric double layer as well as adsorption and desorption processes.

In colloid chemistry a number of methods have been used for the determination of the point of zero charge pH of an oxide surface. This ranges from titrimetric to radiation chemistry approach that deals with scanning electron microscopy.

In this study, the direct effect of aqueous solution acidity on the solid-liquid interfacial free energy and the consequence of this effect on spontaneous imbibition of aqueous solution into borosilicate glass have been exploited for the determination of the point of zero charge pH of this type of glass. What is new in this method is that while the traditional titration method relies on neutralization of surface charges, the present method relies on interfacial free energy changes due to aqueous solution pH changes and the effect of this on the wettability of borosilcate glass surface. Result of point of zero charge pH obtained from the present method has been compared with those obtained using traditional methods. The comparison shows close agreements and this proves the technique used in the present work as a novel method for the determination of the point of zero charge pH of oxide surfaces.

Keywords: pint of zero charge, spontaneous imbibition, contact angle, charge density, excess adsorption

1 Introduction

1.1 Relationship of Capillary Phenomenon to Contact Angle

The point of zero charge pH of an oxide or hydroxide surface is the pH of the aqueous solution in contact with it at which the net surface charge is zero (Sposito, 1998). It is a fundamental surface chemistry property that depends among other things on the dielectric permittivity of the material, metal to oxygen bond length and Pauling bond strength per unit length (Sverjensky, 1994).

A number of approaches have been used in the chemical engineering industry for the determination of this surface parameter. Yoon *et Al.,* (1979) developed a model to calculate this parameter. In this method, Pauling's electrostatic valence principle has been applied to describe the mechanism of surface charging of oxide surfaces in equilibrium with aqueous solutions. This approach has led to the presentation of an equation that can predict point of zero charge pH of oxide surfaces from crystallographic data. Dimitr (1994) showed that by adding electrostatic solvation theory to crystal chemical and electrostatic models the point of zero charge pH of crystalline substances can be quantified. This approach sums up the contributions of Gibbs free energy associated with proton solvation, electrostatic repulsion of protons by cations underlying the surface and electrostatic attraction of protons by oxygen anions near the surface.

Noh and Scwarz, (1989); Bourikas et al., (2003); and Kosmulski (2004) determined the point of zero charge pH by titrimetry. Eggleston and Jordan (1998) used scanning electron microscopy approach to determine the point of zero charge pH of oxide surfaces.

From interface thermodynamic perspective, the interfacial free energy of the system aqueous solution-oxide surface will be affected by the surface charge density due to polar contributions (Van Oss, Good, & Chaudhury, 1988). In view of surface charge density of oxide surfaces depending on pH, the wettability of the system oxide surface-aqueous

solution-vapor will depend on the surface charge density due to the dependence of solid-liquid interfacial tension on pH (Chatelier, Chan, Vasic, Gengenbach, & Griesser, 1995). Also, the extent of surface charging of an oxide surface at a given pH will depend on the difference between aqueous solution pH and the point of zero charge pH of the oxide surface. The objective of this paper is to use a novel approach with a completely different theoretical basis for the determination of the point of zero charge pH an oxide surface. Accordingly, this paper will exploit the oxide surface contact angle dependence on the pH of aqueous solutions for achieving this principal objective.

1.2 Motivation for This Work

1.2.1 Relationship of Capillary Phenomenon to Contact Angle

While other methods described above rely on particular principles to measure the point of zero charge pH of a solid surface, the motivation for the present work derives from the dependence sold-liquid interaction and adsorption phenomena (Barrow, Bowden, Posner, & Quirk, 1980) on the point of zero charge of the solid. Therefore, by invoking Gibbs excess adsorption theory, the effect of adoption and surface charge density on solid-liquid interfacial free energy which has a direct bearing on wettability can be explored. Lipmann (1875) recognized the contribution of externally added electrical field to the interfacial forces due to capillary. Integration of the effect of electric field/surface charge density provides a thermodynamic approach involving entropy maximization of the system vapor-liquid-solid. This approach has yielded modified equations for Laplace and Young equation (Digilov, 2000). Thus, for Laplace equation the following modification holds (Digilov, 2000):

$$\Delta P = \gamma_{LV}\left(\frac{1}{r_1}+\frac{1}{r_2}\right)+\frac{d\gamma_{LV}}{dn}-E_{lv}\sigma_{LV} \quad (1)$$

In which ΔP is Laplace pressure (Pa), γ_{LV} is the liquid vapor interfacial tension (N/m^2), r_1 is the inner radius of curvature of the interface (m), r_2 is the outer radius of curvature (m), n is the curvature (m^{-1}), E_{LV} is the normal to the liquid-vapor interface component of the existing electrostatic field and σ_{LV} is the surface charge density at the liquid vapor interface.

In Eq. 1, the first term in the right hand side is the normal Laplace pressure in the absence of electrostatic field. The second term measures the change of liquid-vapor interfacial tension with curvature due to the electrostatic contribution to the liquid-vapor interfacial tension. The third term is the obvious contribution to Laplace pressure due to electrostatic effect, which is related to the Lipmann effect due to the presence of charges.

For Young's equation, the following modification has been presented (Digilov, 2000):

$$\gamma_{SV}-\gamma_{SL}=\gamma_{LV}\cos\theta_q+\frac{n}{r}-E_{LV}\gamma_{SLV} \quad (2)$$

In which γ_{SV} is solid-vapor interfacial tension (N/m), γ_{SL} is solid liquid interfacial tension (N/m), γ_{LV} interfacial tension (N/m), θ_q is charge dependent contact angle (^{o}) and $E_{LV}\gamma_{SLV}$ is the specific electric driving force of the wetting line.

Equation 1 shows that in the absence of an electric field contribution, we get back to the original Laplace equation. Similarly, Eq. 2 shows that in the absence of an electric field we get back to the original Young's equation where we retain the first two terms on the right hand side of the equation. Here, the second term of the equation refers to the tension correction for Young's equation. Counting on the works of previous researchers, this paper is motivated to use the electrostatic contribution to wetting changes a step further by considering spontaneous imbibition capillary rise under varying pH conditions. This varying in aqueous solution pH is expected to cause variations in surface charge density, which is expected to cause contributions to Laplace and Young's equations similar to that dealt with by previous researchers. In this case, the variations in surface charge density and electric field will be due to ionization of surface hydroxyl functional groups (silanol) on borosilicate glass (Zhuravlev, 1987). The prime objective is to link contact angle and capillary rise to pH and to use this as the basis for determining the point of zero charge pH of Borosilicate glass surface through an appropriate mathematical model.

1.2.2 Dependence of Solid-Liquid Interfacial Tension on Aqueous Solution pH

In the system sold-liquid-vapor there are three fundamental interfacial tensions/energies. They are solid-liquid interfacial tension, liquid-vapor interfacial tension and solid-vapor interfacial tension (Liu, Yao, & Jiang, 2010): Each of

these tensions has two fundamental contributions. They are Lishfitz van der Walls forces and polar contribution, the latter sometimes called electron donor and electron acceptor contribution (van Oss *et al.*, 1988). Generally, polar contributions are pH dependent and for the solid-liquid interface the solid-liquid interfacial tension will consist of two contributions as (Chatelier, et al., 1995):

$$\gamma_{SL} = \gamma_{SL}^{0} + \gamma_{SL}^{ion} \quad 3a$$

Where:

γ_{SL}^{0} = component of solid-liquid interfacial tension at the point of zero charge pH

γ_{SL}^{ion} = free energy per unit area required to form surface charges from surface ionizeable or functional groups relative to the point of zero charge pH at the prevailing aqueous solution pH

The second term on the right hand side of Eq. 3 is pH dependent and strongly coupled to the point of zero charge and therefore, has electrostatic origin

1.2.3 Effect of Solid-liquid Interfacial Tension pH Dependence on Contact Angle

In petroleum engineering and allied disciplines, the theory of wettability quantifies this petrophysical parameter in terms of interfacial tensions between phases as (Liu, Yao, & Jiang, 2010):

$$\cos\theta = \frac{\gamma_{SV} - \gamma_{SL}}{\gamma_{LV}} \quad 3b$$

θ = contact angle

γ_{SV} = solid vapor interfacial tension

γ_{SL} = solid liquid interfacial tension

γ_{LV} = liquid vapor interfacial tension

Hence by recognizing the pH dependence of solid-liquid interfacial tension through the second term of Eq. 3 Young's equation can be modified as:

$$\cos\theta = \frac{\gamma_{SV} - \gamma_{SL}^{0} - \Delta F_{SL}^{ion}(pH)}{\gamma_{LV}} \quad 4$$

This equation shows the dependence of contact angle/wettability on the pH of aqueous solution. It simply means that minimum wettability or maximum contact angle will be attained when the pH dependent component of interfacial tension is a maximum, assuming other interfacial tensions remain constant.

1.3 Mathematical Model

1.3.1 Assumptions

If a capillary tube is dipped into an aqueous solution in a beaker it will rise until an equilibrium height is achieved (Martic, *et al*., 2002). The equilibrium height will depend on the contact angle of the system which reflects wettability. This means that with varying pH of the imbibing fluid, varying surface charge density created by varying pH induced ionization of surface hydroxyl functional groups will cause varying equilibrium heights. To exploit spontaneous capillary imbibition mechanism under varying pH conditions for determining the point of zero charge pH of Borosilicate glass, the following assumptions will be made to render the solid-liquid-vapor system composing of air, a capillary tube and a pH varying imbibing fluid similar to those used by other researchers:

1. At a given capillary rise equilibrium height, there is no heat transfer between the system and the surroundings (Digilov, 2000).

2. The cylindrical model is the simplest pore shape for the mathematical formulation of capillary imbibition and will be assumed in this work.
3. There is adsorption or reaction equilibrium between the walls of the capillary and the imbibing water leading to the formation of a uniform surface charge density
4. For a given charge density there is a mechanical equilibrium in accordance with Young's equation by integrating the electrostatic contribution (Chen, Chiu, & Weng, 2006)
5. Borosilicate glass has amorphous structure (Liu, Yuan, Yan, & Zhao, 2012) at initial aqueous solution pH it will have a net negative surface charge and subsequent adsorption of protons will occur with varying pH reduction

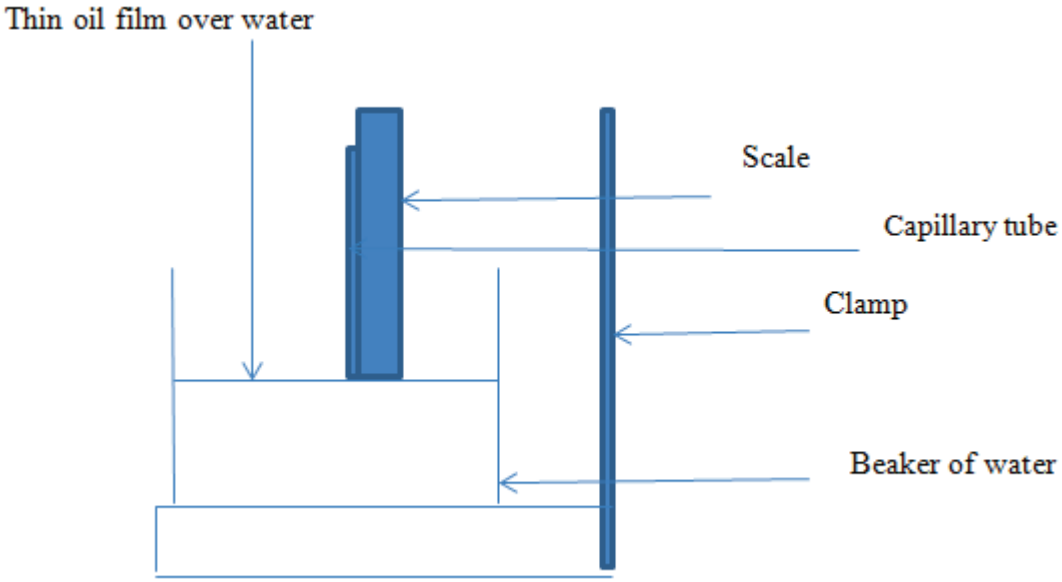

Figure 1. Schematics of capillary imbibition experiments

1.3.2 Mathematical Model Approach

Generally, the surfaces of metal oxides will have hydroxyl functional groups due to the dissociation and chemisorption of water molecules and chemisorption on the oxygen atom on the surface of the oxides (Refson, *et al.*, 1995). For silica surface this leads to the formation of silanols with specific surface densities (Zhuralev, 1987). The surface silanols of silica will undergo acidic and basic ionization reactions in accordance with the following order respectively (Peng & Barteau, 1991):

$$SOH + H_S^+ = SOH_2^+ \quad \text{I}$$

$$SO^- + H_S^+ = SOH \quad \text{II}$$

In which SOH is a surface hydroxyl species, SO^- is a surface deprotonated species, SOH_2^+ is a surface protonated species, H_s^+ is proton near the surface of the solid (silica) and S is a metal attached to a crystal lattice sometimes written as $S \equiv O$

The proton near the surface H_s^+ can be linked to bulk solution hydrogen ion concentration by the work done in transferring a proton from bulk solution to the surface of the solid under the electric field potential due to the surface charge density (Sverjensky, 1994)

Reaction I is typical of acidic conditions while reaction II is typical of basic conditions. Therefore, for a given solution pH, a definite surface charge density exists on the surface of borosilicate glass due to the ionizations reactions. The

objective of the following section is to link this surface charge density to aqueous solution pH and contact angle and to further exploit it as the basis for achieving the principal objective of this paper.

Following Carré, *et al.* (2003), the mechanical equilibrium for the system carbon dioxide, brine and aquifer rock surface can be written as before in accordance with the following equation:

$$\gamma_{VL} Cos\theta = \gamma_{SV} - \gamma_{SW} \quad 5$$

In which γ_{LV} is liquid-vapor interfacial tension [N/m], γ_{SV} is solid-vapor interfacial tension [N/m] γ_{SW} is solid-water interfacial tension [N/m] and θ is the contact angle of the system

Normally, when hydroxyl functional groups such as silanols are in contact with water they will either adsorb protons or ionize depending on the ambient pH. When an acidic solution is added (such as carbon dioxide dissolution and carbonic acid formation) to change the pH, the interfacial tension between water and vapor phase can be considered constant, but the contact angle will change. This is because the contact angle is a function of three interfacial tensions namely the vapor-liquid interfacial tension, the vapor solid interfacial tension and the solid liquid interfacial tension. Literally, the addition of the acid causes pH changes that upset the surface charges of the solid and this impact the solid-liquid interfacial tension in accordance with Eq.4. However, liquid-vapor interfacial tension changes will be negligible if pH control is achieved by using minute drops of acid solution. This is in accordance with the work of Randles and Schiffrin (1966), Figure 4.

Consequently, Eq.5 can be differentiated as:

$$\gamma_{VL} dCos\theta = -d\gamma_{SW} \quad 6$$

Using Gibbs excess adsorption equation, the change in solid-water interfacial tension reads (*Carre et al*., 2003)

$$d\gamma_{SW} = -\Gamma_{H^+} RTd \ln\left|H^+\right| = 2.303\Gamma_{H^+} RTd(pH) \quad 7$$

$$\Gamma_{H^+}, R, T$$

In which Γ is the surface excess adsorption of protons [mol/ m^2], R universal gas constant [J /^{o}K] and T is absolute.

The surface charge density is the result of surface ionization or protonation reactions. For protonation or adsorption reaction Gibbs equation can be written as (Carré, *et al*. 2003):

$$\sigma = \Gamma_{H^+} F \quad 8$$

In which σ is the surface charge density of water-rock interface [C/m^2] and F is Faradays constant [$Cmol^{-1}$]

This formulation is in accordance with the single site model approach (Lu & Smith, 1996) which assumes the presence of only one type of surface hydroxyl group acting as a surface site where dissociation can take place amphoterically leading to protonation or deprotonation.

Putting together Eqs. 6 through 8 yield the following equation:

$$\frac{dCos\theta}{dpH} = -\frac{2.303RT\sigma}{F\gamma_{LV}} \quad 9$$

This equation predicts a turning point at the point of zero charge on silica surface in the context of aqueous solution pH variation. With decreases in wettability following pH decreases as established in a previous research work (Kim, Wan, Kneafsey, & Tokunaga, 2012) the wettability of silica surface will be a minimum at the point of zero charge pH of silica surface.

From Eq. 9 the following can be written:

$$dCos\theta = -\frac{2.303RT\sigma}{F\gamma_{LV}} dp(H) \quad 10$$

The relationship between surface charge density and surface charge potential reads (Atkinson, Posner, & Quirk, 1967)

$$\frac{e\psi}{k_B T} = \sigma\sqrt{\frac{2\pi}{\varepsilon n k_B T}} \quad 11$$

In which ψ is the surface potential of minerals surface [V] and n is the ion density [mol /m^3]

In the following section this equation will be exploited for deriving the pH wettability relationship.

1.4 Applications of Mathematical Model to Spontaneous Imbibition Dynamics

1.4.1 Capillary Rise pH Relationship

In this model, an aqueous solution with varying pH is assumed. The relationship between charge density, potential, dielectric constant of the electrolyte, temperature and solution concentration is written as (Atkinson et al., 1967).

$$\frac{e\psi}{k_B T} = \sigma\sqrt{\frac{2\pi}{\varepsilon n k_B T}} \quad 12$$

The Nernst equation gives (Bowden, Posner, & Quirk, 1977):

$$\psi = -2.303\frac{k_B T}{e}\Delta pH = -2.303\frac{k_B T}{e}\left(pH - pH_{pzc}\right) = \frac{2.303 k_B T}{e}\left(pH_{pzc} - pH\right) \quad 13$$

Wettability or cosine of the contact angle change gives:

$$dCos\theta = -\frac{2.303RT\sigma}{F\gamma_{LV}}dpH \quad 14$$

The relationship between capillary rise and contact angle gives:

$$h_w = \frac{2\gamma_{LV}Cos\theta_c}{\rho g r} \quad 15$$

In which h_w is the spontaneous imbibition rise in a capillary [m], θ_c is the contact angles [deg.], r is the radius of capillary tube [m], ρ is the density of liquid [kg/m^3] and g is the gravitational constant [m/s^2]. All other symbols have already been explained

Equation 23 shows a direct relationship between capillary rise and contact angle, which is a measure of wettability. This shows that capillary imbibition, which is a direct measure of the extent of capillary rise will be greater the greater the water wettability of the capillary glass surface.

Capillary rise is, therefore, a function of wettability at isothermal conditions. Under isothermal conditions therefore the derivative of capillary rise with regard to wettability or cosine of the contact angle is given by:

$$\frac{dh_w}{dCos(\theta)} = -\frac{2\gamma_{LV}}{\rho g r} \quad 16$$

Thus:

$$dCos(\theta) = -\frac{\rho g r}{2\gamma_{LV}}dh_w \quad 17$$

Substitution of Eq. 17 into Eq. 14 for change in cosine of contract angle gives:

$$\frac{\rho g r}{2\gamma_{LV}} dh_w = \frac{2.303RT\sigma}{F\gamma_{LV}} dpH \tag{18}$$

Thus:

$$dh_w = \frac{2.303RT\sigma}{F\rho rg} dpH \tag{19}$$

This implies capillary rise is also a function of pH

In Eq. 13 substitution of the surface potential from Eq. 12 gives:

$$\frac{e}{k_B T}\left[\frac{2.303k_B T}{e}\left(pH_{pzc} - pH\right)\right] = \sigma\sqrt{\frac{2\pi}{\varepsilon n k_B T}} \tag{20}$$

This gives surface charge density as:

$$\sigma = 2.303\left(pH_{pzc} - pH\right)\left(\frac{2\pi}{\varepsilon n k_B T}\right)^{-0.5} \tag{21a}$$

Substitution of this into Eq. 19 gives:

$$dh_w = 2.303\left(pH_{pzc} - pH\right)\left(\frac{2\pi}{\varepsilon n k_B T}\right)^{-0.5} \frac{2.303^2 RT}{F\rho rg} dpH \tag{21b}$$

Hence:

$$dh_w = \left(\frac{2\pi}{\varepsilon n k_B T}\right)^{-0.5} \frac{2.303^2 RT}{F\rho rg}\left(pH_{pzc} - pH\right)dp(H) \tag{22}$$

This can be integrated as:

$$\int_{h_0}^{h} dh_w = \int_{pH_0}^{pH} \left(\frac{2\pi}{\varepsilon n k_B T}\right)^{-0.5} \frac{2.303^2 RT}{F\rho rg}\left(pH_{pzc} - pH\right)dpH \tag{23}$$

In which h_o is the capillary rise at initial pH of aqueous solution [m], h is the capillary rise at a given pH of aqueous solution [m], pH_o is the initial pH of aqueous solution [-] and pH is the final pH of aqueous solution. All other symbols have already been explained.

This gives the following equation:

$$h = -0.5\varsigma pH^2 - \varsigma pH_{pzc}\, pH + \varsigma\left(0.5\, pH_0^2 - pH_{pzc}\, pH_0\right) - h_0 \quad (24a)$$

Thus, for initial height equal to zero, Eq. 24a becomes:

$$h = -0.5\varsigma pH^2 - \varsigma pH_{pzc}\, pH + \varsigma\left(0.5\, pH_0^2 - pH_{pzc}\, pH_0\right) \quad (24b)$$

$$\varsigma = \frac{2.303^2 RT}{F\rho rg}\left(\frac{2\pi}{\varepsilon n k_B T}\right)^{-0.5} \quad (25)$$

This equation shows a parabolic relationship between capillary imbibition height and pH of the aqueous solution. Equation 24 provides a direct experimental advantage because by varying the pH of the aqueous solution the corresponding capillary imbibition height can be measured. By theory, a plot of capillary imbibition height versus solution pH must give a parabolic graph.

1.4.2 Wettability pH Relationship

In order to derive pH cosine of contact angle or wettability relationship the basic equations used before will be recalled as (Atkinson *et al*., 1967):

$$\frac{e\psi}{k_B T} = \sigma\sqrt{\frac{2\pi}{\varepsilon n k_B T}} \quad :$$

In which all symbols have already been explained. Thus:

$$\sigma = 2.303\left(pH_{pzc} - pH\right)\left(\frac{2\pi}{\varepsilon n k_B T}\right)^{-0.5} \quad (26)$$

$$\psi = -2.303\frac{k_B T}{e}\Delta pH = -2.303\frac{k_B T}{e}\left(pH - pH_{pzc}\right) = \frac{2.303 k_B T}{e}\left(pH_{pzc} - pH\right)$$

The derivative of wettability or cosine of the contact angle gives:

$$dCos\,\theta = -\frac{2.303RT\sigma}{F\gamma_{LV}}dpH$$

Substitution for surface charge density from Eq.36 into equation 38 gives:

$$dCos\,\theta = -\frac{2.303R^2T}{F\gamma_{LV}}\left(\frac{2\pi}{\varepsilon n k_B T}\right)^{-0.5}\left(pH_{pzc} - pH\right)dpH \quad (27)$$

Under normal conditions there is pH reduction from near neutral pH to a lower value closer to the point of zero charge

pH of silica surface. The integration limits are the initial pH of formation water to the pH of interest and the wettability (cosine of contact angle) at initial pH (pH_o) to the wettability at a given pH of interest. Application of these limits leads to:

$$\int_{\cos(\theta)_o}^{\cos(\theta)} dCos\theta = -\int_{pH_o}^{pH} \frac{2.303^2 RT}{F\gamma_{LV}} \left(\frac{2\pi}{\varepsilon n k_B T}\right)^{-0.5} \left(pH_{pzc} - pH\right) dp(H) \quad 28$$

In which $\cos\theta_o$ is the cosine of the contact angle at point of zero charge pH [-] and $\cos\theta$ is the cosine of the final contact angle [-]

The final integration gives:

$$\cos(\theta) = \cos(\theta)_o - \frac{2.303^2 RT}{F\gamma_{LV}} \left(\frac{2\pi}{\varepsilon n k_B T}\right)^{-0.5} \left[pH_{PZC}\, pH - \frac{pH^2}{2} \right]_{pH_o}^{pH} \quad 29$$

Expanding the term in the square bracket on the right hand side of the equation gives:

$$\cos(\theta) = \cos(\theta)_o$$

$$+ \frac{2.303^2 RT}{F\gamma_{LV}} \left(\frac{2\pi}{\varepsilon n k_B T}\right)^{-0.5} \left[0.5 pH^2 - pH_{PZC}\, pH + \left(pH_{pzc}\, pH_o - 0.5 pH_o^2\right)\right] \quad 30$$

This equation can be written as:

$$\cos(\theta) = \cos(\theta)_o + \zeta\left[0.5 pH^2 - pH_{PZC}\, pH + \left(pH_{pzc}\, pH_o - 0.5 pH_o^2\right)\right] \quad 31$$

Where:

$$\zeta = \frac{2.303^2 RT}{F\gamma_{LV}} \left(\frac{2\pi}{\varepsilon n k_B T}\right)^{-0.5} \quad 32$$

1.4.3 Theoretical Derivation of the Point of Zero Charge pH

It is interesting to note that in Eq. 24b, capillary rise can be linked to a given pH of aqueous solution. At the same pH of aqueous solution there is a definite wettability. The implication for Eq. 24b is that if contact angle can be calculated using capillary rise data for a given pH, then this contact angle can be plotted against solution pH in accordance with Eq. 31. Since Eq. 31 shows a parabolic relationship between contact angle and pH, the pH derivative of this equation when equated to zero and solved for pH will give the point of zero charge pH of the solid surface. Accordingly, the relationship between capillary rise and contact angle is given as (Jones, n.d.):

$$\cos\theta = \frac{rgh}{\gamma_{LV}} \quad 33$$

Thus:

$$\theta = \cos^{-1}\left[\frac{rgh}{\gamma_{LV}}\right] \quad 34$$

In which θ is the contact angle r is capillary radius, h is capillary imbibition rise and γ_{LV} is liquid-air interfacial tension.

Equation 31 permits a plot of wettability, hereby defined as the cosine of the contact angle (Bhattacharya, Datta, Berg, & Gangopadhyay, 2005) and contact angle respectively versus pH of aqueous solution. Fitting the resulting plots with quadratics models permits determination of the point of zero charge pH of solid surface using maxima and minima principles of differential calculus. This approach will be used in this paper for the determination of the point of zero charge pH of borosilicate glass.

1.5 Experimantal Determination of the Point of Zero Charge pH of an Oxide Surface

1.5.1 pH Measurement

pH was measured using the pH probe pH TESTR 30 (double junction). This is capable of measuring pH to two decimal places with an error of 0.01 pH. pH adjustment of aqueous solution was achieved by using nitric acid.

1.5.2 Brine Preparation and Core Sample Characterization

For synthetic brine experiments involving spontaneous imbibition brine was prepared by using laboratory grade sodium chloride and calcium chloride manufacture by Sigma Aldrich. These bought from Ottawa in Canada were used without further purification.

1.5.3 Density Measurement

Precise density measurement was achieved by first weighing an empty graduated cylinder. The cylinder was then weighed with a known volume of brine sample. The weight difference was divided by the volume of brine to obtain density at ambient conditions. Weights were measured using the Entris weight measuring instrument manufactured by the Sartorium Laboratory Instrument GmbH of Gottingen in Germany. It measures weights to three decimal places.

1.5.4 pH Control

pH control was achieved by preparing 0.25 M of dilute nitric acid solution. Laboratory grade acid was purchased from Sigma Aldrich in Ottawa, Canada. To change the pH of the experimental brine the tip of a 2 mm glass rod was dipped into the acid solution and the experimental brine was stirred using the rod to obtain a uniform solution. This procedure was used to obtain a measurable pH change.

1.5.5 Capillary Tube

Capillary tubes for the experiments were produced by the Chemistry Department of Dalhousie University. Each capillary tube has a diameter of 0.6 mm.

1.6 Experimental Procedures under Ambient Conditions

1.6.1 Capillary Imbibition Experimental Procedures

All spontaneous imbibition experiments involving capillary tube were performed at room temperature. The capillary tube was glued to the side of scale to make it easier to read height rise of the meniscus. The experimental set up is seen in Fig. 2. To avoid evaporation of water from the surface of water in the beaker a thin film of minerals oil was poured on the water. To begin the experiment, the capillary tube with scale is dipped into the beaker with part of the system below water level. The equilibrium height was then read with the surface of water as the zero level. This procedure was used for different pH of the aqueous solution.

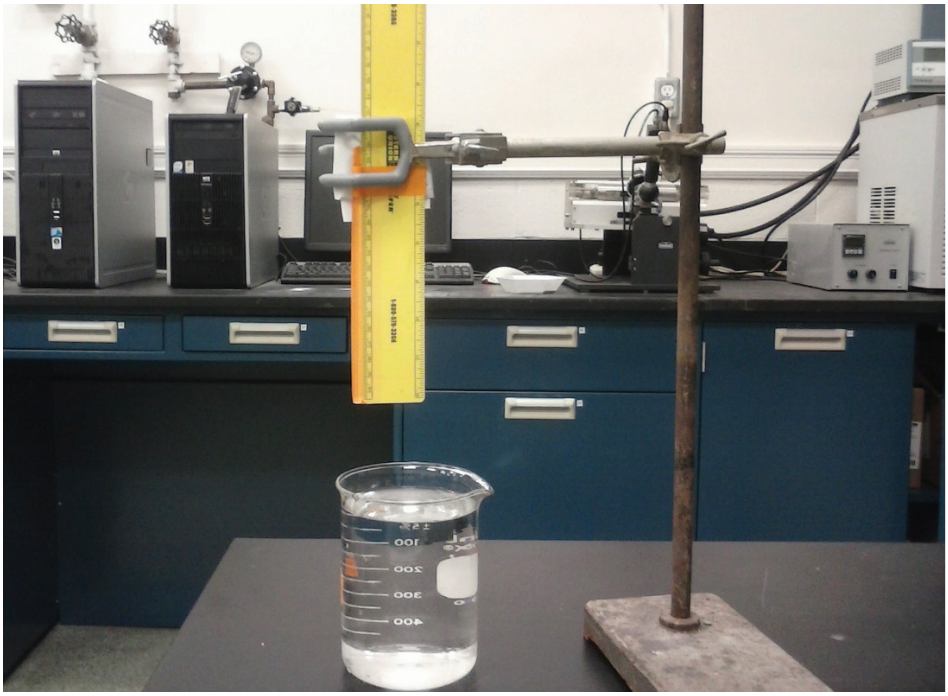

Figure 2. Set up for capillary rise experiment

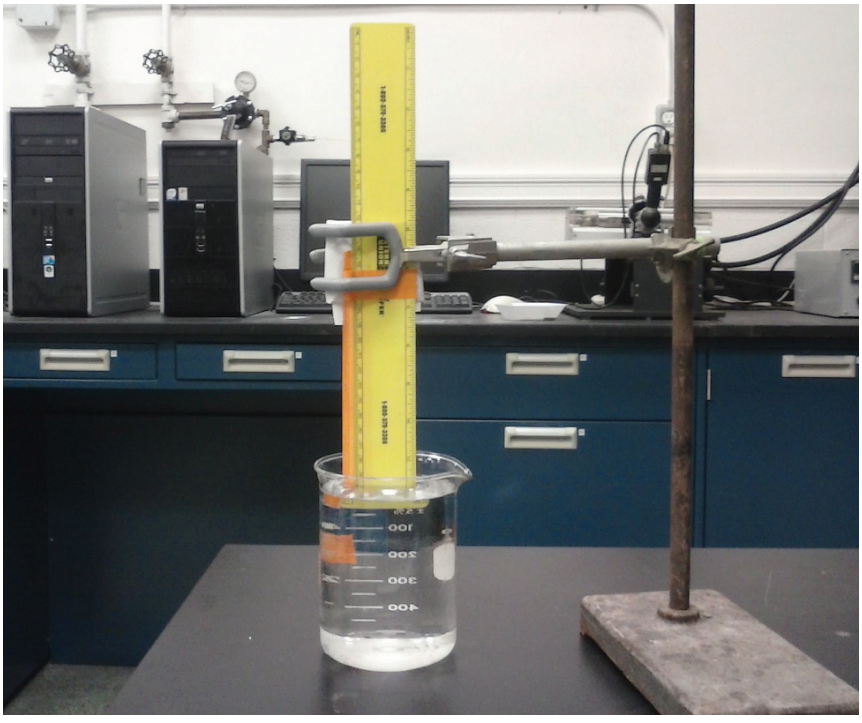

Figure 3. Capillary rise experiments in progress

1.7 Capillary Imbibition Experimental Results and Discussion

Figures 4, 6 and 8 give plots of wettability versus pH with regression coefficients of 0.97, 0.79 and 0.91 respectively while figures 5, 7 and 9 give plots of contact angle versus pH of aqueous solution with regression coefficients of 0.81, 9.99 and 0.91 respectively. These regression coefficients are quite satisfactory.

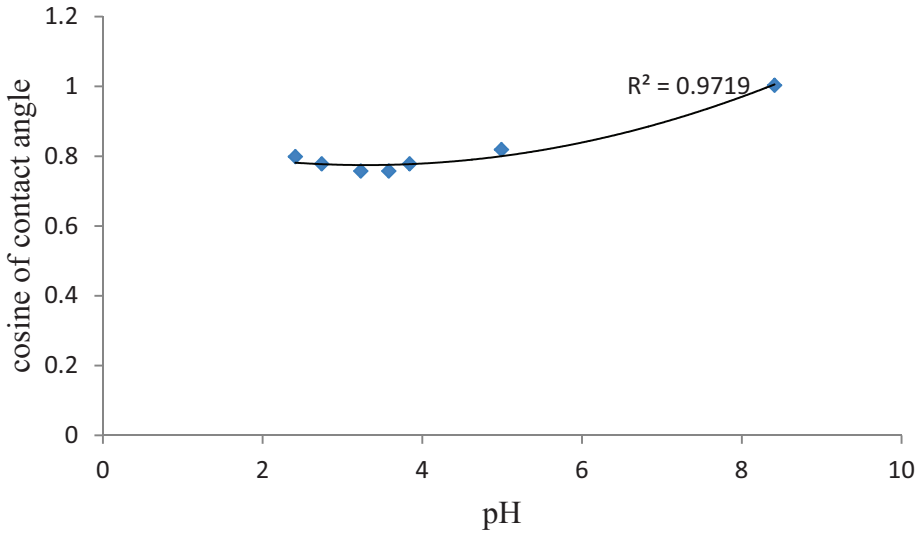

Figure 4. A plot of wettability versus pH of brine for experiment 1 under ambient conditions

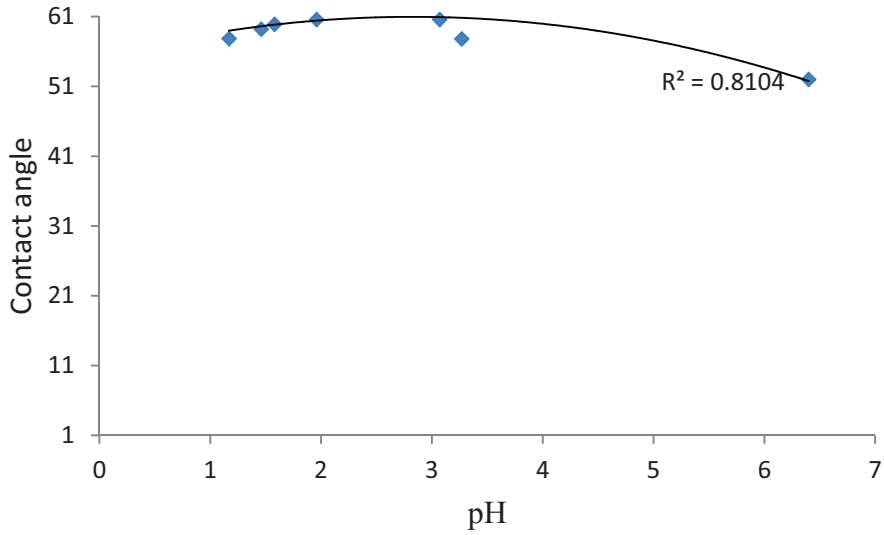

Figure 5. A plot of contact angle versus pH of brine for experiment 1 under ambient conditions

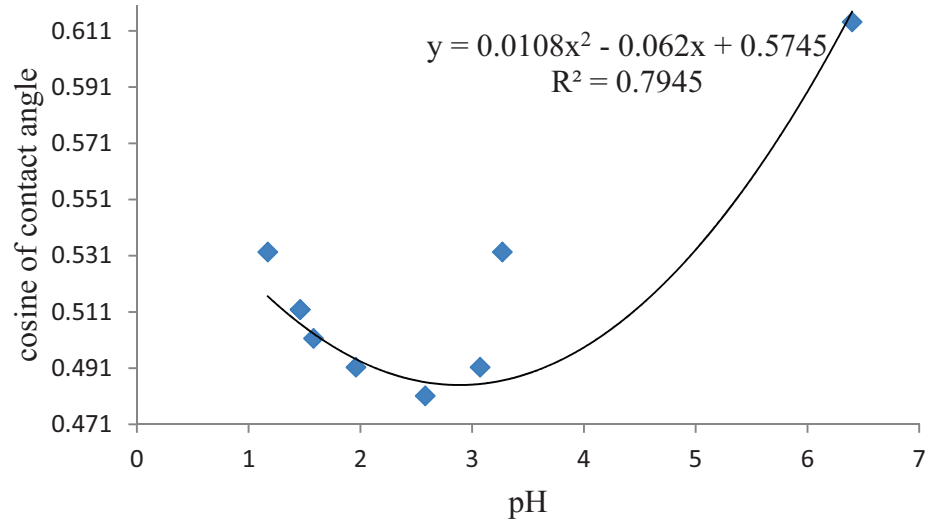

Figure 6. A plot of wettability versus pH of brine for experiment 2 under ambient conditions

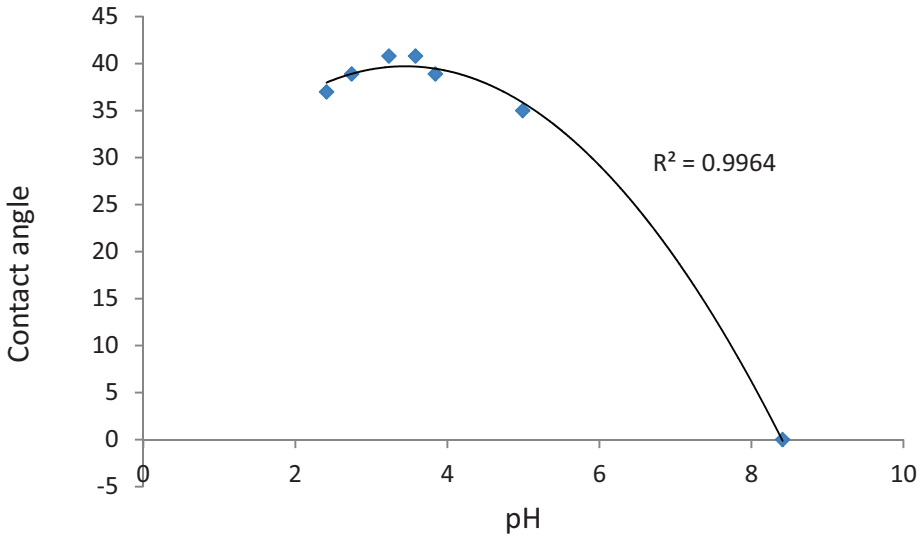

Figure 7. A plot of contact angle versus pH of brine for experiment 2 under ambient conditions

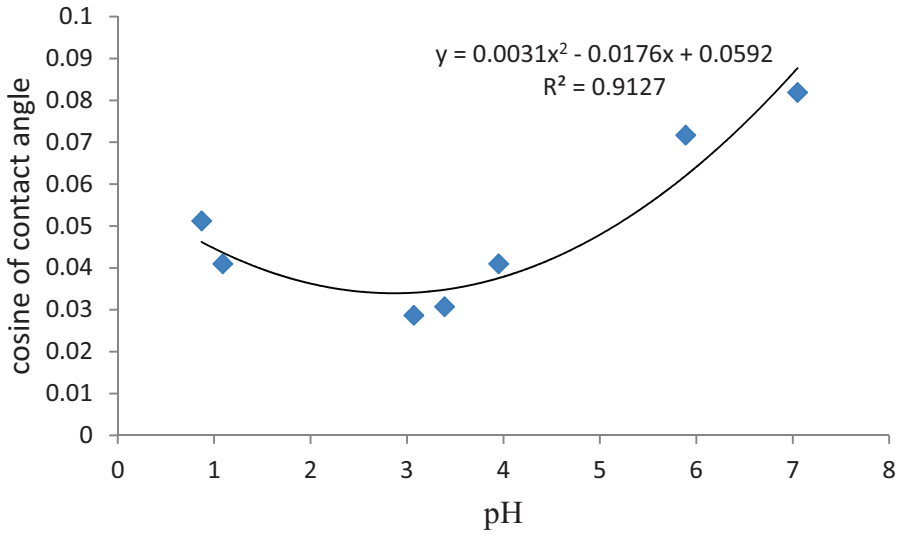

Figure 8. A plot of wettability versus pH of brine for experiment 3 under ambient conditions

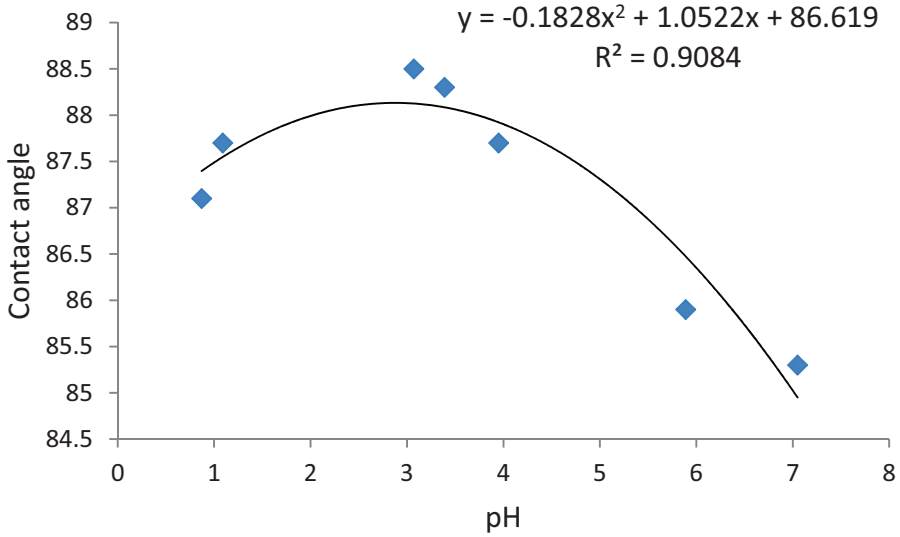

Figure 9. A plot of contact angle versus pH of brine for experiment 3 under ambient conditions

Theoretically at the point of zero charge pH of the solid surface the gradient of the plot of wettability versus pH must be zero because this is the minimum wettability. In order to obtain this pH for the solid surface the quadratic fits equations are differentiated and equated to zero. The pH when the resulting equation is solved is equal to the point of zero charge pH. Using this approach, the following are the point of zero charge pH of borosilicate glass surface for the three experiments

Experiments 1 = 3.30

Experiments 2 = 2.87

Experiment 3 = 2.84

The average is 3.00

2. Comparison with Literature Values

Kyriakos Bourikas *et al.*, (2003) used different techniques to obtain the point of zero charge pH of quartz. The following were their values for five different methods:3.1, 3.3, 3.0, 2.9, 3.2, Ave = 3.14

Information from the capillary glass tube manufacturer indicates it is borosilicate or fused glass. This type of glass is preferred in the laboratory because of its very low thermal expansivity and high boiling point. Zeta potential of borosilicate glass versus pH for borosilicate glass has been made (Barz, Vogel, & Steen, 2009), Appendix C in the

present work. Normalizing the zeta potential with the negative logarithm of the ionic strength results in a collapse of data onto a single curve. The result could be fitted with a curve and the extrapolation of this curve to zero zeta potential that corresponds to the isoelectric point also known as the point of zero charge pH for static conditions gave a range of pH values between 1.7 and 2. In addition to this, Kirby & Hasselbrink, (2004) reported values of the isoelectric point of borosilicate glass to be between 2.6 and 2.8. The average for these literature values gives 2.4. The difference between this and that obtained using spontaneous imbibition is 0.6**.**

3. Conclusion

Results of the experimental work show that the quadratic relationship between wettability and or contact angle derived in this study is theoretically appreciable. Another point of interest is that the quadratic fits give average values of the point of zero charge pH of borosilicate glass from which the capillary tubes are made to be 3 on the average. Appendix A and appendix B show values for silica with close agreement. This is quite within the range of values reported for silica glass, which come from quartz with the same value of point of zero charge pH. The value also agrees with the average value obtained by Kryiakos Bourikas, 2003[5]. The following sums up the principal conclusion of this experiment:

1. Trends in wettability variation with aqueous solution pH agree with the mathematical model.
2. The relationship between wettability and aqueous solution pH using capillary imbibition can be used to obtain information about the point of zero charge pH of glass.

Acknowledgements

In carrying out this research work the authors wish to acknowledge the immense contributions from Mr. Matt Kujath, the engineer for the Department of Process Engineering and Applied Science of Dalhousie University (Halifax, Nova Scotia-Canada) particularly for the great part he played by having capillary tubes manufactured to specification and desired grade. In this regard his contributions enabled the objectives of this research work to be achieved both theoretically and practically.

Appendices

Add appendix A: Point of zero charge of oxides (Kosmulski, 2002)

Material	Description	Salt	T	Method	pH_0
SiO_2	Aerosil OX 50 Degussa	10^{-3}–0.1 mol dm^{-3} NaCl	25	pH iep	<4 if any 2.4
SiO_2	Polysciences	10^{-4}–0.1 mol dm^{-3} KNO_3		iep	<3 if any
SiO_2	Aerosil 380	10^{-2} mol dm^{-3} NaCl, $NaNO_3$	25	iep Acusto	2–4 (if any)
SiO_2	Quartz	10^{-2} mol dm^{-3} NaCl, $NaNO_3$	25	iep Acusto	2–4 (if any)
SiO_2	Duke	10^{-3}–10^{-2} mol dm^{-3} NaCl		iep	2.5–4.5
SiO_2	Quartz, Alfa Aesar	$KOH + HNO_3$		Acusto	2.3
SiO_2	Stöber	10^{-3} mol dm^{-3} KBr		iep	2
SiO_2	Aerosil 380	10^{-3}–0.1 mol dm^{-3} $NaClO_4$	25	iep pH	$\zeta = 0$ at pH <5 <3 if any
SiO_2	Geltech	10^{-3} mol dm^{-3} NaCl, KCl, LiCl, CsCl		Acusto	$\zeta = 0$ at pH 2
SiO_2	Quartz, Sigma	0.1 mol dm^{-3} NaCl, KCl, LiCl, CsCl		Acusto	<2 if any
SnO_2	Cassiterite, natural	None		iep	<3 if any

Appendix B: Point of zero charge pH of some oxides (Parks and De Bruyn, 1962)

Solid	pH: Z.p.c.	pH: Min. solubility	pH: I.e.p. (calcd.)	Comment	Ref.
			1		35
WO_3	0.43	0.43		*a,e*	36
SiO_2	<2			*b,e,f*	37, 38, 16
SnO_2	4.5			*a,e*	16
	(5.5–7.3)			*b,e*	16
TiO_2	6.7			*b,f*	39
	6			*a,e*	16
	(4.7)			*b,c,e*	16
ZrO_2	~4			*b,g*	38
Al_2O_3	6.94 ± 0.37			*a,e*	40
	(8.4)			*b,e*	16
	(9.45)			*b,f*	41
		7.7			42

Appendix C: Zeta potential of borosilicate glass versus pH (Barz *et al*, 2009)

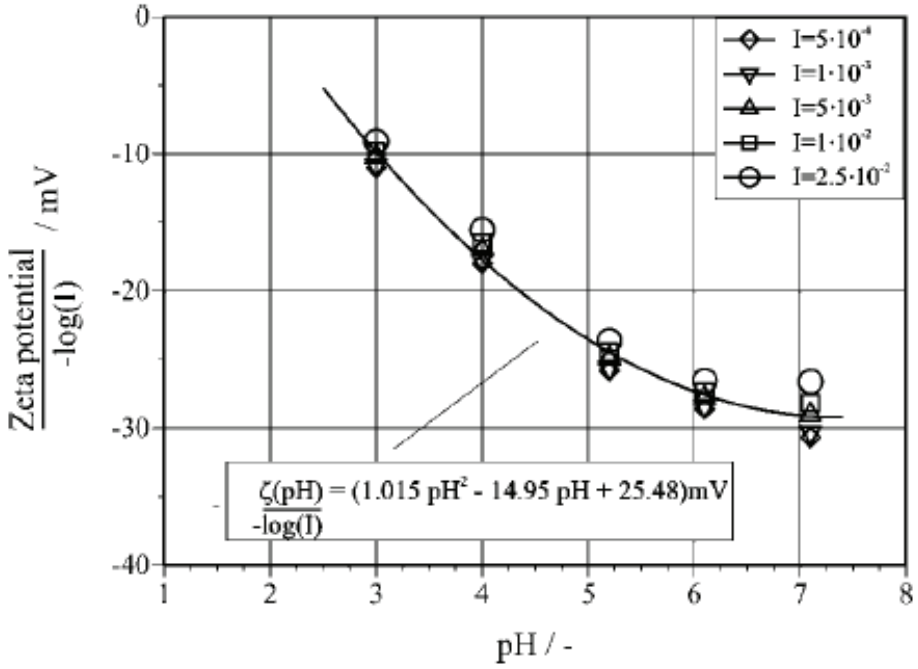

References

Atkinson, R. J., Posner, A. M., & Quirk, J. P. (1967). Adsorption of potential-determining ions at the ferric oxide-aqueous electrolyte interface. *The Journal of physical chemistry, 71*(3), 550-558. https://doi.org/10.1021/j100862a014

Barrow, N. J., Bowden, J. W., Posner, A. M., & Quirk, J. P. (1980). Describing the effects of electrolyte on adsorption of phosphate by a variable charge surface. *Soil Research, 18*(4), 395-404. https://doi.org/10.1071/SR9800395

Barz, D. P., Vogel, M. J., & Steen, P. H. (2009). Determination of the zeta potential of porous substrates by droplet deflection. I. The influence of ionic strength and pH value of an aqueous electrolyte in contact with a borosilicate surface. *Langmuir, 25*(3), 1842-1850. https://doi.org/10.1021/la802949z

Bhattacharya, S., Datta, A., Berg, J. M., & Gangopadhyay, S. (2005). Studies on surface wettability of poly (dimethyl) siloxane (PDMS) and glass under oxygen-plasma treatment and correlation with bond strength. *Journal of Microelectromechanical Systems, 14*(3), 590-597. https://doi.org/10.1109/JMEMS.2005.844746

Bourikas, K., Vakros, J., Kordulis, C., & Lycourghiotis, A. (2003). Potentiometric mass titrations: experimental and theoretical establishment of a new technique for determining the point of zero charge (PZC) of metal (hydr) oxides. *The Journal of Physical Chemistry, B, 107* (35), 9441-9451. https://doi.org/10.1021/jp035123v

Bowden, J. W., Posner, A. M., & Quirk, J. P. (1977). Ionic adsorption on variable charge mineral surfaces. Theoretical charge development and titration curve. *Soil Research, 15*(2), 121-136.

Carré, A., Lacarrière, V., & Birch, W. (2003). Molecular interactions between DNA and an aminated glass substrate. *Journal of colloid and interface science, 260*(1), 49-55. https://doi.org/10.1016/S0021-9797(02)00147-9

Chatelier, R. C., Chan, D. Y., Vasic, Z. R., Gengenbach, T. R., & Griesser, H. J. (1995). Theory of contact angles and the free energy of formation of ionizable surfaces: application to heptylamine radio-frequency plasma-deposited films. *Langmuir, 11*(10), 4122-4128. https://doi.org/10.1021/la00010a078

Chatelier, R. C., Drummond, C. J., Chan, D. Y., Vasic, Z. R., Gengenbach, T. R., & Griesser, H. J. (1995). Theory of Contact Angles and the Free Energy of Formation of Ionizable Surfaces: Application to Heptylamine Radio-Frequency Plasma-Deposited Films. *Langmuir, 11*(10), 4122–4128. https://doi.org/10.1021/la00010a078

Chen, T., Chiu, M. S., & Weng, C. N. (2006). Derivation of the generalized Young-Laplace equation of curved interfaces in nanoscaled solids. *Journal of Applied Physics, 100*(7), 074308. https://doi.org/10.1063/1.2356094

Digilov, R. (2000). Charge-induced modification of contact angle: the secondary electrocapillary effect. *Langmuir, 16*(16), 6719-6723. https://doi.org/10.1021/la991308a

Eggleston, C., & Jordan, G. (1998). A new approach to pH of point of zero charge measurement: Crystal-face specificity by scanning force microscopy (SFM). *Geochimica et Cosmochimica Acta, 62*(11), 1919-1923. https://doi.org/10.1016/S0016-7037(98)00119-7

Jones, A. Z. (n.d.). *Contact Angle & Capillarity - Liquid in a Vertical Tube*. Retrieved from http://physics.about.com/od/physicsexperiments/a/surfacetension_3.htm

Kim, Y., Wan, J., Kneafsey, T. J., & Tokunaga, T. K. (2012). Dewetting of silica surfaces upon reactions with supercritical CO2 and brine: pore-scale studies in micromodels. *Environmental science & technology, 46*(7), 4228-4235. https://doi.org/10.1021/es204096w

Kirby, B. J., & Hasselbrink, E. F. (2002). Zeta potential of microfluidic substrates: 1. Theory, experimental techniques, and effects on separations. *).Electrophoresis, 25*(2), 187-202. https://doi.org/10.1002/elps.200305754

Kosmulski, M. (2004). pH-dependent surface charging and points of zero charge II. Update. *Journal of colloid and interface science, 275*(1), 214-224. https://doi.org/10.1016/j.jcis.2004.02.029

Lippmann, G. (1875). Relations entre les phénomènes électriques et capillaires. *Annles de Chimie et de Physique*(5), (Doctoral dissertation, Gauthier-Villars).

Liu, K., Yao, X., & Jiang, L. (2010). Recent developments in bio-inspired special wettability. *Chem. Soc. Rev., 39*, 3240-3255. https://doi.org/10.1039/b917112f

Liu, Q., Yuan, S., Yan, H., & Zhao, X. (2012). Mechanism of oil detachment from a silica surface in aqueous surfactant solutions: molecular dynamics simulations. *The Journal of Physical Chemistry B, 116*(9), 2867-2875. https://doi.org/10.1021/jp2118482

Lu, W., & Smith, E. H. (1996). Modeling potentiometric titration behavior of glauconite. *Geochimica et cosmochimica acta, 60*(18), 3363-3373. https://doi.org/10.1016/0016-7037(96)00180-9

Martic, G., Gentner, F., Seveno, D., Coulon, D., De Coninck, J., & Blake, T. D. (2002). A molecular dynamics simulation of capillary imbibition. *Langmuir, 18*(21), 7971-7976. https://doi.org/10.1021/la020068n

Noh, J. S., & Schwarz, J. A. (1989). Estimation of the point of zero charge of simple oxides by mass titration. *Journal of Colloid and Interface Science, 130*(1), 157-164. https://doi.org/10.1016/0021-9797(89)90086-6

Peng, X. D., & Barteau, M. A. (1991). Acid-base properties of model magnesium oxide surfaces. *Langmuir, 7*(7), 1426-1431. https://doi.org/10.1021/la00055a023

Randles, J. E., & Schiffrin, D. J. (1966). Surface tension of dilute acid solutions. *Transactions of the Faraday Society, 62*, 2403-2408. https://doi.org/10.1039/tf9666202403

Refson, K., Wogelius, R. A., Fraser, D. G., Payne, M. C., Lee, M. H., & Milman, V. (1995). Water chemisorption and reconstruction of the MgO surface. *Physical Review B, 52*(15), 10823. https://doi.org/10.1103/PhysRevB.52.10823

Sposito, G. (1998). On points of zero charge. *Environmental science & technology, 32*(19), 2815-2819. https://doi.org/10.1021/es9802347

Sverjensky, D. A. (1994). *Zero-point-of-charge prediction from crystal chemistry and solvation theory. Geochimica et Cosmochimica Acta, 58*(14), 3123-3129. https://doi.org/10.1016/0016-7037(94)90184-8

Van Oss, C. J., Good, R. J., & Chaudhury, M. K. (1988). Additive and nonadditive surface tension components and the interpretation of contact angles. *Langmuir, 4*(4), 884-891. https://doi.org/10.1021/la00082a018

Yoon, R. H., Salman, T., & Donnay, G. (1979). Predicting points of zero charge of oxides and hydroxides. *Journal of colloid and interface science, 70*(3), 483-493. https://doi.org/10.1016/0021-9797(79)90056-0

Zhuravlev, L. T. (1987). Concentration of hydroxyl groups on the surface of amorphous silicas. *Langmuir, 3*(3), 316-318. https://doi.org/10.1021/la00075a004

International Journal of Chemistry; Vol. 9, No. 3; 2017
ISSN 1916-9698 E-ISSN 1916-9701
Published by Canadian Center of Science and Education

Uptake of Zn, Pb, Cu and Fe Ions from Spent and Unspent Engine Oil Using Termite Soil

Iwekumo Agbozu[1], Bassey Uwem[1], Boisa Ndokiari[2]

[1]Department of Environmental Management and Toxicology, Federal University of Petroleum Resources, P.M.B 1221, Effurun, Delta State, Nigeria

[2]Department of Chemistry, Rivers State University, P.M.B 5080, Port Harcourt, Rivers State, Nigeria

Correspondence: Iwekumo Agbozu, Department of Environmental Management and Toxicology, Federal University of Petroleum Resources, P.M.B 1221, Effurun, Delta State, Nigeria. E-mail: iwekumo@yahoo.co.uk

Received: February 22, 2017 Accepted: June 4, 2017 Online Published: July 25, 2017

doi:10.5539/ijc.v9n3p85 URL: https://doi.org/10.5539/ijc.v9n3p85

Abstract

Removal of Zn, Pb, Cu and Fe ions from unspent and spent engine oil was studied using Termite soil. Process parameters such as contact time and adsorbent dosage were varied. Values from contact time were used for predicting kinetics equation of their uptake. At optimum time of 40 minutes, percentage adsorption was of the order Fe>Zn>Cu>Pb for both spent and unspent engine oil. Kinetics equation such as Elovich, Intra-particle, Pseudo-first order and Pseudo-second order were tested. Results obtained shows that their sequestering pattern fit into the pseudo-second order kinetics. Initial reaction rates, h (mg/g.min) and α (mg. $g^{-1}min^{-1}$) for all metal ions obtained from Pseudo-second order and Elovich kinetic models followed the trends Zn>Fe>Cu>Pb and Zn>Fe>Pb>Cu respectively in spent engine oil while for unspent engine oil, the trend was Fe>Zn>Cu>Pb for h (mg/g.min) and Zn>Fe>Pb>Cu for α (mg. $g^{-1}min^{-1}$). Electrostatic attraction existing on the surface of the adsorbent assisted in the high initial reaction of Zn and Fe ions, implying good affinity of the ions for the adsorbent. Desorption constant β (g/mg) was of the trend Cu>Pb>Fe>Zn and Cu>Pb>Zn>Fe for spent and unspent engine oils respectively. Intra-particle diffusion constant k_{id} ($mgg^{-1}min^{-1/2}$) followed a similar pattern, revealing strong binding between Zn and termite soil than any of the metal ion. This pilot research has been able to suggest a kinetic process for uptake of the studied ions from spent and unspent engine oil.

Keywords: spent and unspent engine oil, termite soil, metal uptake, adsorption kinetics

1. Introduction

Spent motor oil is an alarming environmental pollutant and is usually obtained after servicing and subsequent draining from automobile and generator engines by auto-repairers (Sharifi *et al*., 2007). Some major pollutants found in spent lubricating oil include polynuclear aromatic hydrocarbons (PAHs) and high levels of heavy metals. Considerable quantities of heavy metals, such as Pb, Zn, Cu, Cr, Ni, and Cd, are contained in used crankcase oil (Vwioko and Fashemi, 2005). Improper disposal of spent engine oil leads to a buildup of essential inorganic nutrients such as phosphorus, calcium, and magnesium, and trace amounts of lead, zinc, iron, copper and cobalt. These elements if in excess accumulate in plant tissues. Although some heavy metals at low concentrations are essential micro nutrients for plants, at high concentrations they could cause high metabolic disorder and growth inhibition for most plant species. Spent engine oils are particularly dangerous to the environment due to their contamination with products of thermal decomposition and mechanical impurities. These pollutants become hardly biodegradable and have carcinogenic properties (Grzegorz *et al*., 2015).

Contaminations of soil with engine oil are rampant in the Nigerian environment and have adversely affected seasonal crops such as maize (Kelechi *et al.,* 2012; Agbogidi *et al*., 2007).

In Nigeria, the Government has not been able to monitor or control the discharge of used oils and grease from the numerous auto- repair workshops littered over the country because they have proven to be very difficult to regulate their activities by virtue of their small size (Ahamefule, 2013).

Several adsorbents such as agricultural waste have been investigated for sequestering of heavy metals from various waste matrices. In recent times, termites soils have been investigated and reported to have high porosity and water infiltration due to buildup of have galleries (Schaefer, 2001; Dangerfield *et al*., 1998) which makes it a suitable

adsorbent for metal removal (Agbozu and Bassey, 2016). Also, pH of termite soil tends to be higher than that of adjacent soils thereby causing an increase in adsorption sites (Holt *et al*., 1998).

Adsorption kinetics is important in the evaluation of the performance of a given adsorbent and underlying mechanisms of sorption. From the kinetic analysis, the solute uptake rate, which determines the residence time required for completion of adsorption reaction, may be established. Also, one can know the scale of an adsorption apparatus based on the kinetic information. Generally speaking, adsorption kinetics is the base to determine the performance of fixed-bed or any other flow-through systems (Dabrowski, 2001). Adsorption kinetics is determined by the following stages: 1) diffusion of molecules from the bulk phase towards the interface space commonly called external diffusion; 2) diffusion of molecules inside the pores internal diffusion; 3) Adsorption-desorption elementary processes (Sharma, 1990).

1.1 Lagergren Pseudo-first Order Model

The pseudo first-order kinetic model (Lagergren's equation) describes adsorption in solid–liquid systems based on the sorption capacity of solids. It assumes that one metal ion (adsorbate) is adsorbed onto one sorption site on the adsorbent surface:

1.2 Pseudo-second Order Model

The pseudo second-order rate expression has been applied for analyzing chemisorption kinetics from liquid solutions. The model assumes that one metal ion (adsorbate) is sorbed onto two sorption sites on the adsorbent surface:

1.3 Elovich Model

Elovich equation is also used successfully to describe second order kinetic assuming that the actual solid surfaces are energetically heterogeneous, but the equation does not propose any definite mechanism for adsorbate–adsorbent relationship.

In order to avert the problem of soil pollution caused by used engine oil, there is need to study the adsorption kinetics of termite soil for the removal of heavy metals (Pb, Fe, Zn, and Cu) from spent and unspent engine oil through adsorption process.

2. Materials and Methods

2.1 Sampling

Termite soil was collected from Ugbomro Community in Uwvie Local Government Area of Delta State, Nigeria at Latitude N 05^{o} 34' 09.8" and Longitude E 005^{o} 50' 23.0".

2.2 Pretreatment

The termite soil was air dried at room temperature for 72 hours and crushed in a mortar. The sample was pretreated to remove non clay material such as carbonate and quartz minerals. A 2M Hydrochloric acid (HCl) was added to 0.6mm particle sized adsorbent to remove heavy metals present in the adsorbent and improve the sorption property of the absorbent. The mixture was stirred for 1 hour and allowed to remain in a plastic for 24hours and then thoroughly washed with distilled water and air dried for 2days. Virgin (unspent engine) oil with Society of Automotive Engineers (SAE) Grade of 20W-50 was used in a generator running at 6 hours daily for one week. Residual engine oil was collected after 42 hours of usage in the generator and labeled as spent engine oil.

2.3 Initial Concentration of Heavy Metals in Adsorbent and Adsorbate

A 0.5g of the termite soil was weighed into a 100ml beaker, and then 20ml of an aqua regia mixture (15ml conc. HCl, 5ml conc. HNO_3 in the ratio of 3:1) was added to the soil sample in the beaker. The sample was then digested using a block digester under fume hood for 15 minutes. The solution was allowed to cool, and then filtered into a 100 ml Pyrex and immediately transferred into 120ml plastic container. Concentrations of heavy metals were determined using atomic absorption spectrophotometer (spectral 220 FX). similarly, 5ml of the spent engine oil sample was measured, and added to a mixture of 20ml HNO_3 and HCl (5ml HCl +15ml HNO_3) (Yong *et al*., 2016). Results from the analysis were used as initial concentration of metal ions. Same process was used for digestion of unspent engine oil.

2.4 Adsorption Techniques

A glass separating funnel was fitted with cotton wool and held firmly in a vertical position with the aid of a retort stand. Atmospheric pressure helped to push the sample through the adsorbent. Adsorption process was carried out at room temperature. Process parameters such as contact time and adsorbent dosage were varied.

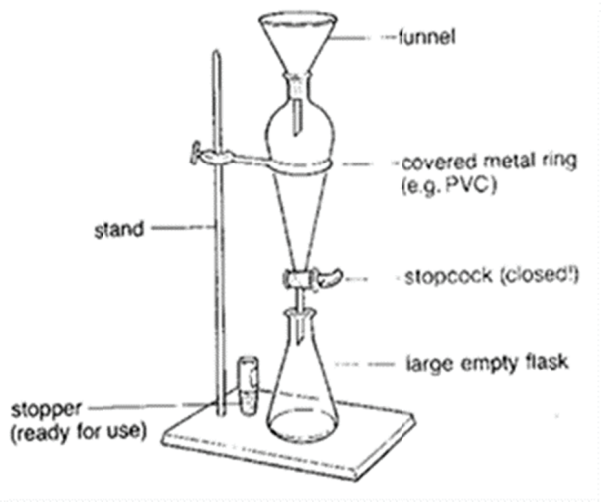

Figure 1. Experimental setup during adsorption process

2.5 Contact Time

A 0.5g of termite soil with mesh size 0.6mm was packed in a column and 5ml of spent engine oil was introduced and allowed to remain in the column for 10, 20, 30 and 40 minutes respectively before elution as shown in Figure 1. After each contact time, the filtrate obtained was digested and the digest was stored in a polyethylene container for metal analysis using the Atomic Adsorption Spectrophotometer. Similar process was used for unspent engine oil.

2.6 Adsorbent Dosage

Adsorbent dosage of 0.1, 0.2, 0.3, 0.4, and 0.5g of 0.6mm mesh size were investigated. The adsorbent was packed in a column; 5ml of spent engine oil was introduced and allowed to remain in the packed column for the studied optimum contact time of 40mins. Thereafter, the filtrate was digested and the digest stored in a polyethylene container for metal determination. Similar process was used for unspent engine oil

2.7 Infra-red Spectrometric Analysis of Termite Soil

In other to determine functional groups present in the adsorbent, 100 mg of the termite soil was dissolved in 2 ml of hexane. Two drops of the mixture was placed on a clean salt (NaCl) plate and the solvent was allowed to evaporate, leaving a cast film of the adsorbent. The cast film of the adsorbent was transferred to the PLC-11M Prism Cell. The resulting sample was scanned using infra-red spectrophotometer M500.

2.8 Data Analysis

The following kinetics equations were explored to determine the movement of various metal ions to the surface of the adsorbent.

Kinetic equations

$$\text{Adsorption capacity } q_e \text{ (mg/g)} = \frac{(C_0 - Ce)v}{m} \quad (1)$$

$$\text{Pseudo first order kinetics Log } (q_e - q_t) = \text{Log } q_e - \frac{k_1}{2.303} \quad (2)$$

$$\text{Pseudo second order kinetics } \frac{t}{q_t} = \frac{1}{k_2 q_e 2} + \frac{t}{q_e} \quad (3)$$

$$\text{Intra-particle diffusion } q_e = k\sqrt{t} + C \quad (4)$$

$$\text{Elovich } q_e = \left(\frac{1}{\beta}\right) \text{In } (\alpha\beta) + \frac{1}{\beta}\text{Int} \quad (5)$$

Where

M is the mass of adsorbent in gram,

C_0 and C_e are initial and final concentration of metal ions,

V is the volume of solution in litres and

q_t is the quantity of metal ions adsorbed at any particular time (mg/g).

β (g/mg) is desorption constant,

α (mg. $g^{-1}min^{-1}$) is the initial reaction rate from Elovich equation

3. Result and Discussion

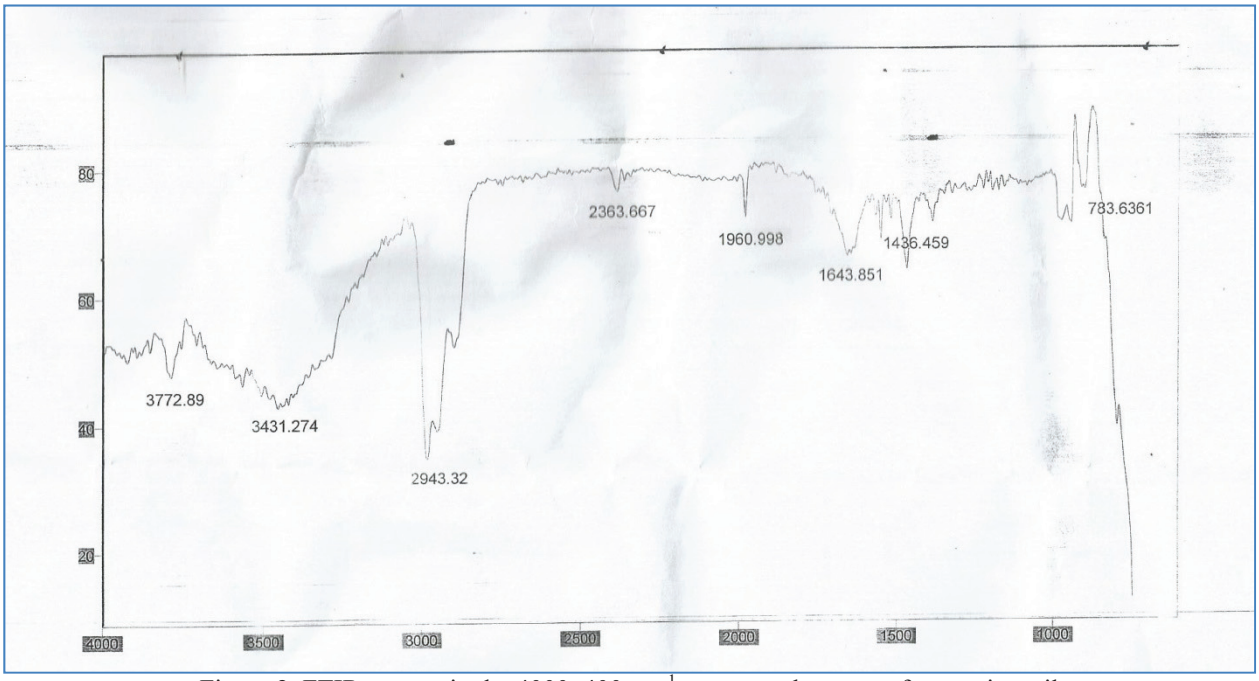

Figure 2. FTIR spectra in the 4000–400 cm^{-1} wave number range for termite soil

From Figure 1.0 the main bands appearing in that spectrum were due to stretching vibrations of OH groups in the range from 3750 –3000 cm^{-1}, which are overlapped to the stretching vibration of N-H; and C–H bond in $–CH_2$ (2943 cm^{-1}). Bending vibrations of methyl groups occurred at 1436 cm^{-1}, (Mano *et al*., 2003).Absorption in the range of 1643–1436 cm^{-1} was related to the vibrations of carbonyl bonds (C=O) of the amide group CONHR (secondary amide, 1643 cm^{-1}) (Marchessault *et al*., 2006).On the basis of interaction with functional group, hydroxide ions present in the adsorbent provide sites for chemisorptions of heavy metals. Surface reaction includes;

$$Zn^{2+}(aq) + 2OH^{-}(aq) \longrightarrow Zn(OH)_2(s)$$

$$Fe^{2+}(aq) + H_2O \longrightarrow Fe^{3+}(aq) + 3OH^{-}(aq) \longrightarrow Fe(OH)_3(s).$$

Similar reaction of Cu and Pb ions give product of their hydroxides. The ease at which this bond would be destroyed by water molecules is dependent on their enthalpies of hydration. The hydration energy for the +2 oxidation states of the studied metal ions are -1946 kJ/mol for Fe (II), -1480kJ/mol for Pb (II), -2046kJ/mol for Zn (II) and -2100kJ/mol for Cu (II) respectively. According to Ayuba and Khuzaifa (2014) stronger enthalpy of hydration leads to better adsorption and reduces the tendency for desorption. Therefore Zn and Cu ions would held strongly on the adsorbent with less ease of leaching away.

Table 1. Initial concentration (mg/l) of metal ions in spent and unspent engine oil

S/N	Metal	Spent engine oil	Unspent engine oil
1	Cu	4.94±0.5289	4.10±0.1405
2	Zn	226.35±8.8114	210.03±7.2351
3	Pb	10.38±0.5876	5.95±0.5896
4	Fe	38.70±3.3560	32.17±1.4351

Table 2. Concentration (mg/l) of metal ions in spent and unspent engine oil after adsorption

Contact time	Spent engine oil				unspent engine oil			
	Cu	Zn	Pb	Fe	Cu	Zn	Pb	Fe
10	4.45	162.07	10.02	34.98	3.82	142.19	5.85	23.57
20	4.00	124.94	9.82	26.00	3.14	132.38	5.64	12.57
30	3.98	115.66	9.60	22.52	2.94	115.51	5.56	10.73
40	3.50	85.33	9.00	12.69	2.66	114.09	5.52	9.29

Table 3. Concentration (mg/l) of metal ions in 0.5g adsorbent

Contact time	Spent engine oil				unspent engine oil			
	Cu	Zn	Pb	Fe	Cu	Zn	Pb	Fe
10	0.49	64.28	0.36	3.72	0.29	67.84	0.10	8.60
20	0.94	101.41	0.56	12.70	0.96	77.65	0.31	19.60
30	0.96	110.69	0.58	16.18	1.16	94.52	0.39	21.44
40	1.44	141.02	1.38	26.01	1.44	95.94	0.43	22.88

Table 4. Concentration (mg/l) of metal ions adsorbed during variation of adsorbent dosage at optimum time of 40 min

Dosage (g)	Spent engine oil				unspent engine oil			
	Cu	Zn	Pb	Fe	Cu	Zn	Pb	Fe
0.1	0.32	50.25	0.01	1.45	0.1	45.01	0.02	5.46
0.2	0.38	62.07	0.23	8.27	0.25	47.77	0.15	8.98
0.3	0.38	61.25	0.28	10.55	0.88	46.89	0.26	15.32
0.4	0.40	70.45	0.72	22.06	0.92	72.08	0.41	16.55

From Table 1, the order of heavy metals in both used and unused engine oil is Zn>Fe>Pb>Cu. The high concentration of zinc obtained may be due to the presence of additives such as Zinc diaryl or dialkyl dithiophosphates; zinc dithiophosphate, and other organometallic compounds found in engine oil which contains heavy metals (Masabumi *et al*., 2008; Rizvi, 2009). The increase in the content of zinc in spent oils in comparison with unspent oil may be the result of the presence of wearing products. Its presence in used oils is mainly connected with bearing wear (Nwosu *et al*., 2008). Copper in used engine oils comes mainly from the wearing products of the bearings, rings, and valve guides; in smaller quantities it is introduced in the form of additives (Palkendo *et al*., 2014). Iron is the most typical engine wear product present in engine oil. Therefore, its concentration in spent oil mainly depends on lubricating conditions inside the engine. Njue *et al*. (1999) reported values of 20-788, 9-1550 and 6.5-170 in mg/l for Pb, Fe and Cu in spent engine oil collected from Nairobi central district in Kenyan.

From Table 2 the order removal of various metal ions using termite soil is as follows: for spent engine oil at 10 minutes Zn > Cu>Fe> Pb, 20 and 30 minutes Zn>Fe>Cu>Pb and 40 minutes Fe > Zn> Cu>Pb for unspent engine oil at10 minutes Zn>Fe>Cu>Pb, 20 to 40 minute Fe>Zn>Cu>Pb. An increase in adsorbent dose resulted to more uptake of metal ions as seen in Table 4. This is due to more porous adsorption sites.

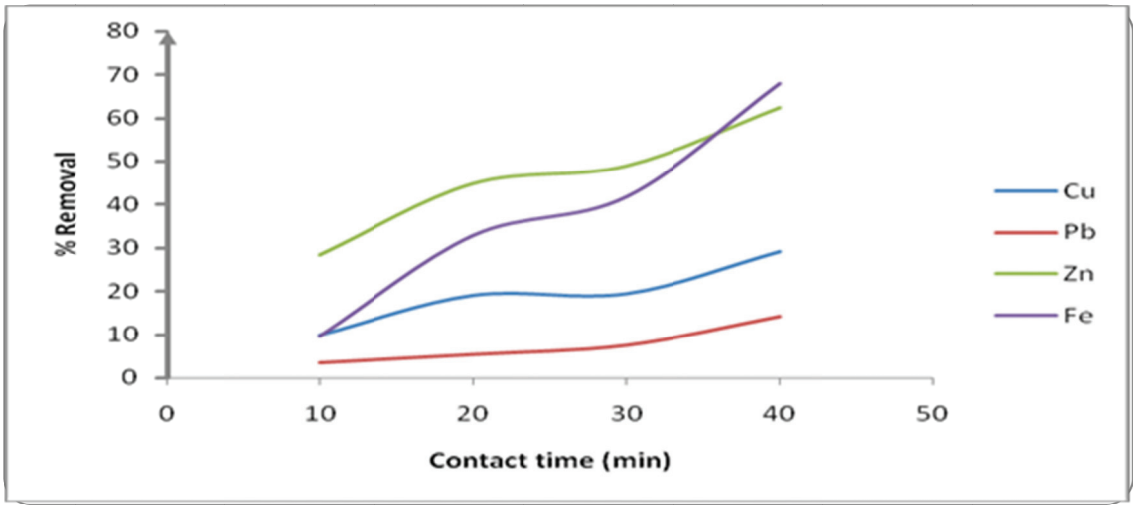

Figure 3. Percentage removal of metal ions from spent engine oil

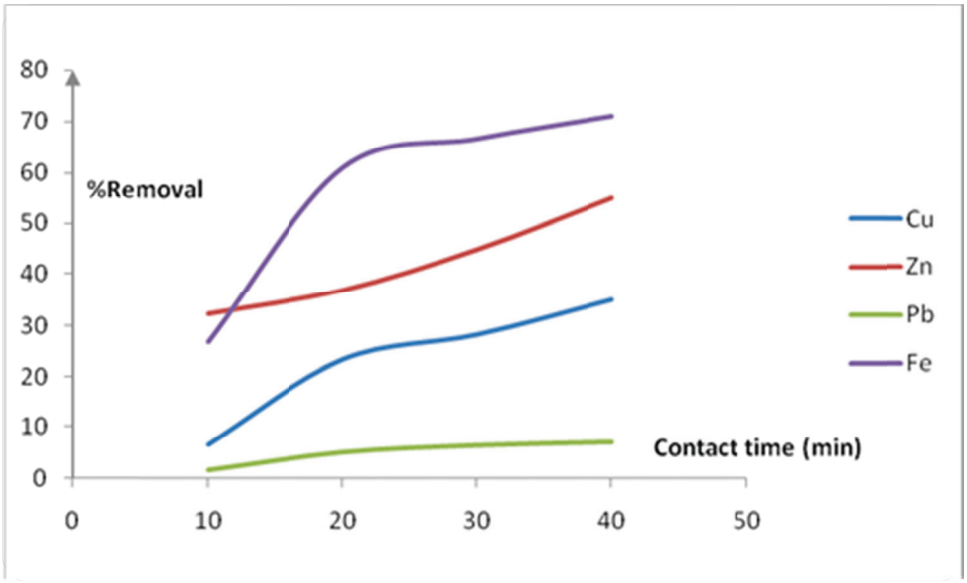

Figure 4. Percentage removal of metal ions from unspent engine oil

Percentage removal of studied metal ions as shown in Fig 3 and 4 increases with increase in contact time was also increased. This occurred as a result of availability of adsorption sites in the adsorbent.

Table 5. Kinetics parameters for spent engine oil

Pseudo first order kinetics				
Parameters	**Zn**	**Pb**	**Cu**	**Fe**
Q_t (mg/g)	1.5922	1.0234	1.4421	1.4928
Q_e (mg/g)	0.0141	0.0146	0.0144	0.2630
$k_1(min^{-1})$	0.0415	0.2349	0.1658	0.0737
R^2	0.967	0.771	0.708	0.876
Pseudo second order kinetics				
Q_t (mg/g)	0.0285	0.02430	0.0285	0.2615
Q_e (mg/g)	0.0141	0.0146	0.0144	0.2630
k_2 (g/mgmin)	0.0188	0.8468	0.7387	0.1535
h (mg/g.min)	0.08921	0.000313	0.000514	0.00366
R^2	0.983	0.905	0.982	0.900
Intra-particle diffusion				
C (mg/g)	-0.062	-0.007	-0.004	-0.179
k_{id} $(mgg^{-1}min^{-1/2})$	0.227	0.003	0.002	0.067
R^2	0.964	0.841	0.912	0.958
Elovich				
α (mg/gmin)	0.1779	0.0011	0.00054	0.01775
β (g/mg)	1.9493	142.8571	333.333	6.71141
R^2	0.956	0.772	0.915	0.931

Q_e (mg/g); experimental adsorption capacity

Q_t (mg/g); theoretical adsorption capacity

Table 6. Kinetics parameters for unspent engine oil

Parameters	Zn	Pb	Cu	Fe
Pseudo first order kinetics				
Q_t(mg/g)	2.8445	1.5031	2.0328	3.1477
Q_e (mg/g)	0.1520	0.0323	0.0144	0.2288
K_1((min^{-1})	0.1359	0.1543	0.1842	0.1404
R^2	0.963	0.733	0.797	0.969
Pseudo second order kinetics				
Q_t (mg/g)	0.2873	0.0433	0.0215	0.4115
Q_e (mg/g)	0.1520	0.0323	0.0144	0.2288
K_2(g/mgmin)	0.0188	0.8468	0.7387	0.1535
h(mg/g.min)	0.0031	0.0027	0.0003	0.0138
R^2	0.982	0.927	0.945	0.964
Intra-particle diffusion				
C(mg/g)	0.0071	0.004	0.007	0.005
K_{id} ($mgg^{-1}min^{-1(1/2)}$)	0.037	0.002	0.003	0.004
R^2	0.941	0.936	0.963	0.952
		Elovich		
α(mg. $g^{-1}min^{-1}$).	0.5354	0.00126	0.001227	0.1724
β ($g.mg^{-1}$)	11.764	111.11	125.00	9.708
R^2	0.979	0.878	0.986	0.921

Q_e (mg/g); experimental adsorption capacity

Q_t (mg/g); theoretical adsorption capacity

Table 5 and 6 gives various parameters for Pseudo-first, pseudo-second, intra-particle and elovich parameters used in describing the factors influencing the movement of metal ions onto available adsorption sites on the adsorbent. It is observed that correlation coefficient for pseudo-first order kinetics is larger compared to other kinetics model, and had theoretical adsorption capacity close to the experimental value. Hence describes the pattern of movement of metal ions to the surface of the adsorbent. Also R^2 for spent and unspent engine are 0.983, 0.905, 0.982, 0.900 and 0.982, 0.927, 0.945, 0.964 respectively is greater compared to other kinetics models.

Graph of $\frac{t}{q_t}$ against t was used in determining initial reaction rate h(mg/g.min) as described by pseudo-second order kinetics. Also plot q_t against Int gave elovich parameter α for initial reaction rate determination. Values obtained shows that Zn and Fe had fast uptake compared to Cu and Pb. The theoretical adsorption capacity also reveals the availability of Cu and Zn ions on the adsorbent surface. Possibly Pb and Cu ions tends to desorp away from the adsorbent upon getting to the surface as evidence from their high desorption constant as seen in the Tables 5 and 6, desorption constant is of the order Cu>Pb>Zn>Fe for spent engine oil Table 5.0 and Pb>Cu>Zn>Fe for unspent engine oil Table 6.0. Values obtained for pseudo-second order kinetics have less difference between theoretical (Q_t) and experimental adsorption (Q_e) capacity

Plot of q_t against $\sqrt{t}$ were used in obtaining intra-diffusion parameters. Intercept C (mg/g) obtained from Tables 5 and 6 are negligible, implying insignificant restriction of boundary layer of the adsorbent for the uptake of the ions. According to Imaga and Abia (2015), for uptake of ions in a heterogeneous system to be best described by intra particle diffusivity the boundary layer C (mg/g) should be equal to zero. Values of boundary layer for the adsorbent during uptake of metal ions were not equal to zero. The observed values shows that the mode of transport is affected by more than one process such as surface adsorption, chemisorptions, ion exchange, precipitation and intra-particle diffusion are occurring concurrently (Igwe *et al*., 2005). Intra-particle diffusion constant (k_{id}) is of the order Zn>Fe>Pb>Cu. This reveals the affinity of the adsorbent (termite soil) with various metal ions. According to Itodo *et al*. (2010) higher values of k_{id} illustrate an enhancement rate of adsorption, which is related to improve bonding between adsorbate and adsorbent particles. Hence Zn ions formed strong bond with the adsorbent compared to other metal ions. Desorption constant 'beta' obtained shows that Zn ions has less potential to be leached from the pores of the adsorbent.

4. Conclusion

Result obtained reveals an increase in concentration of metals in engine oil after usage. This might be attributed to wear and tear of engine parts. However, there was a decrease in their concentration after adsorption. The level of uptake followed the order Fe>Zn>Cu>Pb. Several kinetics models were tested but pseudo-second order kinetics was the best for predicting the kinetics for uptake of the studied metal ions.`.

References

Agbogidi, O. M., Eruotor, P. G., & Akparobi, S. O. (2007) Effects of Time Application of Crude Oil to Soil on the growth of Maize. *Res. J. Environ. Toxicol.*, *1*(3), 116-123. https://doi.org/10.3923/rjet.2007.116.123

Agbozu, I., & Uwem, B. (2016). Kinetic Modeling for removal of Pb, Cd, Ni and Cr ions from Petrochemical effluent using termite Hill. *International Journal of Sciences*, *5*(2), 77-82. https://doi.org/10.18483/ijSci.950

Ahamefule, H. E. (2013). Bioremediation of spent automobile engine oil contaminated sandy loam soil in South-Eastern Nigeria using Maize and Cowpea Test Crops. A Thesis Submitted in Partial Fulfillment of the Requirements for the Award of the degree of Doctor of Philosophy (Ph.D.) in Soil Physics/Conservation. Department of Soil Science Faculty of Agriculture University of Nigeria Nsukka, 20.

Ayuba, A. M., & Khuzaifa, Y. M. (2014). The Effect of Halides on the Adsorption of Cd (II) Onto Groundnut Shell (Arachis hypogeal)-a Thermodynamic Study. Book of Proceeding of the 37th Annual Chemical Society of Nigeria Conference, 262-270.

Dabrowski, A. (2001). Adsorption from theory to practice. *Advances in Colloid and Interface Science,* 93, 135-224. https://doi.org/10.1016/S0001-8686(00)00082-8

Grzegorz, Z., Joanna, S. B., Tomasz, S., Andrzej, K., & Agnieszka, K. (2015). Designation of Chosen Heavy Metals in Used Engine Oils Using the XRF Method. *Pol. J. Environ. Stud., 24*(5), 2277-2283. https://doi.org/10.15244/pjoes/58781

Holt, J. A., Coventry, R. J., & Sinclair, D. F. (1998). Some aspects of the biology and pedological significance of mound-building termites in a red and yellow earth landscape near charters towers, north Queensland. *Australian Journal of Soil Research, 18*, 97–109. https://doi.org/10.1071/SR9800097

Igwe, J. C., Nwokennaya, E. C., & Abia, A. A. (2005). The role of pH in heavy metal detoxification by biosorption from aqueous solution containing chelating agents. *Africa Journal of Biotechnology*, *4*(10), 1109-1112.

Imaga, C. C., & Abia, A. A. (2015) Kinetics and Mechanisms of Sorption Of Lead (II) Ions Using Carbonized And Mercapto-Acetic Acid Modified Sorghum (sorghum Bicolor) Hull of Two Pore Sizes, *Journal of Multidisciplinary Engineering Science and Technology*, *2*(1), 3159-0040.

Itodo, A. U., Abdulrahman, F. W, Hassan, L. G, Maigandi, S. A., & Itodo, H. U. (2010). Intra particle Diffusion and Intra particulate Diffusivities of Herbicide on Derived Activated Carbon. http://www.sciencepub.net/researcher. 74–86.

Kelechi, L. N., Modupe, O. A., & Temitope, O. B. (2012). Effect of time of application of spent oil on the growth and performance of maize (*Zea mays)*. *African Journal of Environmental Science and Technology*, *6*(1), 67-71. https://doi.org/10.5897/AJEST11.061

Marchessault, R. H., Ravenelle, F., & Zhu, X. X. (2006). Polysaccharides for drug delivery and pharmaceutical applications, *American Chemical Society.* https://doi.org/10.1021/bk-2006-0934

Masabumi, M., Hiroyasu, S., Akihito, S., & Osamu, K. (2008). Prevention of oxidative degradation of ZnDTP by microcapsulation and verification of its antiwear performance; *Tribology International, 41*, 1097–1102. https://doi.org/10.1016/j.triboint.2008.01.005

Njue, W., Kinyua, A. M., & Thinguri, M. T. (1999). Determination of heavy metals and sulphur in waste engine oil. *Bulletin. Chemical Society of Ethiopia*, *13*(2), 99-104. https://doi.org/10.4314/bcse.v13i2.21062

Nwosu, F. O., Olu-owolabi, B. I., Adebowalek. O., & Leke, L. (2008). Comparative Investigation of Wear Metals in Virgin and Used Lubricant Oils. *Terrestrial and Aquatic Environmental Toxicology*, *2*(1), 38.

Palkendo, J. A., Kovach, J., & Betts, T. A. (2014). Determination of Wear Metals in Used Motor Oil by Flame Atomic Absorption Spectroscopy. *J. Chem. Educ*., *91*(4), 579. https://doi.org/10.1021/ed4004832

Rauckyte, T., Hargreaves, D. J., & Pawlak, Z. (2006). Determination of Heavy Metals and Volatile Aromatic Compounds in Used Engine Oils and Sludges. *Fuel*, *85*(4), 481. https://doi.org/10.1016/j.fuel.2005.08.004

Rizvi, S. Q. A. (2008). A comprehensive review of lubricant chemistry, technology, selection, and design, ASTM

International, West Conshohocken, PA., 100-112. https://doi.org/10.1520/MNL11464M

Schaefer, C. E. R. (2001). Brazilian Latosols and their B horizon microstructure as long-term biotic constructs. *Australian Journal of Soil Research, 39*, 909–926. https://doi.org/10.1071/SR00093

Sharifi, M., Sadeghi, Y., & Akbarpour, M. (2007). Germination and growth of six plant species on contaminated soil with spent oil. Inter. J. *Environ., Sci. Technol*., *4*(4), 463-470.

Sharma, Y. C., Gupta, G. S., Prasad, G., & Rupainwar, D. C. (1990). Use of wollastonite in the removal of Ni(II) from aqueous solutions, *Water, Air, and Soil Pollution*, *49*, 69. https://doi.org/10.1007/BF00279511

Vwioko, D. E., & Fashemi, D. S. (2005). Growth Response of *Ricinus communis* L. (Castor Oil) in Spent Lubricating Oil Polluted soil. *J. App. Sci. Environ. Manage*, *9*(2), 73-79. https://doi.org/10.4314/jasem.v9i2.17294

Yong, W., Laura, A. B., Erick, H., & Ian, D. B. (2016). Rapid high-performance sample digestion of base metal ores using high-intensity infrared radiation with determination by nitrogen-based microwave plasma optical spectrometry. *Analytical Chemistry Research, 7*, 17-22. https://doi.org/10.1016/j.ancr.2016.02.002

International Journal of Chemistry; Vol. 9, No. 3; 2017
ISSN 1916-9698 E-ISSN 1916-9701
Published by Canadian Center of Science and Education

Reviewer Acknowledgements

International Journal of Chemistry wishes to acknowledge the following individuals for their assistance with peer review of manuscripts for this issue. Their help and contributions in maintaining the quality of the journal is greatly appreciated. Many authors, regardless of whether *International Journal of Chemistry* publishes their work, appreciate the helpful feedback provided by the reviewers.

Reviewers for Volume 9, Number 3

Ahmad Galadima, Usmanu Danfodiyo University, Nigeria

Ahmet Ozan Gezerman, Yildiz Technical University, Turkey

Amer A. Taqa, Mosul University, Iraq

Asghari Gul, Comsats IIT, Pakistan

Ayodele Temidayo Odularu, University of Fort Hare, South Africa

Chanchal Kumar Malik, Vanderbilt University, USA

Diego Antonio Alonso, Alicante University, Spain

Farkhondeh Fathi, University of Toronto, Canada

Greg Peters, University of Findlay, USA

Jiajue Chai, Brown University, USA

Jignasu P. Mehta, Bhavnagar University, India

Juan Rafael Garcia, Research Institute on Catalysis and Pertrochemistry (INCAPE), Argentina

K. Ishara Silva, Rensselaer Polytechnic Institute, USA

Kallen Mulilo Nalyanya, Egerton University, Kenya

Leiming Wang, Konica Minolta Laboratory, USA

Meriem Belhachemi, University of Bechar, Algeria

Monira Nessem Michael, National institute of standards (NIS), Egypt

Mustafa Oguzhan Kaya, Siirt University, Turkey

Priyanka Singh, University of Iowa, USA

R. K. Dey, Birla Institute of Technology (BIT), India

Rabia Rehman, University of the Punjab, Pakistan

Saroj Kumar Panda, Research & Development Center, Saudi Arabia

Sujan Kumar Sarkar, Ruhr University Bochum, Germany

Thirupathi Barla, Harvard University, USA

Vijay Ramalingam, Columbia University, USA

Waseem Hassan, Universidade Federal de Santa Maria, Brazil

Albert John

On behalf of,

The Editorial Board of *International Journal of Chemistry*

Canadian Center of Science and Education

ACADEMIC AND OPEN ACCESS

Canadian Center of Science and Education

CCSENET.ORG

➢ CALL FOR MANUSCRIPTS

International Journal of Chemistry (IJC) is a peer-reviewed, open access journal, published by Canadian Center of Science and Education. It publishes original research and applied articles in all areas of chemistry. Authors are encouraged to submit complete unpublished and original works, which are not under review in any other journals. We are seeking submissions for forthcoming issues. All manuscripts should be written in English. Manuscripts from 3000–8000 words in length are preferred. All manuscripts should be prepared in MS-Word format, and submitted online, or sent to: ijc@ccsenet.org

Paper Selection and Publishing Process

a) Submission acknowledgement. If you submit manuscript online, you will receive a submission acknowledgement letter sent by the online system automatically. For email submission, the editor or editorial assistant sends an e-mail of confirmation to the submission's author within one to three working days. If you fail to receive this confirmation, please check your bulk email box or contact the editorial assistant.

b) Basic review. The editor or editorial assistant determines whether the manuscript fits the journal's focus and scope. And then check the similarity rate (CrossCheck, powered by iThenticate). Any manuscripts out of the journal's scope or containing plagiarism, including self-plagiarism are rejected.

c) Peer Review. We use a double-blind system for peer review; both reviewers' and authors' identities remain anonymous. The submitted manuscript will be reviewed by at least two experts: one editorial staff member as well as one to three external reviewers. The review process may take two to four weeks.

d) Make the decision. The decision to accept or reject an article is based on the suggestions of reviewers. If differences of opinion occur between reviewers, the editor-in-chief will weigh all comments and arrive at a balanced decision based on all comments, or a second round of peer review may be initiated.

e) Notification of the result of review. The result of review will be sent to the corresponding author and forwarded to other authors and reviewers.

f) Pay the publication fee. If the submission is accepted, the authors revise paper and pay the publication fee.

g) Send printed journals by post. After publication, two hard copies of the journal will be sent to the corresponding author.

h) Publication notice. The authors and readers will be notified and invited to visit our website for the newly published articles.

More Information

E-mail: ijc@ccsenet.org

Website: http://ijc.ccsenet.org

Paper Submission Guide: http://submission.ccsenet.org

Recruitment for Reviewers: http://recruitment.ccsenet.org

➢ JOURNAL STORE

To order back issues, please contact the editorial assistant and ask about the availability of journals. You may pay by credit card, PayPal, and bank transfer. If you have any questions regarding payment, please do not hesitate to contact the editorial assistant.

Price: $40.00 USD/copy Shipping fee: $20.00 USD/copy

ABOUT CCSE

The Canadian Center of Science and Education (CCSE) is a private for-profit organization delivering support and services to educators and researchers in Canada and around the world.

The Canadian Center of Science and Education was established in 2006. In partnership with research institutions, community organizations, enterprises, and foundations, CCSE provides a variety of programs to support and promote education and research development, including educational programs for students, financial support for researchers, international education projects, and scientific publications.

CCSE publishes scholarly journals in a wide range of academic fields, including the social sciences, the humanities, the natural sciences, the biological and medical sciences, education, economics, and management. These journals deliver original, peer-reviewed research from international scholars to a worldwide audience. All our journals are available in electronic form in conjunction with their print editions. All journals are available for free download online.

Mission

To work for future generations

Values

Scientific integrity and excellence

Respect and equity in the workplace

CONTACT US

General

Tel: 1-416-642-2606

Fax: 1-416-642-2608

E-mail: info@ccsenet.org

Website: www.ccsenet.org

Mailing Address

1120 Finch Avenue West

Suite 701-309

Toronto, ON., M3J 3H7

Canada

Visiting Address

9140 Leslie St., Suite 110

Richmond Hill, Ontario, L4B 0A9

Canada

The journal is peer-reviewed
The journal is open-access to the full text
The journal is included in:

Academic Journals Database
CABI
CAS
EBSCOhost
Elektronische Zeitschriftenbibliothek EZB
Google Scholar
JournalTOCs
LOCKSS
NewJour
Open J-Gate
PKP Open Archives Harvester
Standard Periodical Directory
Ulrich's
Universe Digital Library
WorldCat

International Journal of Chemistry
Quarterly

Publisher Canadian Center of Science and Education
Address 1120 Finch Avenue West, Suite 701-309, Toronto, ON., M3J 3H7, Canada
Telephone 1-416-642-2606
Fax 1-416-642-2608
E-mail ijc@ccsenet.org
Website http://ijc.ccsenet.org

ISSN 1916-9698